THE UNIVERSITY OF QUEENSLAND

AUSTRALIA

Inflammation-driven bone formation in ankylosing spondylitis: Characterisation of the proteoglycan-induced spondylitis mouse model

Hsu-Wen Tseng

Master of Science

A thesis submitted for the degree of Doctor of Philosophy at

The University of Queensland in 2015

The University of Queensland Diamantina Institute

Abstract

Ankylosing spondylitis (AS) is a chronic inflammatory arthritis characterised by severe inflammation of the axial skeleton followed by bone formation that can lead to ankylosis. The mechanisms mediating the transition from inflammation to bone formation are poorly understood due to the limited availability of relevant bone samples. Therefore, we used the proteoglycan-induced spondylitis (PGISp) mouse model to delineate the morphological changes during axial disease development. This mouse model develops spondylitis followed by ankylosis, mimicking the clinical progression seen in patients with AS.

The first part of this project aimed to characterise the disease progression across a 43-week time-course in the PGISp mouse model. The principal assessment for analysing spinal disease was a semi-quantitative histological score that assessed joint inflammation, joint destruction (including intervertebral disc (IVD), cartilage and bone) and excessive tissue formation (peri-joint mesenchymal tissue expansion or fibrocartilage formation). Early inflammation initiated at the periphery of the IVD and was followed by varying levels of disc, cartilage and bone damage. In the advanced stages of disease, excessive tissue formation and ectopic chondrocyte expansion, ectopic bone and osteophyte formation were the key features. Abnormal tissue formation was always associated with IVD destruction, which was the result of inflammation, indicating that inflammation-derived IVD destruction is a prerequisite for induction of excessive tissue formation and the subsequent osteoproliferation.

Current therapies for AS include non-steroidal anti-inflammatory drugs (NSAIDs), tumour necrosis factor (TNF) inhibitors and physiotherapy. However, these therapies aim to alleviate symptoms but cannot prevent syndesmophyte formation; hence new, more effective, therapeutic strategies are required. Genome-wide association studies have shown that AS is strongly associated with prostaglandin E2 (PGE2) receptor subtype 4 (EP4), which plays regulatory roles in both inflammation and bone formation. The involvement of EP4 in AS has not been examined. The second objective of this thesis was to examine the hypothesis that blocking EP4 can suppress disease progression by inhibiting both inflammation and bone formation. PGISp mice were prophylactically administered with ONO-AE1-329 (an EP4 agonist) or ONO-AE2-227 (an EP4 antagonist)

for 16 weeks. Indomethacin, an NSAID, was included as a positive control of PGE2 signalling inhibitor. None of the treatments significantly altered peripheral arthritis or axial disease progression. Use of EP4 agonist or antagonist did not change bone mineral density and bone mineral content as measured by dual-energy X-ray absorptiometry. The large variation of disease onset and features within each experimental group confounded the analysis.

The third objective was to test the hypothesis that inflammation-derived IVD destruction is a prerequisite for excessive tissue formation. To suppress the onset and severity of inflammation development, a combination of high dose etanercept plus high dose prednisolone was administered in the initial stage of axial disease development. This anti-inflammatory therapy was found to significantly suppress peripheral inflammation and delay disease onset. It also reduced axial inflammation and led to a trend toward reduced IVD destruction, bone erosion, cartilage damage and excessive tissue formation. Suppressing inflammation ameliorated disease progression supporting that early and aggressive anti-inflammatory intervention might mediate genuine clinical improvements with respect to structural damage.

In conclusion, enthesitis and excessive cartilage/bone formation were the key features of the PGISp mouse, making it a suitable model for understanding the pathological mechanisms that are involved in the transition from inflammation to osteoproliferation. The IVD destruction driven by inflammation is a prerequisite for induction of osteoproliferation. Therefore, early intervention with anti-inflammatory therapy might prevent structural damage and further suppress excessive tissue formation.

Declaration by author

This thesis is composed of my original work, and contains no material previously published or written by another person except where due reference has been made in the text. I have clearly stated the contribution by others to jointly-authored works that I have included in my thesis.

I have clearly stated the contribution of others to my thesis as a whole, including statistical assistance, survey design, data analysis, significant technical procedures, professional editorial advice, and any other original research work used or reported in my thesis. The content of my thesis is the result of work I have carried out since the commencement of my research higher degree candidature and does not include a substantial part of work that has been submitted to qualify for the award of any other degree or diploma in any university or other tertiary institution. I have clearly stated which parts of my thesis, if any, have been submitted to qualify for another award.

I acknowledge that an electronic copy of my thesis must be lodged with the University Library and, subject to the policy and procedures of The University of Queensland, the thesis be made available for research and study in accordance with the Copyright Act 1968 unless a period of embargo has been approved by the Dean of the Graduate School.

I acknowledge that copyright of all material contained in my thesis resides with the copyright holder(s) of that material. Where appropriate I have obtained copyright permission from the copyright holder to reproduce material in this thesis.

Publications during candidature

Peered-reviewed papers

1. Benham H, Rehaume LM, Hasnain SZ, Velasco J, Baillet AC, Ruutu M, Kikly K, Wang R, Tseng HW, Thomas GP, Brown MA, Strutton G, McGuckin MA, Thomas R (2014) IL-23-mediates the intestinal response to microbial beta-glucan and the development of spondyloarthritis pathology in SKG mice. *Arthritis Rheumatol*: 66:1755-1767
2. Haynes KR, Pettit AR, Duan R, Tseng HW, Glant TT, Brown MA, Thomas GP (2012) Excessive bone formation in a mouse model of ankylosing spondylitis is associated with decreases in Wnt pathway inhibitors. *Arthritis Res Ther.* 14:R253.

Conference abstracts

1. Tseng HW, Pitt ME, Glant TT, McRae A, Kenna TJ, Brown MA, Pettit AR, Thomas GP. Endochondral bone formation and advanced enthesitis are key features of PGISp mouse model of ankylosing spondylitis. Australian Rheumatology Association 54th annual scientific meeting (Oral presentation), 2013
2. Tseng HW, Pitt ME, Glant TT, McRae A, Kenna TJ, Brown MA, Pettit AR, Thomas GP. Endochondral bone formation and advanced enthesitis are key features of PGISp mouse model of ankylosing spondylitis. Translational Research Institute Symposium (TRI) (Poster presentation), 2013
3. Tseng HW, Pitt ME, Glant TT, McRae A, Kenna TJ, Brown MA, Pettit AR, Thomas GP. Endochondral bone formation and advanced enthesitis are key features of PGISp mouse model of ankylosing spondylitis. Princess Alexandra Hospital Symposium (Poster presentation), 2013
4. Tseng HW, Pitt ME, Glant TT, McRae A, Kenna TJ, Brown MA, Pettit AR, Thomas GP. Endochondral bone formation and advanced enthesitis are key features of PGISp mouse model of ankylosing spondylitis. Australian Society for Medical Research Queensland postgraduate student conference (Poster presentation), 2014
5. Tseng HW, Pitt ME, Glant TT, McRae A, Kenna TJ, Brown MA, Pettit AR, Thomas GP. Endochondral bone formation and advanced enthesitis are key features of PGISp

mouse model of ankylosing spondylitis. 44th IBMS international Sun Valley workshop (Poster presentation), 2014

Publications included in this thesis

No publications included.

Contributions by others to the thesis

Dr Gethin Thomas, Dr Allison Pettit and Professor Matthew Brown significantly contributed to the conception and design of the projects, interpretation of research data and editing this thesis. Miss Miranda Pitt significantly contributed to performing mRNA expression analysis. Professor Tibor Glant kindly provided cartilage extract needed in the entire project and technical advice. Dr Allan McRae significantly contributed to statistical analysis of unsupervised cluster analysis. Dr Tony Kenna significantly contributed to experimental design, non-routine technical work and data interpretation.

Statement of parts of the thesis submitted to qualify for the award of another degree

Chapters 2, Figure 2.2F (page 61) and 2.3E (page 64) submitted for Miss Miranda Pitt's HBSc Honours, The University of Queensland, 2013, degree awarded 6th of December 2013.

Acknowledgements

First and foremost I wish to thank my supervisors. My principle supervisor Dr Gethin Thomas has supported me academically and emotionally throughout my study, and his vast knowledge was elemental in the conception and progression of this project; I thank him for his patience in allowing me to learn and progress at my own pace, and encouraging me during periods of frustration. I appreciate his great and continual assistance and patience in my writing and improving my presentation. My co-supervisor Dr Allison Pettit, whose expertise in histology, bone biology and immunology added considerably to my project. I am grateful for her incredible patience in devoting time to reading and editing/rewriting my thesis. I have been very lucky to have supervisors who always made time to meet regularly with me whenever I needed guidance. Thanks to my co-supervisor Professor Matthew Brown for accepting me into this big family and providing extensive clinical insight into to my project. Other than my supervisors, I wish to thank Dr Tony Kenna, whose expertise in immunology has provided much assistance in the design and execution of aspects of this project, Dr Tibor Glant, who kindly provided me the human cartilage extract, shared his experiences and welcomed me to visit his lab and Dr Allan McRae who helped me with the unsupervised clustering analysis. Appreciation also goes out to my other thesis committee members, Dr Liza Raggatt, Dr Antje Blumenthal, Professor Dietmar Hutmacher and Dr Nyoman Kurniawan, for their insightful comments.

I must express my gratitude to Miranda Pitt, who did the hard work analysing mRNA expression profile during her honours degree. Poh-Lynn Low, Karena Pryce and Patricia Keith gave me a hand in my big tissue collection. Knowledgeable Eugene Lau always had answers for my questions. Thanks to Philip Robinson, Linda Bradbury and Steven Truong for their clinical inputs. Katelin Haynes shared her experience with this animal model and histological experiments. Dr Karine Mardon, Dr Nana Sunn and Nathan Boase, from CAI and TRI imaging facilities, helped me with setting up CT imaging protocols, acquiring images, troubleshooting and analyses. The histology and animal experiments would not have been completed without the assistance from UQ Biological resource facilities in PA hospital, AIBN, PACE and TRI; the histology facilities in QIMR and TRI; and the microscopy facility in TRI.

Thanks to Diamantina Institute, the University of Queensland and TRI for providing all the research resources and educational support I needed to complete my work. I would also like to acknowledge the financial support I received from the UQ international scholarship.

I must also express my thanks to the whole Brown group for creating such a friendly and cheerful working environment, and many people's efforts to keep the lab running smoothly. The encouragements from Aideen McInerney-Leo, Jessica Harris, Erika de Guzman, Shannon Waldron, Sharon Song, Syndia Lazarus, Kelly Hollis, Kim Gardner, Lawrie Wheeler, and Brooke Gardiner. Special thanks to my editors, Katie Cremin, Aimee Hanson, Lisa Anderson and Mary-Ellen Costello, for making my thesis readable.

Last but not least, I must thank my parents, sister and brother for their constant support and encouragements throughout my life. My parents gave me opportunities to pursue a higher education and study abroad. My sister and brother are my best friends whom I can share everything with. Thanks God for blessing me with such a nice family and placing so many helpers around me.

Keywords

Ankylosing spondylitis, proteoglycan-induced spondylitis mouse model, enthesis, intervertebral disc destruction, chondroidal bone formation, osteophyte, ectopic bone, spondyloarthropathy, arthritis, osteoproliferation

Australian and New Zealand Standard Research Classifications (ANZSRC)

ANZSRC code: 060699 Physiology not elsewhere classified, 60%

ANZSRC code: 110799 Immunology not elsewhere classified, 40%

Fields of Research (FoR) Classification

FoR code: 0699 Other Biological Sciences, 60%

FoR code: 1107 Immunology, 40%

Table of Contents

List of Figures

List of Appendix Figures

List of Tables

List of Abbreviations used in the thesis

Abbreviation	Full name
AIA	Adjuvant-induced arthritis
ANK	Progressive ankylosis
ARE	AU-rich elements
AS	Ankylosing spondylitis
ASAS	Assessment of SpondyloArthritis international Society
ASSERT	Ankylosing Spondylitis Study for the Evaluation of Recombinant Infliximab Therapy
β-cat	β-catenin
BMC	Bone mineral content
BMD	Bone mineral density
BMP	Morphogenetic protein
C1-7	Cervical vertebrae
CAI	Carbonic anhydrase I
CAIA	Collagen antibody-induced arthritis
CIA	Collagen-induced arthritis
cAMP	Cyclic adenosine monophosphate
Comp	Cartilage oligomeric matrix protein
Col2a1	Type II collagen, α 1
COX	Cyclooxygenase
CRP	C-reactive protein
CT	Computed tomography
DAB	Diaminobenzidine
DDA	Dimethyldioctadecylammonium
DKK-1	Dickkopf-1
DXA	Dual x-ray absorptiometry
EAE	Encephalomyelitis
ECM	Extracellular matrix
EDTA	Ethylenediaminetetraacetic acid disodium salt dihydrate
EP1-4	PGE2 receptor subtype 1-4

ER	Endoplasmic reticulum
ERAP	Endoplasmic reticulum aminopeptidases
ESR	Erythrocyte sedimentation rate
ETN	Etanercept
FBS	Fetal bovine serum
GWAS	Genome-wide association studies
GSK-3β	Glycogen synthase kinase 3
H&E	Haematoxylin and eosin
HRP	Horseradish peroxidase
HLA	Human leukocyte antigen
hβ2m	Human β2-microglobulin
hTNFtg	Human TNF transgenic mice
IBD	Inflammatory bowel disease
IFN	Interferon
IHC	Immunohistochemistry
IND	Indomethacin
IVD	Intervertebral discs
L1-6	Lumbar vertebrae
LRP	low-density lipoprotein receptor-related protein
MHC	Major histocompatibility complex
MRI	Magnetic resonance imaging
MMP	Metalloproteinase
mSASSS	Modified Stoke Ankylosing Spondylitis Spinal Score
NSAIDs	Non-steroidal anti-inflammatory drugs
OASIS	Outcome Assessments in Ankylosing Spondylitis International Study
PBS	Phosphate-Buffered Saline
PCR	Polymerase chain reaction
PI3K	Phosphatidylinositol 3-kinases
PG	Proteoglycan
PGIA/PGISp	Proteoglycan-induced arthritis/ spondylitis mouse model
PGE2	Prostaglandin E2
PKB/AKT	Protein kinase B

PRD	Prednisolone
PTGER4	PGE2 receptor subtype 4
QPCR	Quantitative real-time reverse transcription PCR
RA	Rheumatoid arthritis
RANKL	Receptor activator of nuclear factor-κB ligand
rhG1	Recombinant human G1
RT	Room temperature
SCID	Severe combined immunodeficiency
Sfrp	Secreted frizzled-related proteins
SI	Sacroiliac
SNP	Single nucleotide polymorphisms
Sox9	Sex determining region Y- box 9
SOST	Sclerostin
SpA	Spondyloarthropathies
SPF	Specific pathogen-free
T1-13	Thoracic vertebrae
TBS	Tris-buffered saline
TCF/LEF	T cell factor/lymphoid enhancer binding factor
TCR	T cell receptor
TGF-β	Transforming growth factor-β
TNF	Tumour necrosis factor
TNFR	TNF receptor
TNFΔARE	Deletion of the ARE in the TNF 3'UTR
TRANCE	TNF-related activation-induced cytokine
TWEAK	TNF-related weak inducer of apoptosis
3'UTR	3'-untranslated region
Wnt	Wingless
ZAP	Zeta-chain-associated protein kinase 70

1 Chapter 1: Literature review

1-1 Clinical features of AS

Ankylosing spondylitis (AS) is an auto-immune inflammatory arthritis belonging to the spondyloarthropathies (SpA) that affects 0.35-1% of the population in the United States [1]. SpA is a broad group of related diseases sharing similar clinical symptoms, such as axial disease, peripheral arthritis, enthesitis, dactylitis, uveitis, psoriasis and inflammatory bowel disease (IBD). Other diseases in the SpA spectrum are psoriatic arthritis, reactive arthritis, enteropathy-related spondylitis and arthritis, and undifferentiated SpA [2].

AS is the major subgroup of SpA and the prevalence in white European population is 0.5% [3]. Inflammation in the axial skeleton, including spine and sacroiliac (SI) joints, leads to morning stiffness, chronic low back pain, decreased spinal mobility and restricted chest expansion [2]. The disease often initiates before the age of 30 and targets men two-three times more often than women. Large joints are also frequently involved, such as hips and heels. In the advanced stages, disability is mainly the result of syndesmophyte formation, a consequence of excessive ectopic bone formation that bridges the adjacent vertebrae and can eventually fuse the whole spine [4].

1-2 Pathogenesis of AS

1-2.1 Genetic factors

Human leukocyte antigen (HLA)-B27 is carried by 80-95% of AS patients and the subtype HLA-B*2705 has the strongest correlation with AS [3]. The most validated hypotheses proposed to explain how HLA-B27 links to AS are arthritogenic peptide hypothesis and ER stress hypothesis.

If AS were a monogenic disease associated only with HLA-B27, the disease concordance rate of HLA-B27 positive dizygotic twins and HLA-B27 monozygotic twins should be approximately the same. However, the rates of HLA-B27 positive dizygotic twins and HLA-B27 monozygotic twins were 23% and 63% respectively [5]. This indicates that AS is highly heritable, but the presence of HLA-B27 alone is not causative. Genome-wide association studies (GWAS) also found many non-major histocompatibility complex (MHC)

genes to be associated with the risks of developing AS [6]. Many of them are involved in the regulation of immune responses suggesting these single nucleotide polymorphisms (SNP) might augment the auto-immunity (Table 1-1). Genes associated with radiographic progression include several MHC molecules, such as HLA-DRB1, HLA-B and HLA-DQA1, as well as other genes mainly involved in bone anabolic and catabolic pathways (Table 1-2) [7-9].

Table 1-1 Non-MHC candidate genes associated with AS and their regulatory roles in immune system.

SNP	Chromosome	Position	Nearby gene(s)	Function
rs6600247	1p36	25177701	*RUNX3* (Runt-related transcription factor 3)	Development of CD8 T cells [10] and IFN-γ producing Th17 [11].
rs11209026	1p31	67478546	*IL23R* (IL-23 receptor)	IL-23 receptor signalling induces IL-17 and IL-22 production.
rs41299637	1q32	199144473	*KIF21B* (kinesin family member 21B)	KIF21B is involved in organelle transportation, such as $GABA_A$Rs [12]. Increased KIF21B expression is associated with multiple sclerosis and Alzheimer's disease [13].
rs6759298	2p15	62421949	Intergenic	
rs12186979	5p13	40560617	*PTGER4* (Prostaglandin E2 receptor subtype 4)	PGE2/EP4 enhances Th1 differentiation and Th17 expansion [14]. It is also important in bone homeostasis (see below).
rs30187	5q15	96150086	*ERAP1* (Endoplasmic reticulum aminopeptidase 1)	Peptide trimming and MHCI complex assembling (see below).

SNP	Chromosome	Position	Nearby gene(s)	Function
rs6871626	5q33	158759370	*IL12B* (IL-12p40 submit)	A shared subunit of pro-inflammatory cytokines, IL-12 and IL-23.
rs1128905	9q34	138373660	*CARD9 (*caspase recruitment domain family, member 9*)*	An adaptor protein that participates in pattern recognition receptor signalling [15].
rs1860545	12p13	6317038	1. *LTBR* (lymphotoxin B receptor) 2. *TNFRSF1A (*Tumour necrosis factor receptor superfamily, membrane 1. Also known as TNFRI)	1. LTβR is required for lymphoid organogenesis and development of conventional and γδ T cell [16]. 2. TNFRI is ubiquitously expressed and mediates most TNF-induced inflammation [17].
rs9901869	17q21	42930205	*TBX21 (*T-Cell-Specific T-Box Transcription Factor T-Bet)	A transcription factor enhances Th1 development while suppresses Th17 differentiation [18].
rs2836883	21q22	39388614	Intergenic	
rs4129267	1q2	152692888	*IL6R* (IL-6 receptor)	Required for IL-6 signalling which is dysregulated in a number of autoimmune

SNP	Chromosome	Position	Nearby gene(s)	Function
				diseases.
rs1801274	1q23	159746369	*FCGR2A* (Fc receptor γ IIa, FcγRIIA, CD32)	A receptor of IgG Fc region of IgG1-4, regulates phagocytosis of immune complex[19].
rs12615545	2q31	181756697	*UBE2E3* (ubiquitin-conjugating enzyme E2E3)	The function of UBE2E3 is unclear. Other ubiquitin-conjugating enzymes regulate both innate and adaptive immune responses [20, 21].
rs4676410	2q37	241212412	*GPR35* (G protein-coupled receptor 35)	A tryptophan metabolite-sensing receptor expressed on innate immune cells [22]. Activation of GPR35 in human iNKT cells reduces IL-4 production [23].
rs17765610	6q15	90722494	*BACH2* (BTB and CNC homology 1, basic leucine zipper transcription factor 2)	A transcriptional factor that regulates B cell differentiation and regulatory T cell development [24].
rs1250550	10q22	80730323	*ZMIZ1* (zinc finger, MIZ-type containing 1. Also known as	A transcriptional co-activator that interacts and enhances p53 [25] and Smad3/4 [26]

SNP	Chromosome	Position	Nearby gene(s)	Function
			ZIMP10)	transcriptional activity.
rs11190133	10q24	101268715	*NKX2-3* (NK2 homeobox 3)	NKX2-3 regulates the development of secondary lymphoid organs [27, 28].
rs11065898	12q24	110346958	*SH2B3 (*Src homology 2-B adaptor protein 3. Also known as Lnk)	SH2B3 negatively regulates the development of lymphocytes and dendritic cells [29].
rs11624293	14q31	87558574	*GPR65* (G protein-coupled receptor 65. Also known as T-cell death-associated gene 8)	It suppresses inflammatory cytokine expression in macrophages and inhibits lymphocyte and eosinophil apoptosis [30]
imm_16_28525386	16p11	28525386	1. *IL27p28* 2. *SULT1A1* (sulfotransferase family, cytosolic, 1A, phenol-preferring, member 1)	1. One subunit of IL-27 which enhances Th1 but suppresses Th2 and Th17 differentiation and induces IL-10 production by T cells [31]. 2. Sulfotransferases are associated with different types of cancers, including breast, prostate cancer, lung, bladder and

SNP	Chromosome	Position	Nearby gene(s)	Function
				colorectal cancer [32].
rs2531875	17q11	23172294	*NOS2* (nitric oxide synthase 2, inducible nitric oxide synthase)	Converts L-arginine to nitric oxide (NO) and L-citrulline. NO mediates vasodilation, infection clearance and favours Th1 differentiation [33]. Elevation of serum nitrite level has been reported in active SpA patients [20]
rs35164067	19p13	10386181	*TYK2* (tyrosine kinase 2)	Mediates IFN, IL-12 and IL-23 pathways and is important in both innate and adaptive immune responses [34]. Deficiency of Tyk2 protects anti-type II collagen antibody-induced arthritis in mice [35]
rs7282490	21q22	44440169	*ICOSLG* (inducible T-cell co-stimulator ligand. Also known as ICOSL)	Expressed on antigen presenting cells and regulates T cell differentiation. The IBD-associated risk allele decreased cytokine production upon the activation of pattern-

SNP	Chromosome	Position	Nearby gene(s)	Function
				recognition receptors [36].

Table 1-2 Non-MHC genes associated with radiographic progression [7-9]

SNP	Chromosome	Position	Gene	Function
rs12725747	1q42	226173544	*WNT9A* (wingless-type MMTV integration site family, member 9A)	Inhibits chondrogenesis and enhances chondrocyte hypertrophy via decreasing *Col2a1* and *Sox9,* while increasing *Runx2* and *Col10a1* mRNA expression [37].
rs2228545	2q33	203128957	*BMPR2* (bone morphogenetic protein receptor, type II)	One BMP receptor subunit. (See below)
rs27911	5p15	14760378	*ANKH (*ANKH inorganic pyrophosphate transport regulator)	Exports inorganic pyrophosphate [38]. Loss-of-function mutation [39] and deficiency [40] leads to joint ankylosis in mice.

SNP	Chromosome	Position	Gene	Function
rs928501	6q23	132317130	*CTGF* (connective tissue growth factor. Also known as CCN2)	A matricellular protein that is required for forming endochondral ossification [41]. It also enhances M-CSF/RANKL-mediated osteoclastogenesis [42]
rs1236913	9q32	124173300	*PTGS1* (prostaglandin-endoperoxide synthase 1. Also known as prostaglandin G/H synthase and cyclooxygenase or COX-1)	Converts arachidonic acid to prostaglandin.
rs7909264	10q23	88679764	*BMPR1A* (bone morphogenetic protein receptor, type 1A)	One BMP receptor subunit. (See below)
rs470504 rs470558	11q22	102163899	*MMP1* (matrix metallopeptidase 1. Also known as collagenase 1)	A collagenase. The expression level is increased in RA synovial fluid [43]. Overexpressing *Mmp1* reduces osteoblast markers in human periodontal ligament cells [44]
rs833843	12q13	47650658	*WNT10B* (wingless-type MMTV integration site family, member 10B)	Induces osteoblastogenesis and increases bone mass [45].
rs851056	17q11	39192708	*SOST* (sclerostin)	Antagonizes Wnt signalling by

SNP	Chromosome	Position	Gene	Function
				binding to Wnt receptor LRP5/6 [46].
rs8092336	18	58187063	*RANK* (tumour necrosis factor receptor superfamily, member 11a. Also known as TNFRSF11A)	Receptor for RANKL on myeloid-derived dendritic cells and activated T cells. Important in osteoclast differentiation and lymph node development [47].
rs30187 rs27044	5q15	96150086	*ERAP1* (Endoplasmic reticulum aminopeptidase 1)	Peptide trimming and MHCI complex assembling (see below).
rs8176785	11p15	20761862	*NELL1* (NEL-like 1. Also known as)	Induces osteoblast differentiation and controls normal synostoses [48]
rs1801253	10q25	115795046	*ADRB1*(adrenoceptor beta 1)	Adrb1$^{-/-}$ mice had decreased femur bone mineral density (BMD), cancellous bone volume/total volume (BV/TV), cortical size, and cortical thickness [49].
rs241453	6p21	32904204	*TAP2* (transporter associated with antigen processing 2)	Transports cytosolic peptides into the endoplasmic reticulum, to facilitate MHCI peptide complex formation.

1-2.2 Arthritogenic peptide hypothesis

The HLA-B27 molecule is one of the type I major histocompatibility complex (MHCI), which presents endogenous peptides to CD8 T cells. MHCI peptide complex formation occurs in the endoplasmic reticulum (ER), in which peptides are trimmed by endoplasmic reticulum aminopeptidases 1 and 2 (ERAP1 and 2) and loaded into the peptide pocket of MHCI. Association between ERAP1 and AS has been reported in AS patients [50] and restricted to HLA-B27 positive cases [51]. The protective ERAP1 SNP, rs30187 (p.Lys528Arg) and rs17482078 (p.Arg725Gln) decreased peptide trimming activity [51]. Therefore, aberrant peptide trimming and presentation might participate in the development of AS.

The arthritogenic peptide hypothesis suggests that HLA-B27 is particularly predisposed to present peptides likely derived from environmental pathogens that induce immune responses that cross-react with self-antigens. A number of autoantibodies have been found to react with proteins involved in connective tissue matrix assembling, ossification and bone remodelling, including glypican 3 and 4, chondromodulin 1, osteoglycin and osteonectin [52]. Proteoglycan (PG)-specific T cells have been reported in AS patients [53] and the cytotoxic T cell responses against chondrocytes could be enhanced by an underlying pro-inflammatory environment, such as elevated interferon (IFN)-γ [54]. Histological examination of the femoral head taken from AS patients showed that the accumulation of T cells in the bone marrow was significantly higher in the presence of remnant articular cartilage compared to the areas where articular cartilage had been completely resorbed. This suggests that T cells might react with proteins in the cartilage matrix [55].

Many studies have been undertaken to understand the origin of arthritogenic peptides with no consensus emerging. Unanswered questions include how these peptides are processed and loaded into HLA-B27, which immune cells are the major pathological inflammatory cells and which self-antigens are required to substantiate this hypothesis.

1-2.3 Misfolding of HLA-B27 induces ER stress

Induction of ER stress by misfolded HLA-B27 is another hypothesis of the pathogenesis of AS [56]. The protein folding process of HLA-B27 molecules is slower and with higher mis-

folding frequency compared to other MHCI subtypes [57]. Altered ERAP1 activity might affect the assembling of HLA-B27 and peptides [51]. The misfolded HLA-B27 molecules induce ER stress that up-regulates inflammatory responses, such as IL-23/IL-17 [57, 58]. However, Kenna *et al.,* demonstrated that expression of ER stress markers in peripheral blood mononuclear cell and ileal biopsies were not different between AS patients and healthy control [59]. Neither the presence of HLA-B27, ERAP1 genotypes nor the disease activity were correlated with ER stress level [59]. These results suggest HLA-B27 and ERAP1 may regulate disease through an ER stress-independent pathway.

The trigger of AS remains unclear; however, all genetic factors, pathogens and above hypotheses suggest that dysregulated inflammatory responses are related to disease development and progression.

1-2.4 Interaction between host immune system and microbiome

The frequent coexistence of gastrointestinal inflammation with AS suggests a role for the gut microbiome [60]. Costello *et al.,* examined the microbial profile in terminal ileal biopsies using 16S rRNA gene sequencing and demonstrated significantly different microbiome communities in AS and healthy control. [61]. HLA-B27/hβ2m transgenic rats [62] and SKG mice [63], two SpA animal models, have reduced intestinal inflammation as well as arthritis when raised in a germ-free environment suggesting the gut microbiome play important roles in disease development. Moreover, the very distinct gut microbiome populations in both models prior to disease onset support that microbial signature was altered by genetic background [63, 64]. These results suggest that the interaction between genetic factors, intestinal bacteria and host immune system are critical in initiating and developing AS.

1-3 Disease features of AS

1-3.1 Inflammation

Increased erythrocyte sedimentation rate (ESR), C-reactive protein (CRP), IL-6, IL-12, transforming growth factor beta-β (TGF-β), IL-17A, and IL-23 levels in AS patients compared to control suggests an elevated systemic inflammatory status [65, 66]. Although there are no specific inflammatory markers in AS, associated polymorphisms of IL-23 receptor suggest that IL-23, and/or its downstream cytokines, might facilitate pro-

inflammatory pathways in AS. The increased portion of IL-23 receptor expressing cells in AS peripheral blood mononuclear cells, as well as the increased IL-23 receptor expression level on individual T cells suggests that more effector cells can respond to IL-23 in AS [67]. The findings that IL-17+CD4+T cells [68] or IL-17+$\gamma\delta$ T cells [67] are increased in AS patients further support the hypothesis that IL-23 signalling is more active in AS patients. The most direct evidence supporting the pathological role of IL-23 was demonstrated by Sherlock *et al.*, whose group showed that overexpressing IL-23 alone can induce enthesitis and osteoproliferation [69]. Therefore, inhibitors targeting the IL-23/IL-17 pathway have been developed and considered for AS.

Inflammation in the enthesis, also known as enthesitis, is a hallmark feature of SpA and AS. Low back pain and reduced spinal mobility are the results of local inflammation of the spine and SI joints. The axial skeleton contains numerous ligaments, such as those attached to the IVD, anterior/posterior longitudinal ligaments, ligamenta flava, ischial tuberosity, iliac crest and interspinous/supraspinous ligaments [70]. Peripheral entheses are also commonly affected in SpA, including the Achilles tendon, fascia plantaris and epicondylus humeri lateralis [71].

In addition to enthesitis, bone marrow oedema and synovitis are also inflammatory features of AS seen on magnetic resonance imaging (MRI) short τ inversion recovery sequence [72]. The concept of the “enthesis organ” suggests that enthesis is not only the interface between bone and ligament, but also the neighbouring tissues, such as periosteal fibrocartilage, bursa, fat, synovium and subchondral bone marrow [70]. Studies have shown that enthesitis, synovitis and subchondral bone marrow oedema are coincident in affected joints [73]. The high stress concentration in entheses increases the possibility of microdamage, which might result in a stimulus for immune cells from the synovium and bone marrow to interact directly with collagens and PG, the potential auto-antigens highly present in the cartilage and enthesis [74, 75]. In comparison with mechanical-induced enthesitis, bone marrow oedemas, which implies inflammation, is more severe in HLA-B27 positive patients suggesting the presence of HLA-B27 exacerbates the inflammation induced by the initial mechanical stress [76].

1-3.2 Bone formation

The most distinctive radiographic feature of spinal disease in AS is syndesmophyte formation at the vertebral corners as a result of excessive tissue formation [77]. Normal bone development processes and signalling pathways, such as intramembranous, endochondral and chondroidal ossification, are involved in the pathological bone formation in AS but are switched on temporally and/or anatomically inappropriately [73, 78, 79].

In normal bone development, intramembranous ossification is the process in which mesenchymal cells differentiate directly into osteoblasts after condensation [80]. Intramembranous bone formation is the main mechanism of flat bone formation. Endochondral ossification accounts for the majority of bone formation in the body[81]. During endochondral ossification, mesenchymal cells differentiate into chondrocytes, which then produce cartilage matrices, such as type II collagen and aggrecan. Chondrocytes eventually undergo hypertrophy and express type X collagen and metalloproteinase (MMP)-13. Chondrocyte hypertrophy is accompanied by vascular invasion that allows the formation of marrow and brings in osteoprogenitors, which differentiate into osteoblasts and deposit bone matrix on the remnant cartilage scaffold [81].

An alternative bone formation process involving cartilage formation is chondroidal ossification, in which cartilage directly transforms into bone (Figure 1.1) [78]. An *in vitro* study showed chondrocytes within cartilage explants could express osteogenic markers after culture, such as type I collagen, alkaline phosphatase, osteopontin, suggesting transformation of chondrocyte to an osteogenic cell phenotype [82]. Consequently these transformed chondrocytes produced osteoid in the lacunae resulting in transitions from cartilage to bone. Recently, Yang *et al.,* used cell lineage tracing to demonstrate that type X collagen expressing cells can give rise to osteoblasts and osteocytes *in vivo,* further supporting plasticity between these cell types [83].

Examination of 26 entheses, the common sites of excessive bone formation during either ageing or SpA, taken from cadavers demonstrated that spur development involves intramembranous, endochondral and chondroidal ossification [78]. However, the unclear

cartilage-bone boundary, the rarity of hypertrophic chondrocytes and vascular invasion suggested chondroidal ossification dominated during spur formation (Figure 1.1) if a cartilage template was involved [78].

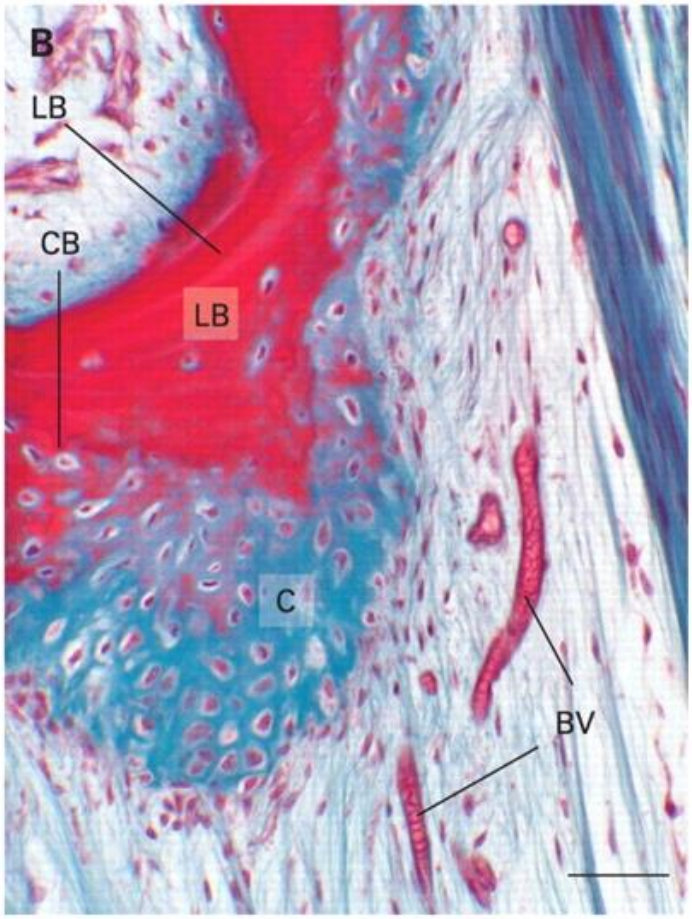

Figure 1.1: An example of chondroidal ossification [78].

Benjamin *et al.*, used Masson trichrome stain to demonstrate the chondroid bone (CB) in a spur at the tibial attachment of the anterior cruciate ligament. C, cartilage; CB; chondroid bone; BV, blood vessel; LB, lamellar bone. Scale bar: 50 mm.

1-3.3 Bone formation signalling

Dysregulated bone formation-related signalling pathways are involved in pathological bone formation, particularly the prostaglandin E2 (PGE2), canonical wingless (Wnt) and bone morphogenetic protein (BMP) signalling pathways.

1-3.3.1 PGE2 signalling

PGE2 is converted from arachidonic acid by constitutively active cyclooxygenase (COX)-1 and inducible COX-2 followed by PGE synthase. PGE2 exerts its effects through PGE2 receptor subtypes 1-4 (EP1-4, Figure 1.2) [84]. EP2 and EP4 are G stimulatory (Gs) protein-coupled receptors that activate cyclic adenosine monophosphate (cAMP)/protein kinase A (PKA) or phosphatidylinositol 3-kinases (PI3K)/ protein kinase B (PKB or Akt) pathways. EP3 activates G inhibitory (Gi) protein and decreases cAMP production. EP1 activates phospholipase C and regulates intracellular calcium concentration. Inhibition of COX decreases the production of different types of PGs, and Non-steroidal anti-inflammatory drugs (NSAIDs) are non-selective COX inhibitors.

PGE2 exerts anabolic roles in bone primarily through EP2 and EP4. EP2 and EP4 agonists have been shown to improve fracture healing [85-87] and osteoporosis in ovariectomised rats [88, 89]. EP3 mRNA expression was undetectable in either osteoblastic MC3T3-E1 cell line [90] or growth plate chondrocytes [91]. Unlike EP2 and EP4, EP1 deficiency has been shown to improve fracture healing by increasing osteoblastogenesis and remodelling [92]. PGE2 is an important regulator mediating anabolic responses upon sensing mechanical stress. PGE2 up-regulates gap junction protein connexin 43 expression on osteocytes through EP2 [93]. Connexin 43 facilitates PGE2 release [94] hence form a positive feedback loop with PGE2. PGE2 is upregulated in tendon after repetitive mechanical loading suggesting it is also involved in mechanoregulation in tendon [95].

In AS patients, NSAIDs have been shown to retard new syndesmophyte formation when given in high-dose or continuously [96, 97]. Furthermore, an SNP near *PTGER4,* which encodes PGE2 receptor subtype 4 (EP4), has been reported to be associated with AS suggesting that PGE2/EP4 signalling might be involved in the disease. Therefore,

inhibiting EP4 might be a therapeutic target for suppressing both inflammatory symptoms and osteoproliferation.

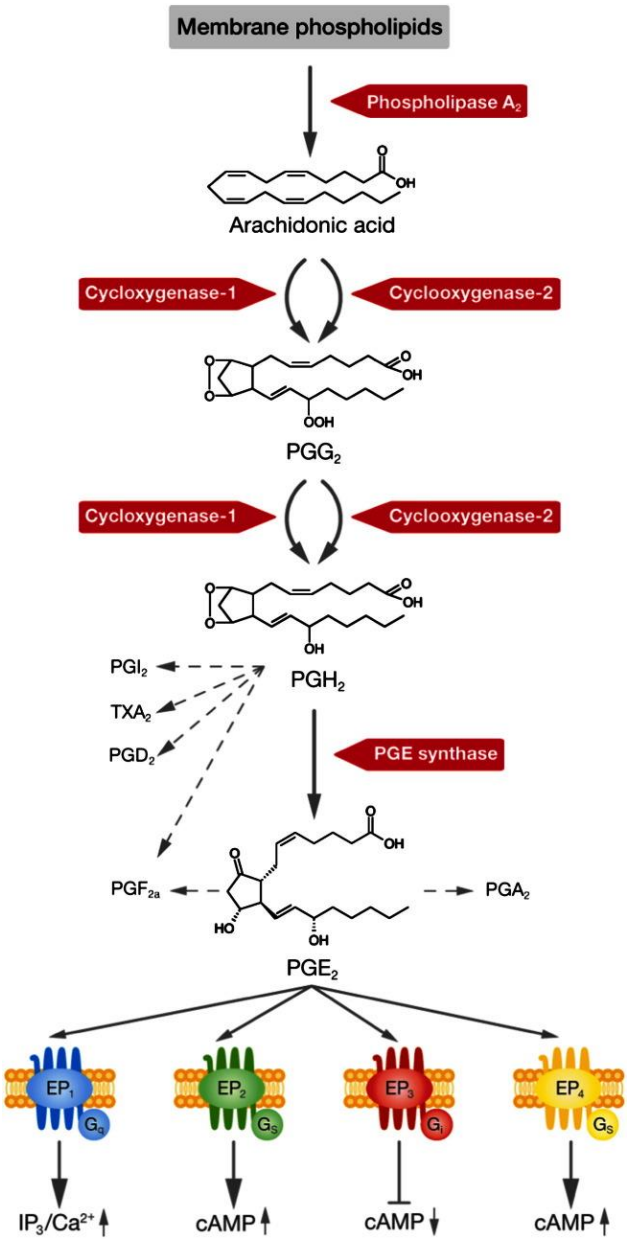

Figure 1.2: PGE2 synthesis and PGE2 receptors EP1-4. [84]

PG, prostaglandin; TXA2, thromboxane A2; IP3, inositol trisphosphate; cAMP, cyclic adenosine monophosphate; Gs, G stimulatory; Gi, G inhibitory

1-3.3.2 Wnt signalling

The canonical Wnt signalling pathway regulates bone development (Figure 1.3) [98]. Wnt ligands that activate the canonical Wnt/β-catenin signalling pathway include Wnt1, 3a, 7b and 10. These ligands bind to the frizzled receptors and low-density lipoprotein receptor 5/6 (LRP5/6). In the absence of Wnt ligands, β-catenin is phosphorylated by glycogen synthase kinase 3 (GSK-3β) and degraded by the ubiquitin/proteasome-dependent pathway. Ligand binding inhibits GSK-3β hence hypophosphorylated β-catenin remains stable and translocates to the nucleus and interacts with T cell factor/lymphoid enhancer binding factor (TCF/LEF). Wnt signalling is regulated by several endogenous antagonists, such as sclerostin and dickkopf-1 (DKK-1). Sclerostin defects are associated with high bone mass diseases, sclerosteosis and Van Buchem disease [99]. DKK-1 expression is inversely correlated with bone mineral density [100].

Increased serum Wnt-3 levels [101] and decreased serum sclerostin and DKK-1 levels [102, 103], as well as the number of sclerostin-positive osteocytes in zygapophysial joints of AS patients [104], suggests the activation of Wnt signalling in AS patients. Decreased DKK-1 and sclerostin expression is associated with the excessive tissue formation in the PG-induced spondylitis (PGISp) mouse model [105]. Moreover, anti-DKK-1 not only rescues TNF-mediated bone destruction, but also induces osteophyte formation in human TNF transgenic (hTNFtg) mice [102]. These support that up-regulated Wnt signalling pathway might be involved in excessive bone formation.

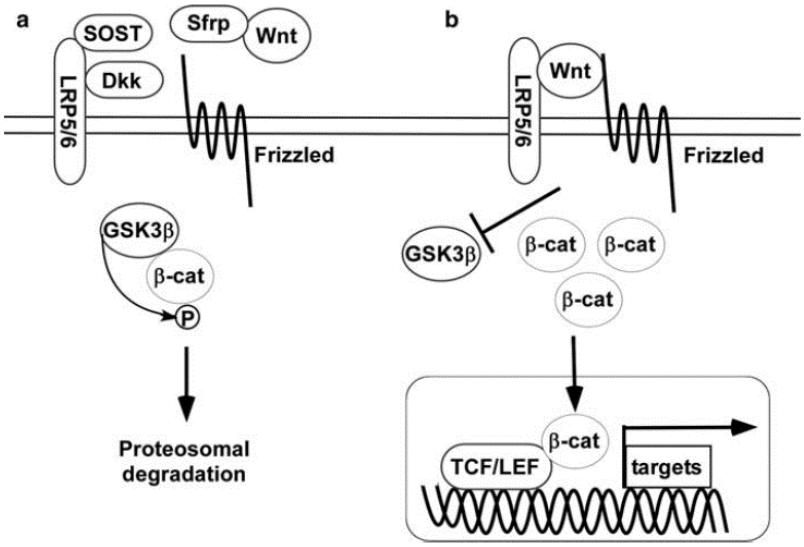

Figure 1.3: Canonical Wnt signalling pathway [98].

LRP, low-density lipoprotein receptor-related protein; SOST, sclerostin; DKK, dickkopf; Sfrp, secreted frizzled-related proteins; β-cat, β-catenin; GSK3β, glycogen synthase kinase-3 β; TCF/LEF, T cell factor/lymphoid enhancer binding factor.

1-3.3.3 BMP signalling

BMP belongs to TGF-β superfamily that comprises approximately 30 members [106]. BMP ligand binding triggers dimerization of type I and II BMP receptors and activates the kinase that phosphorylates Smad 1, 5 and 8. Phosphorylated Smad 1, 5 and 8 then translocate to the nucleus with Smad 4 to activate gene transcription (Figure 1.4). Noggin, an endogenous BMP inhibitor, binds to BMPs and blocks the downstream signalling pathway [107]. BMP 2, 4 and 7 are differentially expressed during various stages of endochondral ossification and play important roles from mesenchymal condensation to bone development [108]. Conditional deletion of *BMP2* and *BMP4* controlled by *Prx1* limb enhancer, which is expressed in limb bud mesenchyme, leads to severe limb developmental defects [109]. Misexpressing noggin in embryonic limb inhibits mesenchymal condensation and chondrocyte differentiation suggesting BMP signalling is required for chondrogenesis [110].

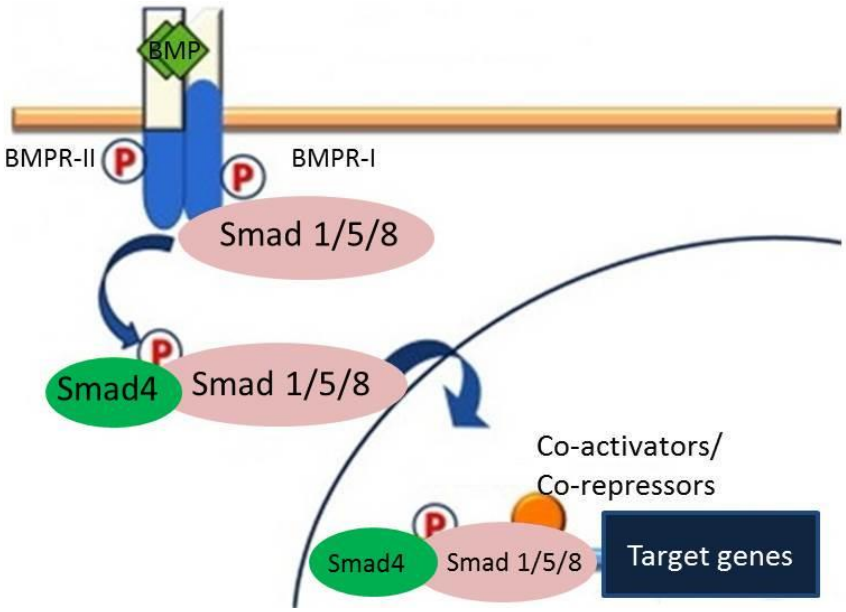

Figure 1.4: BMP-Smad signalling [107]

Aberrant BMP signalling is associated with skeletal disease. Fibrodysplasia ossificans progressiva is a rare autosomal dominant disorder featured by congenital malformation of the great toe and heterotopic bone formation in muscle and connective tissues after birth. Higher expression of BMP-4 [111] and mutation in ACVR1, a BMP type I receptor are the underlying pathogenic mechanisms of fibrodysplasia ossificans progressiva [112].

Evidences of BMP activation have been found in AS patients and animal models. Increased serum BMP-2, 4 and 7 concentrations have been reported in AS patients with more radiographic progression compared to those without spinal fusion [103, 113]. Activation of the BMP-Smad pathway also contributes to chondroproliferation and ankylosis in HLA-B27/hβ2m transgenic rats [114]. Blocking BMP signalling by overexpressing noggin reduced clinical scores and ankylosis in DBA mice, a spontaneous SpA animal model [108], suggesting BMP signalling might play important roles in joint ankylosis.

These studies suggest that PGE2/EP4, Wnt and BMP, are associated with pathological bone formation. However, when, how and where these signalling pathways are activated/dysregulated in AS is still poorly understood.

1-4 Current therapy

Current AS therapies primarily aim to relieve inflammatory symptoms. The first-line treatment includes NSAIDs and physiotherapy to reduce inflammation, pain and improve spinal mobility [115]. High-dose and continuous use of NSAID has been shown to retard new syndesmophyte formation compared to low-dose and on-demand treatment [96, 97]. However, some patients do not tolerate long-term use of NSAIDs due to adverse gastrointestinal, renal and cardiovascular side effects [116].

TNF blockade is an alternative option. Five TNF blockers, Simponi (golimumab), Remicade (infliximab), Humira (adalimumab), Cimzia (certolizumab) and Enbrel (etanercept), have been shown to improve AS functional indices and decreased inflammatory lesions on MRI imaging [117-123]. When comparing different studies, a higher percentage of patients with shorter mean disease duration had 20% and 40% improvement from baseline using the Assessment of SpondyloArthritis international Society (ASAS) ASAS20 and ASAS40 criteria respectively and ASAS partial remission (Table 1-2). However, despite the rapid inflammation remission, TNF blockers only partially retard but do not prevent radiographic progression [124-127].

Table 1-3: Effects of disease duration on treatment outcome

Treatments	**Mean disease duration**	**Study duration**	**Effects on Inflammation**	**Ref**
Infliximab 5 mg/kg	17.2 months	16 weeks	ASAS40: 61.1% ASAS partial remission: 55.6%	[119]
Infliximab 5 mg/kg+ naproxen 1000 mg daily	1.76 years	28 weeks	ASAS20: 81%	[128]

Treatments	Mean disease duration	Study duration	Effects on Inflammation	Ref
			ASAS40:75.2% ASAS partial remission: 61.9%	
Infliximab 5 mg/kg	7.7 years	24 weeks	ASAS20: 61.2% ASAS40: 47% ASAS partial remission: 22.4%	[118]
Infliximab 5 mg/kg	16.4±8.3 years	12 weeks	ASAS20: ~70% ASAS partial remission:~22%	[129]
Etanercept 25mg twice/ week or Etanercept 50 mg/week	2.4 years (Non-radiographic axial SpA)	12-24 weeks	12 weeks: ASAS20: 52.4% ASAS40: 33.3 % 24 weeks: ASAS20: 71.2% ASAS40: 51.9 %	[130]
Etanercept 25mg twice/week	2.6 years	48 weeks	ASAS20: 85% ASAS40: 70%	[122]
Etanercept 25 mg twice/week	10.7 years	12-96 weeks	12 weeks: ASAS20: 64% ASAS40: 45%	[131, 132]

Treatments	Mean disease duration	Study duration	Effects on Inflammation	Ref
			24 weeks: ASAS20: 63% ASAS40:45% 48 weeks: ASAS20: 74% ASAS40: 61% 96 weeks: ASAS20: 74% ASAS40: 62%	

Other biological therapies, previously tested in other inflammatory diseases, have also been investigated for efficacy in AS; however; most do not show therapeutic effects. For example, anakinra, an IL-1 receptor antagonist [133]; rituximab, a B-cell depleting agent [134]; and tocilizumab, a monoclonal antibody targeting IL-6 receptor [135] only moderately improve inflammatory symptoms and functional indices. The ongoing unmet medical needs for an effective, if not curative treatment for AS, motivate ongoing investigation of different therapeutic regimens. GWAS findings as discussed in Table 1-1 implicated several potential therapeutic targets, such as the IL-23/Th17 pathway. Ustekinumab neutralizes IL-12p40, a subunit of both IL-12 and IL-23, improved AS functional index and MRI scores [136]. Secukinumab, an anti-IL-17 monoclonal antibody, significantly reduced inflammatory symptoms in a small group of AS patients [137]. These promising results provide support for targeting other GWAS identified AS candidate genes,

such as *ERAP1* and *PTGER4,* rather than adapting therapies used for other inflammatory therapies.

1-5 Animal models of AS

The difficulty of obtaining bone biopsies has limited the understanding of AS disease progression. Animal models provide a complementary method to study AS. An ideal animal model should mimic the symptoms of enthesitis, spondylitis and ankylosis. Additional extra-articular symptoms, such as IBD, uveitis and psoriasis are preferred as well. Several animal models have been used for understanding the association between inflammation and osteoproliferation and for testing therapeutic approaches. The benefits and drawbacks of each animal model are discussed below.

1-5.1 HLA-B27/hβ2m transgenic rat

Based on the strong association between HLA-B27 and AS, several lines of HLA-B27 transgenic rat models have been developed in Lewis or Fisher rats by introducing human HLA-B*2705 heavy chain and the invariant chain β2-microglobulin (hβ2m), which stabilizes the confirmation of MHC [138]. The initial symptom is gastrointestinal inflammation followed by other inflammatory features present in SpA, such as peripheral arthritis, spondylitis, enthesitis and psoriasis [138]. In addition to inflammation, chondrocyte proliferation and syndesmophyte formation, were observed in the peripheral joints and spine [139]. The copy number of HLA-B27 and hβ2m molecules has a threshold effect on the susceptibility to spontaneous arthritis/spondylitis. Two rat lines that are homozygous for transgene loci that bear fewer than 7 copies of both HLA-B27 and hβ2m remained healthy [140]. Hemizygous expression of at least 55 copies of HLA-B27 molecule with 66 copies of hβ2m [140] or 20 copies of HLA-B27 molecule with 35 copies of hβ2m [141] are required for the development of arthritis/ spondylitis. Gastrointestinal inflammation is absent in the latter rat line suggesting gut disease and arthritis can be independent [141]. However, HLA-B27/hβ2m transgenic rats remain healthy in a germ-free environment indicating that gut flora is important in priming immune responses and required for disease initiation [62].

The disease observed in the HLA-B27/hβ2m transgenic rats is immune system-dependent and transferable by bone marrow, splenocytes and lymphoid cells [142, 143]. Although HLA-B27 belongs to MHCI and presumably presents antigens to CD8 T cells, depletion of CD8αβ T cells did not ameliorate the symptoms [144, 145]. On the contrary, CD4 T cells could transfer the disease more efficiently than CD8 T cells [142].

Consistent with human AS pathology, the IL-23/Th17 response is also activated in arthritic joints [146] and inflamed gut tissues [147] of the HLA-B27/hβ2m transgenic rat model. The IL-23/Th17 pathway can be induced by a response triggered by misfolded HLA-B27 [147, 148]. Alternatively or simultaneously, aberrant dendritic cell function might also be involved in enhancing IL-23/Th17 in the HLA-B27/hβ2m transgenic rats [149].

Histological evidence showed that peripheral and axial entheses were affected in the HLA-B27/hβ2m transgenic rats [138]. Severe inflammation, bone erosion and chondroproliferation were observed simultaneously at affected sites [139]. The chondrocyte proliferation and hypertrophy have been suggested to be the result of activation of the BMP/Smad pathway [114]. Anti-TNF treatment started prior to disease onset fully prevented the disease. Interestingly, delayed treatment decreased arthritis and gut inflammation but failed to inhibit the activation of BMP/Smad pathway [114, 150]. This result supports that early treatment is required for preventing both inflammation and syndesmophyte formation.

Overall the HLA-B27/hβ2m transgenic rat is an important animal model of SpA, particularly with respect to disease mechanisms related to HLA-B27 molecule and their interaction with environmental factors. However, the transgene copy number-dependent outcomes suggest that the model may be biased as a consequence of supra-pathophysiologic representation of this disease pathway. Therefore, the disease progression in rats might be different from patients, in whom the interactions between multiple factors might be required to overcome other disease induction and severity thresholds.

1-5.2 DBA1 Mice

Grouping adult male DBA/1 mice from different litters results in spontaneous arthritis particularly in the hind limbs, which is characterised by swelling and erythema in the interphalangeal and metatarsophalangeal joints and also enthesitis in the ankle joints [151]. Arthritis is accompanied with typical psoriasis symptoms, including dactylitis, nail deformity and dermatitis [152]. Proliferation of fibroblasts and chondrocytes leads to ankylosis of the ankle in this model [153].

The proliferation of synovial tissues and infiltration of mononuclear and polymorphonuclear leukocytes near entheses were present in the arthritic joints [152]. Arthritis and dermatitis depend on IFN-γ and IL-17 [154, 155]. However, T cells are less important in the disease progression of DBA/1 mice, because neither deficiency of α/β nor γ/δ T cells altered disease progression [153]. The presence of neutrophils and expression of chemokine (C-X-C motif) (CXCL) 1 and 2 and their corresponding receptors suggests the innate immune responses might play a role in DBA/1 mice [152, 156]. Neither etanercept, a TNF blocker, [157] nor dexamethasone [156] showed remarkable effects on clinical symptoms.

This model has been used to study enthesopathy. Phosphorylation of Smads, indicating BMP activation, has been shown in fibroblasts as well as proliferating and hypertrophic chondrocytes within developing osteophytes [108]. Inhibition of BMP/Smad signalling pathway by overexpressing the endogenous BMP antagonist, noggin, demonstrated a decrease in both clinical scores and ankylosis in this model [108]. However, the absence of axial pathology suggests that the DBA/1 mouse model is a better model of SpA, that has higher predominance of peripheral disease, rather than AS in which axial disease is a defining feature.

1-5.3 SKG mouse model

The SKG mouse model carries a point mutation in the SH2 domain of Zeta-chain-associated protein kinase 70 (ZAP-70) (ZAP-70^{W163C}) [158]. ZAP-70 is a tyrosine kinase downstream of T cell receptor (TCR) signalling that regulates both positive and negative selection during T cell development [159]. Sakaguchi *et al.,* demonstrated that this mutation altered the threshold of thymic selection thus it increased the pool of self-reactive

T cells, which led to spontaneous polyarthritis and bone destruction mimicking RA [158]. Ruutu et al., demonstrated that systemic delivery of curdlan induces not only RA-like arthritis, but also features resembling SpA, such as enthesitis, spondylitis, sacroiliitis, Crohn's like ileitis, dactylitis, unilateral uveitis, psoriasis-like skin disease and osteophyte formation [160].

In a specific pathogen-free (SPF) environment, SKG mice remain arthritis-free, unless treated with fungal cell wall components, such as zymosan or β-glucans (curdlan) [161]. Germ-free environment has been shown to prevent ileitis and significantly reduce the severity of curdlan-induced spondylitis and arthritis [63]. Increase in highly self-reactive CD4+ T cells induced by the ZAP-70 mutation alone is not sufficient for full disease development and incidence in this model as neutrophils, macrophages, IL-1, IL-6, IL-17 and TNF-α are all also involved [162, 163]. Anti-mouse IL-23 antibody and IL-17 deficiency both prevent the development of peripheral arthritis, spondylitis and ileitis [160]. Interestingly, IL-22, another cytokine down-stream of IL-23 signalling, mediates enthesitis but protects the intestine from inflammation [164].

Overall, the enthesitis, gastrointestinal disease, spondylitis, uveitis and dermal inflammation support the SKG mouse as a good model for SpA rather than specifically AS. This model does add further support to the hypothesis that IL-23 signalling pathway is involved in the development of SpA disease.

1-5.4 TNF overexpressing mouse

Deletion of the AU-rich elements (ARE) in the 3'-untranslated region (3'UTR) of *Tnf* (TNFΔARE) leads to increased TNF accumulation [165]. The resulting phenotype includes polyarthritis, bilateral sacroiliitis, mild to moderate spondylitis and Crohn's-like IBD by the age of 4 weeks [165-167]. The human TNF transgenic mouse model (hTNFtg) has similar peripheral and axial arthritis but does not present with the Crohn 's like IBD [98].

Over-activation of TNF signalling in mesenchymal cells alone induces gastrointestinal symptoms and arthritis [168]. Different forms of TNF receptor (TNFR) play different roles in SpA. TNFRI is related to both gut disease and arthritis; however, deletion of TNFRII ameliorated gut disease but exacerbated the joint inflammation in the TNFΔARE mouse

model [165]. Interestingly, T cells only contribute to the development of IBD, but not arthritis in these mice [165]. This may provide some explanation for variance in the responsiveness of these disease features to different interventions.

Robust induction of osteophyte formation and SI joint fusion in the hTNFtg mice requires the additional hit of blocking DKK-1 activity [102, 166]. This suggests that the combination of unrestrained TNF and Wnt signalling can lead to overt excessive bone formation. However, it is noteworthy that overexpression of TNF induces a severe erosive phenotype with relatively mild osteoproliferation [102, 166, 169], suggesting that osteoproliferation is not a direct predominant sequela of TNF-driven inflammation. This may explain why monotherapy using anti-TNF drugs does not effectively prevent syndesmophyte formation.

Reducing mechanical stress ameliorated enthesitis and osteophyte formation in TNFΔARE mice [169]. Since enthesitis occurs more frequently in weight-bearing joints of AS patients, it is possible that entheseal mechanical stress-induced micro-damages and subsequent repair-associated inflammation may be a trigger of disease or at least osteoproliferation in AS.

Although TNF overexpression models demonstrate the interaction between TNF and Wnt signalling, the severe erosion and lack of consistency in spontaneous osteoproliferation indicate that it has limitation as a model of AS.

1-5.5 IL-23, IL-17 or IL-22 overexpression

A direct association between IL-23 and SpA has been demonstrated using the IL-23 overexpression mouse model [69, 170]. Increasing systemic IL-23 levels using minicircle DNA dose-dependently induced enthesitis in peripheral joints, IVD and SI joints. Mice also develop psoriasis and aortic root inflammation, but not gastrointestinal symptoms. Increased bone remodelling, severe bone erosion and chondro/osteoproliferation leading to osteophyte formation are evident in this model.

IL-17 and IL-22 are both downstream cytokines of IL-23; however, IL-17 overexpression does not lead to arthritis. On the other hand, IL-22 overexpression not only induced spondylitis but also up-regulated bone formation-related gene expression, but induction of

osteoproliferation was not confirmed [69]. These models provide strong evidence for a role of IL-23, likely via IL-22 induction, in peripheral arthritis, spondylitis, sacroiliitis and psoriasis. The symptoms of this model resemble SpA, rather than AS specifically. Additionally, the model is likely biased due to dependence on supra-physiologic expression of a single pro-inflammatory cytokine pathway. However, it does provide further weight to the argument that the IL-23 cytokine pathway may represent a dominant inflammatory process in SpA/AS and is consequently an attractive therapeutic target

1-5.6 Proteoglycan (PG)-induced arthritis (PGIA)/spondylitis (PGISp) mouse model and other PG-relevant autoimmune arthritic model

Aggrecan, the major type of proteoglycan in articular cartilage, has been suggested to contain autoantigens in RA and AS [53]. Aggrecan is composed of a central core protein (globular domains, G1, G2 and G3, and an interglobular domain) attached by hundreds of glycosaminoglycan side chains (chondroitin sulfate or keratan sulfate) [171]. Several animal models have shown that proteoglycan extracted from human cartilage or G1 domain-specific autoimmune responses lead to peripheral and axial arthritis in the arthritis-susceptible BALB/c mice [172-177], and full disease development requires multiple epitopes on G1 [171]. Since these mouse models develop similar symptoms, these models will be discussed together in below section. The generic term “PG” will be used when referring this mouse model as aggrecan is the major type of proteoglycans in cartilage. Moreover, study had shown that deglycosylated crude cartilage extracts including all types of proteoglycans and highly-purified aggrecan were both used in studies and induce disease to similar extent.

Multiple injections of PG were required to induced peripheral arthritis and spondylitis in the PGISp mouse model [174]. Glant *et al.,* showed the spondylitis followed peripheral arthritis and consequently progressed to ankylosis due to extensive cartilage formation bridging the adjacent vertebral bodies [176]. However, this study predominantly focused on the development of peripheral arthritis, therefore detailed analysis of disease development within spine has not been undertaken.

Some PG-related models also displayed extra-articular symptoms common in SpA. For example, uveitis has been reported in mice overexpressing PG-specific TCR after PG immunization [178], and mild intestinal inflammation has been found in recombinant human G1 domain (rhG1)-treated mice (Dr Tibor Glant, personal communication, 2013).

T lymphocytes have been shown to play important roles in PG-induced arthritis. Transferring splenocytes from arthritic mice to Severe combined immunodeficiency SCID mice replicates the arthritic symptoms of donor mice, while T cell depletion abolishes the effects [179]. Reconstitution of G1 domain-specific TCR expressing T cells in SCID mice can restore the susceptibility to arthritis [175, 177]. These studies further support the requirement of PG-specific T cells for disease development. Among all the T cell populations, Th1 has been reported to dominate in PG and rhG1-induced inflammatory responses delivered via intraperitoneal injection; while Th17 is the predominant cell population mediating the inflammatory responses when mice are immunized through subcutaneous injection of PG/rhG1 [180-182]. The Th2 cytokine, IL-4, and regulatory T cells are protective in PGISp mice supporting that PG-induced autoimmune arthritis is a Th1/Th17-skewed disease [183-185].

The genetic factors, excluding MHC-related genes, controlling axial disease were studied by crossing arthritis-susceptible BALB/c with MHC-matched arthritis-resistant DBA/2 mice [186]. Although spondylitis correlated with onset and severity of peripheral arthritis in BALB/c mice, axial disease became independent of peripheral arthritis after the F2 generation. Linkage analysis showed that two spondylitis-related gene loci, *pgis1* and *pgis2*, are linked to the axial disease in F2 mice [187]. Interestingly, combination of DBA/2-derived *pgis1* and BALB/C-derived *pgis2* result in the highest disease susceptibility. The loci include many genes related to immune responses, such as the IL-1 family gene cluster that had been reported in AS [187].

Haynes *et al.,* demonstrated that expression of the Wnt signalling inhibitors, sclerostin and DKK-1, were significantly decreased in PGISp mice, suggesting that activation of Wnt signalling may be the causative mechanism of excessive cartilaginous tissue formation in the spine [105]. Therefore, down-regulation of Wnt signalling pathway inhibitors may lead to the activation of Wnt signalling and excessive tissue formation.

Although severe IVD destruction is not a common features of AS patients, the PGISp mouse model displays a similar disease progression to that of AS patients and has the advantage of being a more physiologic antigen-driven response; therefore, it is currently the ideal choice for studying inflammation-driven bone formation in the spine and pelvis.

Table 1-4: Summary of features of SpA/AS animal models

Animal model	Arthritis	Ankyloses	Pathogens	Gut disease	Uveitis	Psoriasis
HLA-B27/ hβ2m transgenic rats	Peripheral and axial	Peripheral and axial	Yes	Yes	No	Yes
DBA/1 mice	Peripheral	Peripheral.	Not reported	Not reported	Not reported	Yes
Curdlan-treated SKG mice	Peripheral and axial	Peripheral and axial	Yes	Yes	Yes	Yes
TNF-overexpressing mouse models (hTNFtg and TNFΔARE)	Peripheral and axial	Only reported in peripheral after anti-DKK-1 treatment	Not reported	Only in TNFΔARE mice	Not reported	Not reported

Animal model	Arthritis	Ankyloses	Pathogens	Gut disease	Uveitis	Psoriasis
IL-23 Overexpression	Peripheral and axial	Only reported in peripheral	Not reported	No	Not reported	Yes
PGISp and other PG relevant mouse models	Peripheral and axial	Peripheral and axial	Not reported	rhG1-treated mice	PG-TCR transgenic mice	Not reported

1-6 Inflammation and bone formation

1-6.1 Do syndesmophytes develop from inflammatory lesions?

How inflammation links to syndesmophyte formation remains an open question. If the inflammation is required for bone formation, syndesmophytes should develop from vertebral corners that were either previously or are currently affected by inflammation. Furthermore, anti-inflammatory therapies should prevent syndesmophyte formation.

The location of inflammation on MRI and syndesmophytes on X-ray provides clues about the temporal and spatial correlation of these disease features. The percentage of vertebral corners with active inflammation, resolved inflammation and without inflammation at baseline that developed new syndesmophyte in two years were 0%, 16-20% and 2-5% respectively [125, 188]. It appears that vertebral corners with resolved inflammation have higher incidence to develop syndesmophytes. However, more than 80% of vertebral corners with resolved inflammation did not progress to syndesmophytes in the study period suggesting that either these lesions might have a slow and/or variable radiographic progression rate or that regressed inflammation is not solely predictive of syndesmophyte formation. The sensitivity of radiography is limited and it is possible that early osteoproliferative events were not detected by this imaging modality. Therefore, while this study is suggestive, it is not conclusive regarding when, where and how syndesmophyte formation is initiated and progressed. The affected vertebrae only account for less than 20% of all vertebral corners scored, and the percentage varies depending on readers [125, 189]. More than 57% of new syndesmophytes developed at vertebral corners without MRI-determined prior inflammation [190, 191]. Therefore it is also possible that MRI imaging approach was not sensitive enough to detect mild inflammation, or the imaging time points failed to catch acute and transient inflammatory events [192].

Fatty lesions on MRI T1-weighted sequence that develop more frequently either in bone marrow or excavated bone after resolution of inflammation is another hallmark of axial SpA [193-197]. However, the inflammation-fatty metaplasia-syndesmophyte formation axis was not found in all cases [191]. A long-term longitudinal study from the early inflammatory phase through to ankylosis is required for understanding the association between inflammation, fat metaplasia and bone formation.

1-6.2 Can anti-inflammatory therapies inhibit syndesmophyte formation?

Direct regulation of bone formation signalling by inflammatory cytokines has been studied *in vitro*. TNF and TNF-related weak inducer of apoptosis (TWEAK) increased DKK-1 and sclerostin expression in synovial cells and osteoblast cell cultures [102, 198, 199]. *In vivo* studies showed anti-DKK-1 treatment resulted in osteophyte formation and SI joint fusion in hTNFtg mice [102, 166]. Anti-TNF treatment has been shown to decrease serum DKK-1 level in both RA and AS patients [102, 200]. The “TNF-brake hypothesis” suggests that increased TNF during the inflammatory phase upregulates the expression of Wnt inhibitor, DKK-1, which suppresses bone anabolic pathway in matured lesions [201]; consequently TNF blockade removes this inhibition and accelerates radiographic progression. This hypothesis suggests that anti-TNF therapy will lead to more syndesmophyte formation. While anti-TNF treatment has not provided further protection against syndesmophyte formation compared to NSAIDs and physiotherapy over a two to four-year period, it does not exacerbate this process [124, 125, 127, 202-204].

To date, most studies demonstrate a similar radiographic progression in anti-TNF and conventional treatments using the modified Stoke Ankylosing Spondylitis Spinal Score (mSASSS) score, a scoring system ranging 0-72 used to investigate structural change in the cervical and lumbar spine (Table 1-4). Only a few recent reports suggest that anti-TNF can retard the rate of radiographic progression (Table 1-5). The discrepancy in demonstrated effect on radiographic outcome might be due to variation in study duration and when treatment started. The effects of deceleration by anti-TNF might take more than four years to become evident [126, 205]; most of the earlier studies examining this treatment outcome were shorter than four years. Haroon *et al.,* demonstrated that initiating anti-TNF treatment within ten years of disease onset was more efficacious at retarding radiographic progression than patients in which treatment was delayed for more than ten years [206]. Furthermore, AS patients with delayed diagnosis of longer than 8 years showed less improvement in inflammation markers and higher radiographic progression rate compared to those with an early diagnosis, even though both groups had received treatment for a similar time span [207]. AS patients that had syndesmophytes at baseline had more severe radiographic progression than those without baseline syndesmophytes

regardless of the treatment [202, 203, 205, 206]. The benefits of early treatment with anti-TNF have been shown to prevent the activation of BMP/Smad signalling pathway in HLA-B27/hβ2m transgenic rats [114] suggesting that timing of anti-inflammatory intervention has impact on the treatment outcome.

Taken together, while inflammation may have a role in suppressing bone formation signalling and compromise bone repair; anti-TNF therapy does not accelerate syndesmophyte formation. On the contrary, early intervention prior to the initiation of osteoproliferation might be most beneficial for retarding/preventing radiographic progression.

Table 1-5: TNF blockers have no effects on syndesmophyte formation

Treatments	Disease duration	Study duration	Baseline mSASSS	Change of mean mSASSS score	Ref
Etanercept (25 mg) vs OASIS (TNF naive)	Etanercept: 10±8.5 years OASIS: 12±9.8 years	2 years	Etanercept:16±8.3 OASIS: 19±20.8	Etanercept: 0.91±2.45 OASIS: 0.95±3.18 (*p*=0.083)	[124]
Infliximab (5mg/kg) vs conventional treatment (GESPIC cohort)	Infliximab: 15.5(3-35) years GESPIC: 5.5(1-10) years	2 years	Infliximab: 12.1 GESPIC: 5.9	1. All patients (*p*=0.92): Infliximab:0.7±2.8 GESPIC: 0.4±2.7 2. Patients with baseline syndesmophyte (*p*=0.085): Infliximab: 0.5±3.5	[202]

Treatments	Disease duration	Study duration	Baseline mSASSS	Change of mean mSASSS score	Ref
				GESPIC: 2.2±4.8 3. Patients without base line syndesmophyte: no significant difference	
ASSERT (infliximab 5 mg/kg for 48 weeks or Placebo for 24 weeks →infliximab 5 mg/kg) vs OASIS	ASSERT: 10.2±8.7 years OASIS: 9.9±8.8 years	2 years	ASSERT: 17.7±17.9 OASIS:17.5 ±15.1	ASSERT: 1.0±3.2 OASIS: 0.9±2.6 (*p*=0.541)	[118, 127, 208]
Placebo for 24 weeks→ golimumab 50 mg	Golimumab 50 mg: 11.0 (6.0–18.0) years	4 years	golimumab 50 mg: 11.7±16.4 golimumab 100mg:	1. Compare treatment groups (*p*=0.16):	[203]

Treatments	Disease duration	Study duration	Baseline mSASSS	Change of mean mSASSS score	Ref
vs golimumab (50 mg and 100mg) With vs without baseline syndesmophyte	Golimumab 100mg: 9.5 (4.0–18.0) years Placebo: 16.0 (5.0–25.0) years		13.5±18.9 Placebo: 16.1±8.7	Golimumab 50 mg:1.3±4.1 Golimumab100mg: 1.0±5.6 Placebo: 2.1±5.2 2. Effects of baseline syndesmophyte (regardless of treatment) (p<0.0001): All patients with syndesmophyte: 2.8±5.9 All patients without baseline syndesmophyte: 0.2±1.2 3. Among patients with baseline: Syndesmophyte:	

Treatments	Disease duration	Study duration	Baseline mSASSS	Change of mean mSASSS score	Ref
				Golimumab 50 mg:2.1±5.0 Golimumab100mg: 2.9±6.5 Placebo: 3.6±6.2 4. Among patients without baseline syndesmophyte: Golimumab 50 mg:0.1±0.9 Golimumab100mg: 0.4±1.6 Placebo: -0.1±0.5	
Adalimumab 40 mg every other week vs OASIS	Adalimumab: 11.2±9.3 years OASIS: 11.3±8.7 years	2 years	Adalimumab: 19.8±19.3 OASIS: 15.8 ± 17.6	Adalimumab: 0.8±2.6 OASIS: 0.9±3.3 (*p*=0.771)	[204]

Treatments	Disease duration	Study duration	Baseline mSASSS	Change of mean mSASSS score	Ref
Anti-TNF (infliximab, etanercept, adalimumab) vs standard	Anti-TNF: 18.2±11.4 years Standard: 15 ±10 years	2 years	Anti-TNF: 14.5±16.1 Standard: 10±12.1	Anti-TNF: 1.4±1.9 Standard: 1.5±3.1	[125]

OASIS: Outcome Assessments in Ankylosing Spondylitis International Study

GESPIC: GErman SPondyloarthritis Inception Cohort

ASSERT: Ankylosing Spondylitis Study for the Evaluation of Recombinant Infliximab Therapy

Table 1-6: TNF blockers might retard syndesmophyte formation

Treatments	Mean disease duration	Study duration	Baseline mSASSS	Change of mean mSASSS score or number of syndesmophytes	Ref
Infliximab vs Herene histological cohort (TNF	Infliximab:	8 years	Infliximab: 13.2±17.6	mSASSS score in 8 years:	[126]

Treatments	Mean disease duration	Study duration	Baseline mSASSS	Change of mean mSASSS score or number of syndesmophytes	Ref
inhibitor naïve, but can take NSAID)	15.8±8.5 years Herene: 20.7±5.7 years		Herene:14.2±13.8	1. mSASSS score Infliximab: 20.2±21.4 Herene: 25.9±17.8 (*p*<0.001) 2. Mean number of syndesmophyte: Infliximab: 1.0±0.6 Herene: 2.7±0.8 (*p*=0.007)	
5 mg/kg infliximab vs OASIS cohort	Infliximab: 19.0±23.4 years	4 years	Infliximab: 11.6±15.3 OASIS: 12.7±17.4	Infliximab: 1.6±2.6 OASIS:4.4	[205]

Treatments	Mean disease duration	Study duration	Baseline mSASSS	Change of mean mSASSS score or number of syndesmophytes	Ref
	OASIS: 11.7±9.3 years				
TNF blockers)vs TNF blocker naive (NSAID users) Initiating TNF blocker treatment within or after 10 years	TNF blocker: 16.47±11.8 years Naïve: 16.38±14.4 years	>3.9 years	TNF blocker: 10.6±14.9 Naïve: 8.2±13.8	Patients delay >10 years had higher rate of mSASSS progression than <10 years (p=0.03)	[206]

1-7 Aim of this thesis

To date, the transition from inflammation to osteoproliferation is poorly understood, largely due to the limited availability of bone biopsies. What triggers osteoproliferation, the signalling mediators involved in osteoproliferation as well as the tipping point for activation of bone formation are all questions still unanswered in AS. Therefore, the aims of this thesis are as follow:

Chapter 2: The temporal and sequential association between inflammation and excessive tissue formation will assist understanding the transition between these two phases. Therefore, the aim of chapter 2 is to characterise the axial disease progression from initial to advanced stages by an in-depth histological characterisation of the PGISp mouse model.

Chapter 3: The results of Chapter 2 showed that the primary anabolic feature of the PGISp mouse model at 24 weeks post priming was presented as cartilaginous excessive tissue formation. However, whether these cartilaginous tissues could directly become mineralised or convert to bone was unclear. The aim of Chapter 3 is to investigate the nature of the excessive tissue further and whether it mineralises in a longer-term study.

Chapter4: Previous GWAS demonstrated a strong association between AS and *PTGER4*, which encodes EP4. Since PGE2/EP4 regulates both inflammation and bone formation, we hypothesized that this signalling is involved in AS development. The aim of chapter 4 is to study whether modulating EP4 signalling is a potential therapeutic regimen for AS.

Chapter 5: The results from Chapter 2 lead to our next hypothesis that inflammation results in IVD destruction, which is the prerequisite for the excessive tissue formation. Therefore, the aim of Chapter 5 is to test whether early and aggressive intervention with anti-inflammatory treatment, using a combination of high dose etanercept and prednisolone, can suppress inflammation and consequently reduce IVD damage and attenuate progression to excessive tissue formation.

2 Chapter 2: Inflammation is a prerequisite for osteoproliferation in the PGISp mouse model of ankylosing spondylitis

2-1 Foreword

The aim of chapter 2 is to characterise disease progression from the early to advanced stages in the PGISp mouse model as a model of the inflammation-osteoproliferation transition seen in AS. By detailed analysis of this disease progression we have provided some insights into following questions: 1) whether the enthesis is the site of disease initiation, 2) is the inflammation necessary for radiographic disease progression and 3) what is the nature of the pathological osseous tissue laid down. Chapter 2 has been prepared as a draft manuscript for submission for publication.

Inflammation is a prerequisite for osteoproliferation in the PGISp mouse model of ankylosing spondylitis

Tseng HW[1], Pitt ME[1], Glant TT[2], McRae AF[1,3], Kenna TJ[1,] Brown MA[1], Pettit AR[4*], Thomas GP[1*]

Authors' affiliations

[1]Tseng HW, MSc, Pitt ME, BSc, Brown MA, MD, PhD, Thomas GP, PhD, Kenna TJ, PhD, McRae AF, PhD: University of Queensland Diamantina Institute, Translational Research Institute, Australia; [2]Glant TT, MD, PhD: Section of Molecular Medicine, Department of Orthopedic Surgery, Rush University Medical Center, Chicago, IL, USA; [3] McRae AF, PhD: University of Queensland, Queensland Brain Institute; [4]Pettit AR, PhD, University of Queensland, Mater Research, Translational Research Institute, Australia;

* These authors contributed equally to this study

Grant support

This study was supported by NHMRC project grant #APP1006450. HWT was supported by a University of Queensland PhD Scholarship. ARP is supported by NHMRC Career Development Fellowship #519744. MAB is supported by NHMRC Senior Principal Research Fellowship APP1024879 and TTG by the NIH/NIAMS (R01 AR062991).

Running title:

Inflammation drives osteoproliferation in a mouse model of ankylosing spondylitis.

Address for correspondence:

Dr Gethin P Thomas, The University of Queensland Diamantina Institute, Translational Research Institute, 37 Kent Street, Woolloongabba, QLD 4102, Australia. Tel: +61 (0)7 3443 7048; Fax: +61 (0)7 3443 6966; Email: gethin.thomas@uq.edu.au

Or

Dr Allison R Pettit, Mater Research-UQ, Translational Research Institute, 37 Kent St, Woolloongabba, QLD 4102, Australia. Tel: +61 (0)7 3443 7575; Fax: +61 (0)7 3163 2550; Email: allison.pettit@mater.uq.edu.au

2-2 Abstract

Objective

Ankylosing spondylitis (AS) is an immune-mediated arthritis affecting the axial skeleton, in which inflammation is followed by osteoproliferation and frequently ankylosis. The inflammation-bone formation transition is poorly understood, and a key question is whether inflammation is required for osteoproliferation. This study used the proteoglycan (PG)-induced spondylitis (PGISp) mouse model to delineate the morphological and molecular changes during disease progression.

Methods

The spine morphology of the PGISp mice was defined by a semi-quantitative histological scoring system evaluating inflammation, joint destruction and excessive tissue formation (osteoproliferation). Spinal mRNA expression was analysed by real-time PCR. Matrix components were identified using immunohistochemistry.

Results

Disease initiated with inflammation at the periphery of the intervertebral disc adjacent to the longitudinal ligament, reminiscent of enthesitis, and was associated with up-regulated Tnf and metalloproteinases. Destruction of vertebral disc, cartilage and bone were then observed at later time points. Advanced disease was characterised by reduced inflammation, excessive tissue formation and ectopic chondrocyte expansion. These distinct features differentiated the affected mice into early, intermediate and advanced disease stages. Excessive tissue formation was only observed in vertebral joints if the disc was destroyed as a consequence of the early inflammatory process. Excessive tissue and ectopic chondrocytes were enriched in cartilaginous components. Elevated spinal expression of cartilage markers *Col2a1*, *Sox9* and *Comp* indicated upregulated chondrogenesis. Osteophytes were rare but more prevalent in intermediate and advanced disease.

Conclusion

The inflammation-driven intervertebral disc (IVD) destruction in the PGISp mouse was prerequisite for the subsequent excessive tissue formation, which is driven by chondroidal ossification.

2-3 Introduction

Ankylosing spondylitis (AS) is a chronic inflammatory arthritis predominantly affecting the axial skeleton. The disease is characterised by inflammation at entheses, which is followed by an osteoproliferation phase that often leads to ankylosis of affected joints. Current treatments, including non-steroidal anti-inflammatory drugs (NSAID), physiotherapy and tumour necrosis factor (TNF)-inhibitor biologic therapies, function to relieve symptoms, and in the case of TNF-inhibitors reduce inflammation.

Axial and peripheral entheses, where ligaments attach to the bone, are often affected by inflammation causing pain and stiffness [72]. Ankylosis in AS patients results from the development and fusion of syndesmophytes, defined as bony bridges growing at the vertebral corners. Multiple mechanisms of bone formation have been proposed to underlie the osteoproliferation in AS including intramembranous, endochondral, and chondroidal ossification [73, 209]. The causative pathological mechanisms that initiate and perpetuate the excessive bone formation remain unknown. There is an ongoing debate regarding whether inflammation is the direct trigger of this osteoproliferation. Whilst there is evidence that NSAIDs and TNF-inhibitors slow osteoproliferative disease, this effect is at best partial and ankylosis still progresses despite treatment with these agents.

In AS patients, longitudinal magnetic resonance imaging (MRI) and radiographic imaging can be used to follow the disease progress, although the resolution and sensitivity are not sufficient to show correlations at the detailed anatomical level. Collection of serial biopsies from spinal lesions of AS patients would substantially aid elucidation of detailed mechanistic changes underlying the inflammatory responses and the mechanism of bone formation. A few studies have been performed on sacroiliac joint biopsies from patients undergoing hip replacement and in zygapophyseal joints from spinal surgeries [55, 73, 209-211]. Such studies, although informative, are limited by sample size and location, coupled with being predominantly obtained from late-stage disease patients in whom the inflammation-osteoproliferative transition has already occurred. Disease relevant animal models thus present a valuable approach to elucidating mechanisms underlying disease progression in the axial skeleton Time course studies in spinal samples from animal

models present as a powerful approach to elucidate the full progression of AS, particularly to investigate the mechanistic link between inflammation and osteoprolifieration.

We aimed to better delineate the disease progression in AS by studying the proteoglycan (PG)-induced spondylitis (PGISp) mouse model. The PGISp mouse model was chosen for its good recapitulation of AS clinical features including development of both inflammation and osteoproliferation in the spine in response to the PG epitope immune stimulus [105, 176].

To characterise disease progression, we performed a six-month-time time course in PGISp mice spanning from the onset through to advanced disease with regular sampling occurring throughout disease progression. We developed a novel histological scoring system that measured the broad array of disease features occurring during disease progression. We used histology, immunohistochemistry (IHC), and gene expression data to describe events more precisely within affected joints. Additionally, multiple matrix markers were assessed to identify and characterise ectopic formation of cartilage and bone.

2-4 Materials and methods

2-4.1 Mouse model, immunization and collection

The PGISp model was established by treating three month old female IL-4$^{-/-}$ BALB/c mice with 2 mg of human cartilage extract (PG) together with 2 mg of dimethyl dioctadecyl ammoniumbromide (DDA, Sigma-Aldrich, St. Louis, MO) as described previously (Haynes et al [105]). IL-4 deficiency did not change disease presentation but led to higher disease incidence and severity over wild type BALB/c mice [183]. Therefore, IL4-/- mice were used in the present study. Treatment was delivered via intraperitoneal injections, administered in three-week intervals over a 6 week period. Age-matched naïve female IL-4 $^{-/-}$ BALB/c mice were used as controls.

Spine samples including thoracic and lumbar vertebrae were collected 6, 8, 10, 12, 16 and 24 weeks after the first PG injection. Between 12 to 17 mice were collected at each time point from each of the naïve or PGISp groups.

2-4.2 Histology

Spine samples from 5-10 mice at each time point from each of the naïve or PGISp group were fixed in 4% paraformaldehyde (Sigma-Aldrich) for 48-72 hours followed by decalcification in 14% ethylenediaminetetraacetic acid disodium salt dihydrate (EDTA, Sigma-Aldrich) for 3-4 weeks. The embedded spine samples were cut into 5 μm serial sections along the sagittal plane using a standard rotary microtome. The sections were deparaffinised with xylene and graded ethanol and then rehydrated in tris-buffered saline (TBS, 50mM Tris, 150mM NaCl, pH=7.4) before staining with Mayer's haematoxylin and eosin (H&E) or toluidine blue (0.01% toluidine blue O (Sigma) in 0.1% sodium chloride solution (pH = 2.0)). Sections were immersed in the stain solution for 2 minutes followed by an ethanol wash before being mounted in mounting medium (POCD scientific, NSW).

Semi-Quantitative Histological Scoring

Histological scoring criteria outlined in Table 2-1 were developed to capture the broad range of inflammatory, anabolic and catabolic changes that occur within the vertebral joints of the spine in this AS model. Representative images of scoring criteria are shown in the

appendix. Scoring was performed on one H&E and one toluidine blue stained section from each sample. Only samples with correct sagittal orientation and ≥ 6 IVDs in spine section plane were included in the analysis. An average of 9 vertebral joints was scored in each mouse. Anterior and posterior sides of each joint were scored separately and then averaged to generate the final score for any given joints. Joints with a score above zero within any of the criteria categories were defined as affected joints and mice that had at least one affected IVD were defined as affected mice. PGISp mice with normal spine morphology were excluded from further spinal disease incidence and progression analyses. For the qPCR analysis this was not possible and all the mice from each group were analysed. The disease progression was measured by averaging scores of all vertebral joints within one mouse. Blinded scoring was not possible since the feature were quite distinct between early and late stages.

Table 2-1: Histological score criteria

Category	Score	Criteria
Inflammation	0	Normal
	1	Minor infiltration of inflammatory cells at periphery of the joint
	2	Moderate infiltration – inflammatory pannus < 50% joint area
	3	Marked infiltration – inflammatory pannus > 50% joint area
IVD destruction	0	Normal
	1	Less than 50% disc destruction
	2	More than 50% disc destruction
	3	Total disc destruction/only necrotic disc left
Cartilage damage	0	Normal
	1	Some loss of endplate cartilage and/or growth plate cartilage
	2	Severe loss of endplate cartilage and some growth plate cartilage damage

	3	Severe loss of endplate cartilage and severe growth plate cartilage damage
Bone erosion	0	Normal
	1	One or a few small areas of resorption in original vertebral bone.
	2	Numerous areas of obvious focal resorption in original vertebral bone or several areas of severe destruction.
Excess tissue Formation (excluding inflammatory infiltrate)	0	Normal
	1	Mesenchymal cell invasion/ expansion
	2	Moderate fibrocartilage formation (<50% of the original disc area)
	3	Extensive fibrocartilage formation (>50% of the original disc area)
Ectopic chondrocytes	0	Normal
	1	Single small area
	2	Single large area
	3	Multiple areas

2-4.3 Immunohistochemistry

Sagittal sections (4μm) were rehydrated and subjected to different antigen retrieval processes depending on the primary antibody. For types I and II collagen, spine sections were digested in pre-warmed 25% trypsin (Biocare Medical, Concord, NSW, Australia) for 10 minutes at room temperature (RT). For type X collagen, sections were incubated in 0.1 U/ml chondroitinase ABC (Sigma-Aldrich) in tris-acetate buffer (0.1M Tris, 30mM Acetate buffer, 10mM EDTA, pH6.5) for 2 hours at 37°C. No antigen retrieval was performed for osterix antibody. All sections were incubated in 3% H_2O_2 for 30 minutes at RT to inactivate endogenous peroxidases. Samples were further blocked in Sniper Blocking Reagent (Biocare Medical) for 10 minutes and 10% foetal bovine serum for 1 hour at RT. For type I and II collagen and osterix staining, the sections were incubated with rabbit anti-type I or II collagen or osterix antibodies or equivalent concentration of normal rabbit IgG for 1 hour at RT. For type X collagen staining, the sections were incubated with rabbit anti-type X

collagen anti-serum or equivalent concentration of rabbit serum overnight at 4°C. After washing in TBS, sections were incubated in MACH1 Horseradish peroxidase (HRP) polymer reagent (Biocare Medical) for 30 minutes and detected using Diaminobenzidine (DAB) chromogen (Biocare medical). Sections were counterstained in acidified haematoxylin (Sigma). Antibody, normal rabbit IgG and serum details are listed in Table 2-2.

Table 2-2: Antibodies for immunohistochemistry

Antibody	Concentration (dilution)	Catalogue number	Company
Rabbit anti-Type I collagen	0.5 μg/ml (1:2000)	C7510-13	USBioLogical, Swanpscott, MA
Rabbit anti-Type II collagen	0.5 μg/ml (1:2000)	Ab34712	Abcam, Cambridge, UK
Rabbit anti-Type X collagen antiserum	1:8000	LSL-LB-0092	Cosmo bioco, Tokyo, Japan
Rabbit anti-Osterix	0.2 μg/ml (1:4000)	Ab22552	Abcam, Cambridge, UK
Rabbit IgG	Same concentration as antibody	Sc-2027	Santa Cruz Biotechnology, Santa Cruz, CA
Rabbit serum	1:8000	R9133	Sigma, St. Louis

2-4.4 RNA extraction and quantitative real-time PCR

The spine samples from 5-8 PGISp or 5-7 age-matched naïve female mice at each time point were flash-frozen in liquid nitrogen and stored at -80°C. Spine samples were homogenized separately in Trizol (Life Technologies, Mulgrave, Victoria, Australia), and RNA was extracted according to the protocol described previously [105]. Synthesis of cDNA was conducted using a Tetro cDNA synthesis kit (Bioline) following the

manufacturer's instructions. Gene expression was measured by SYBR Green-based quantitative real-time reverse transcription PCR (qPCR) using the Sensimix SYBR kit and run on a ViiA7 Real-Time PCR System (Life Technologies). Primer sequences are listed in Table 2-3. PCR conditions were 10 minutes at 95˚C followed by 50 cycles of 15 seconds at 95˚C and 45 seconds at 60˚C. The expression of individual genes was normalized to β-actin and gene expression quantified using the ΔCT equation.

Table 2-3: Primers for real-time PCR

Gene	Accession Number	Forward Primer (5'-3')	Reverse Primer (3'-5')
β-actin	NM_007393	GATTACTGCTCTGGCTCCTAG	GACTCATCGTACTCCTGCTTG
Col2a1	NM_031163	GCAGAGATGGAGAACCTGGTA	AGCCTTCTCGTCATACCCCT
Comp	NM_016685	GTCCAAGAAGAATGACGATCAGA	ACAGTTGTCAGCTACATTTCGT
Mmp3	NM_010809	GATGAACGATGGACAGAGGATG	TGTGGAGGACTTGTAGACTGG
Mmp13	NM_008607	GCCATTTCATGCTTCCTGATG	AGACTGGTAATGGCATCAAGG
Sox9	NM_011448	CGACCCATGAACGCCTT	GTCTCTTCTCGCTCTCGTTC
Tnfα	NM_013693	AGACCCTCACACTCAGATCA	TCTTTGAGATCCATGCCGTTG

Cartilage oligomeric matrix protein (Comp); Matrix metalloproteinase (MMP); Tumour necrosis factor alpha (Tnfα); Type II collagen, α 1 (col2a1); Sex determining region Y- box 9 (Sox9)

2-4.5 Statistics

Data was analysed by Mann-Whitney or Kruskal-Wallis tests analysis using PRISM 6 (GraphPad Software, La Jolla, CA). *P*-values less than 0.05 were considered significant. Unsupervised analysis was conducted using the hclust function in R. Histological scores of affected IVD of affected mice were averaged and computed using hierarchical cluster analysis using Ward's method.

2-5 Results

2-5.1 PGISp axial joint histopathology progresses from inflammation to osteoproliferation.

To characterise axial disease progression in PGISp mice, H&E stained sections from spines collected across a disease time course (weeks 6, 8, 10, 12, 16 and 24 post the first PG injection) were semi-quantitatively scored according to the criteria outlined in Table 2-1. These assessment criteria scored inflammation, vertebral disc destruction, bone erosion and excess tissue formation (mesenchymal tissue expansion or fibrocartilage formation) in the vertebral joints as well as ectopic chondrocyte formation. Histological scoring of these major disease histopathology features was used to model axial disease progression in the PGISp mice. All the vertebral joints and IVDs in naïve mice appeared normal throughout the time course and were treated as a single mouse group for statistical analysis.

The PGISp mice exhibited early disease by 6 weeks post PG priming with 60% of mice having either 1 or 2 mildly affected vertebral joints (Figure 2.1A). By 8 weeks post the first PG injection, every PGISp mouse had at least one affected vertebra, with 50% of all vertebral joints affected (Figure 2.1A). The majority of joints were only mildly affected at 8 weeks, but severe inflammation was observed in a small percentage (Figure 2.1A). Averaging the inflammatory score of all the vertebral joints in individual affected PGISp mice across the time course showed that the inflammation score peaked at 12 weeks (Figure 2.1B), with 18-19% of affected joints severely inflamed (Figure 2.1A). At both 10 and 12 weeks post PG priming, the inflammation score was significantly elevated (Figure 2.1B). There was heterogeneity in inflammation severity at any time point both between and within individual animals, with some vertebral joints showing no inflammation while others had significant joint damage (Figure 2.1B). Average inflammation severity reduced from 16 weeks post PG priming (Figure 2.1A). Taken together, these observations show that inflammation is the earliest detectable axial histopathological feature in the PGISp model but it is a transient disease process.

Histopathological features of the disease reflecting destruction or tissue formation demonstrated a progressive or sustained disease process. Most reached maximal score at 24 weeks post priming, much later than was observed with inflammation (Figure 2.1C-E).

Initiation of disc destruction (Figure 2.1C), bone erosion (Figure 2.1D), cartilage damage (Figure 2.1E) and excessive tissue formation (Figure 2.1F) were evident from 8 weeks post priming. Disc destruction and bone erosion were significantly increased from week 10 onwards in PGISp compared to naïve mice (Figure 2.1C and D, respectively). Disc destruction (Figure 2.1C) and bone erosion (Figure 2.1D) peaked at the same time as inflammation (Figure 2.1B) but subsequently plateaued, consistent with them being irreparable tissue changes driven by the inflammatory processes. Excessive tissue (Figure 2.1E) and ectopic chondrocyte formation (Figure 2.1F) increased steadily from week 10 through to week 24. A notable feature was that in all the mice analysed, severe inflammation and significant excessive tissue formation did not occur simultaneously within the same joint, consistent with these features representing early and late stages of PGISp progression respectively. Another feature of late stage disease was cartilage damage, which was not significantly elevated compared to naïve or 6-week mice until 16 weeks post PG priming. This suggests that this destructive event is more likely a secondary consequence of other joint changes initiated by the inflammatory process.

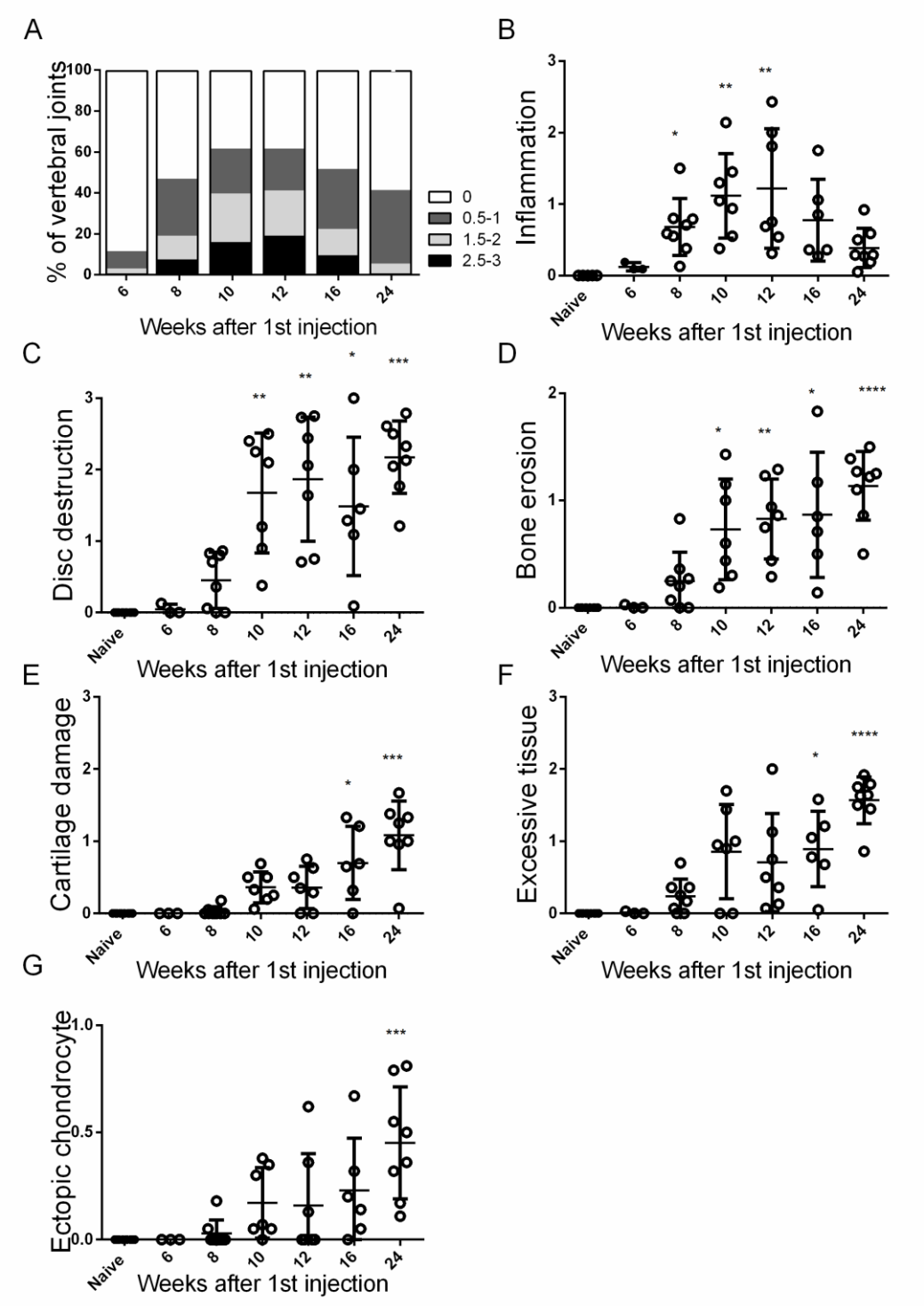

Figure 2.1: PGISp mouse model disease progression.

(A) The severity of inflammatory infiltrate is represented by the percentages of different scores at each time point. Axial disease progression is described by the features of; **(B)** inflammation, **(C)** disc destruction, **(D)** bone erosion, **(E)** cartilage damage, **(F)** excessive

tissue formation and **(G)** ectopic chondrocyte formation. Each point represents the average scores of all vertebral joints within each affected mouse at the particular time points (3-10 mice/time point). The results are shown as mean ± SD and analysed by a Kruskal-Wallis test with posttest Dunn correction. ****p<0.0001, ***p<0.001, **p<0.01, *p<0.05 compared to naïve.

2-5.2 Inflammation drives tissue damage and disc destruction in PGISp mice

Detailed histological assessment across the time course exemplified the heterogeneity of disease progression between different animals and even between individual vertebral joints, similar to that reported in AS [212]. At the 6-week time point, the earliest detected feature of inflammation was accumulation of inflammatory cells at the periphery of the IVD adjacent to the annulus fibrosus (Figure 2.2A). At 8 weeks post priming, while all mice were affected, within any given PGISp mouse both affected (Figure 2.2B, joints 2-4) and unaffected (Figure 2.2B, joints 1 and 5) vertebral joints were observed and there was a broad range of inflammation severity within the spine (Figure 2.2B, joints 2-4). Inflammatory pannus invading into the disc space drove IVD destruction, resulting in joint space narrowing (Figure 2.2B, space between black arrows) and was often associated with bone erosion (Figure 2.2C, black arrowheads). Early hyaline cartilage damage, including eroded surfaces defined by excavated and empty chondrocyte lacunae, was confined to areas exposed to inflammatory infiltrate (Figure 2.2C, yellow dash line represents eroded cartilage surface).

Severe inflammation was characterised by marked infiltration of the AF by inflammatory cells, including polymorphonuclear cells, vascular structures and increased density of mixed morphology mesenchymal cells (Figure 2.2C and D). In severely inflamed joints, periosteal expansion and inflammatory cell invasion frequently extended along the cortical surface of the vertebral body, possibly following the spinal ligaments, suggesting an entheseal and/or periosteal pathology (Figure 2.2E, arrow). Overall the histopathology features suggest that the inflammatory process drives the IVD destruction and focal bone and cartilage damage.

TNFα, and MMP-3 and -13 have been implicated in AS inflammatory processes and have been correlated with disease activity [213-215]. Therefore, mRNA expression of these genes in the whole spine was measured by qPCR (Figure 2.2F). The basal level of *Mmp3* in unaffected mice was very low across the time course. PG immunisation induced a dramatic elevation of *Mmp3* at 8 weeks and expression levels of this transcript remained significantly higher in PGISp mice at all later time points (Figure 2.2F). *Mmp13* was significantly elevated at weeks 12 and 16 in PGISp spines. *Tnf* expression was significantly increased in PGISp mice at 8 and 16 weeks (Figure 2.2F). These data suggest that the inflammation-driven tissue remodelling molecular cascades are established by 8-10 weeks post immunisation and decrease in parallel with inflammation during the later disease stages.

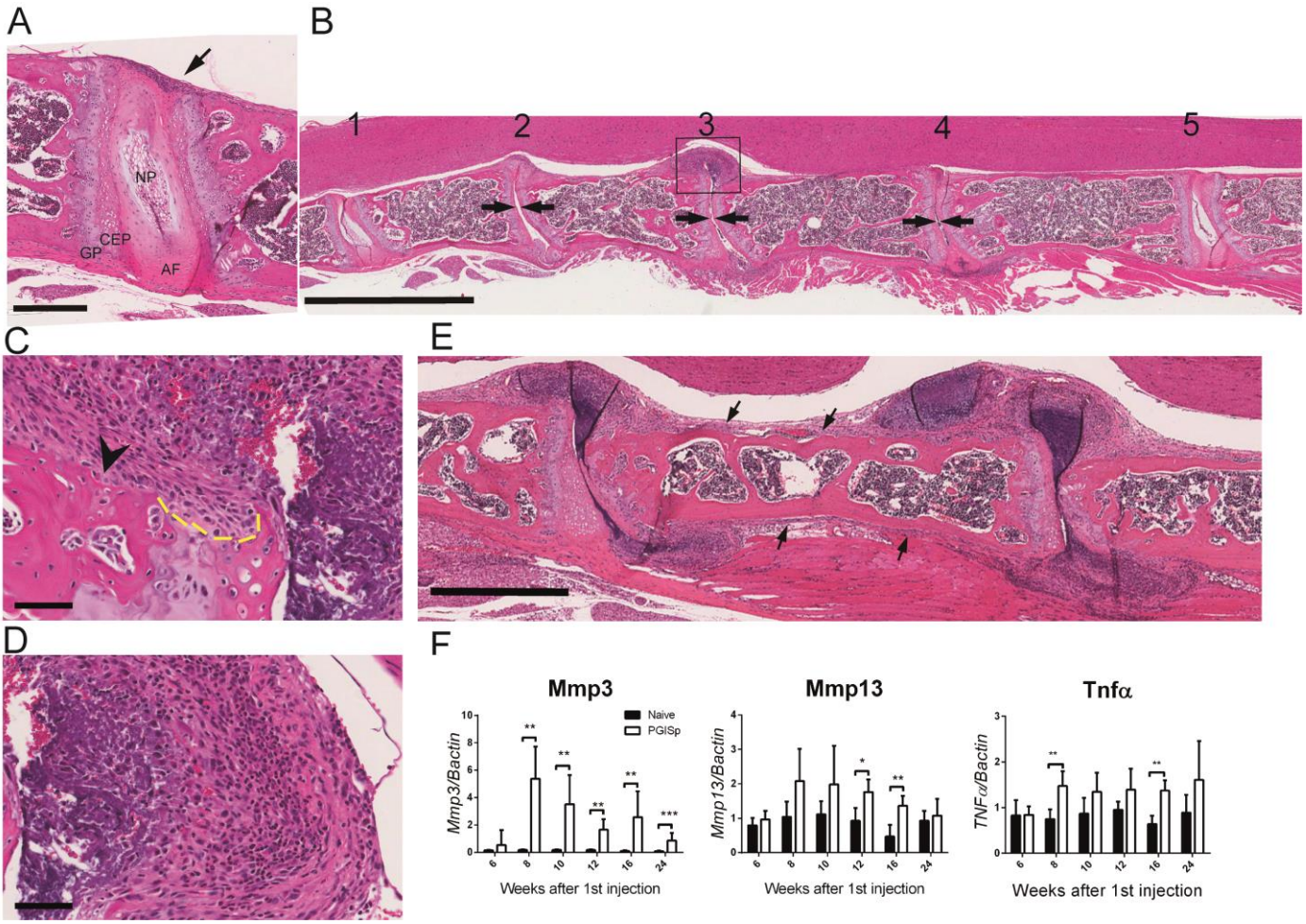

Figure 2.2: Progression of spinal inflammation in PGISp mice.

(A) Representative H&E stain of mild inflammation in an 8-week time point mouse. Inflammatory cells accumulate at the periphery of the disc (arrow), but the rest of the IVD appears normal. NP: nucleus pulposus; AF: annulus fibrosus; CEP: cartilaginous endplate; GP: cartilaginous growth plate. **(B)** Variable disease penetrance in a 8-week PGISp mouse; (1) and (5) unaffected IVDs, (2) disc destruction combined with early chondrocyte formation, (3) severe inflammation and disc destruction (4) moderate inflammation with incomplete disc destruction. **(C)** Magnification of the boxed area in (B) shows bone erosion (arrowhead) and cartilage damage. The yellow dashed line indicates the eroded cartilage surface. **(D)** Magnification of the boxed area in (B) demonstrates large numbers of mononuclear cells presenting in the affected joints. **(E)** inflammation expansion along the longitudinal ligament (black arrows) **(F)** mRNA expression of *Mmp3*, *Mmp13* and *Tnf* in whole spine was analysed by qPCR and normalized to *β-actin*. Black bars represent naïve and open bars represent PGISp mice. Expression levels are presented as mean ± SD. ***p<0.001, **p<0.01, *p<0.05 compared to naïve at the same time point, Mann-Whitney test. Scale bar: (A) 300μm, (B) 2mm, (C-D) 60μm and (E) 700 μm.

2-5.3 Disease-associated anabolic tissue pathology

Expansion of mesenchymal cells, predominantly fibroblast- (Figure 2.3Ai,ii, arrowheads) and chondrocyte-like, (Figure 2.3Ai,ii, arrows) was found in the bulging residual annulus fibrosus of affected vertebral joints and extending along the vertebral periosteal surface. The chondrocyte-like cell phenotype included rounded or polygonal morphology within a dense predominantly basophilic extracellular matrix (ECM). In advanced disease, ectopic cartilaginous tissue increased as the inflammatory cell infiltrate and density of fibroblast-like mesenchymal cells declined (Figure 2.3B, black arrows). Our results showed the ectopic chondrogenesis only occurred following disc destruction, with residual necrotic disk tissue frequently evident (Figure 2.3A-B, asterisks). Ectopic cartilage-like tissue containing embedded chondrocytes in columnar formation was also observed in some mice parallel to the vertebral periosteal surface, possibly associated with longitudinal ligament attachment points (Figure 2.3C, yellow arrowheads). Interestingly, inflammation was also noted in similar regions of other mice (Figure 2.2E, black arrows).

To elucidate the composition of the ectopic ECM present at sites of PGISp excess tissue formation, the distribution of different types of collagen was analysed by IHC (Figure 2.3D). In unaffected vertebral joints, the annulus fibrosus and hyaline cartilage had high PG content (toluidine blue positive) and predominantly contained type II collagen. Type I collagen was weakly present in annulus fibrosus and strongly expressed by vertebral bone. In affected joints, the majority of the excessive tissue had a high PG content and contained both type II and type X collagens, verifying pathologic cartilage expansion. Expression of type X collagen suggested that some chondrocytes were hypertrophic. Consistent with previous findings [105], weak collagen type I staining seen at the periphery of excessive tissue areas potentially indicated progression towards a more boney phenotype.

Spinal mRNA expression of cartilage matrix components and cartilage-forming regulatory proteins fluctuated during disease progression (Figure 2.3E). Expression of cartilage components *Col2a1* and *Sox9* were decreased at 8 and 6 weeks post priming respectively. From 10 weeks onwards, as inflammation peaked and excessive tissue formation increased, *Comp* was significantly elevated. *Col2a1* was up-regulated at week

12 whilst *Sox9* increased at weeks 10 and 24. This trend suggests cartilaginous matrix expression was increased in PGISp mice after the peak of inflammation.

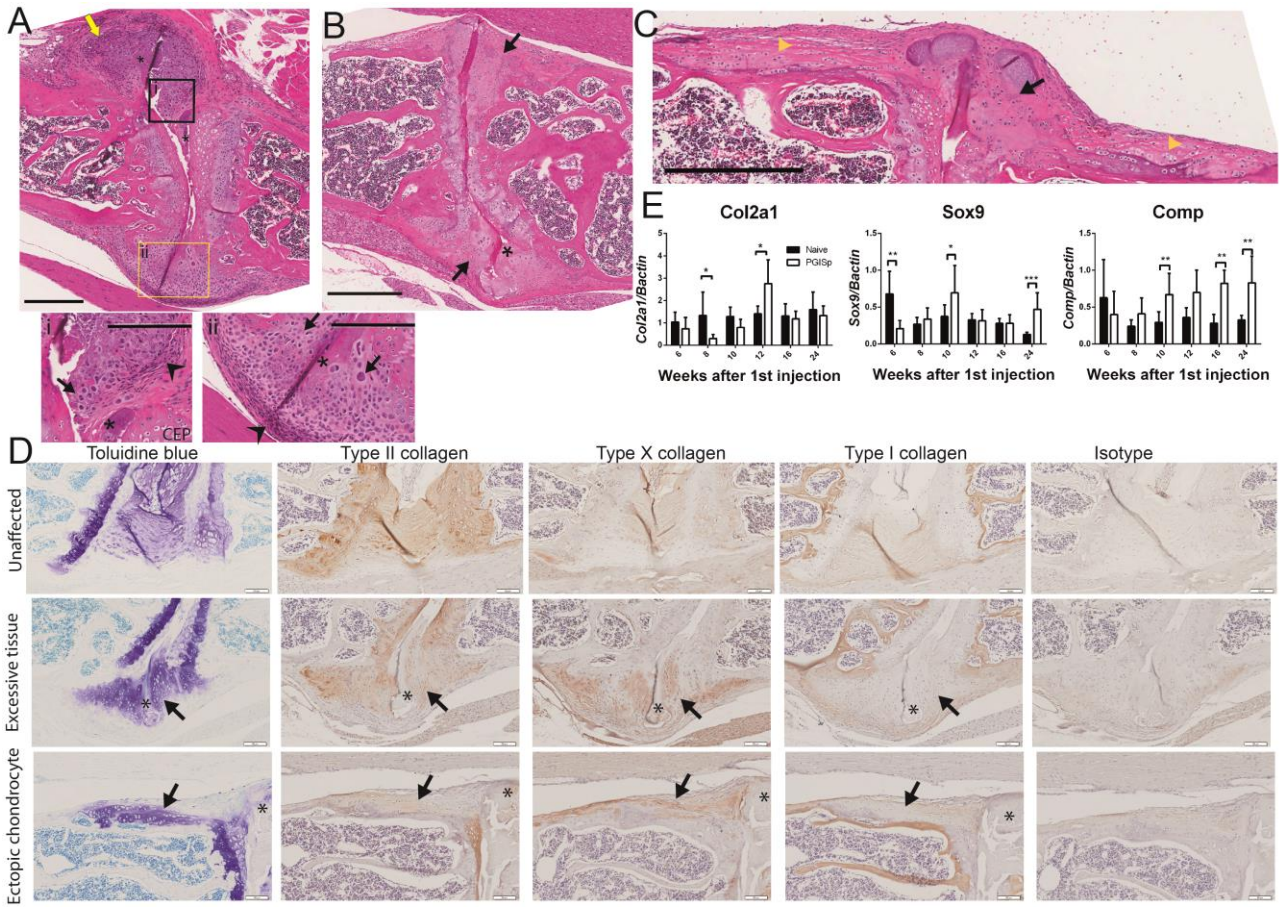

Figure 2.3: Excessive tissue and ectopic chondrocyte formation are key features of advanced disease.

(A) A 12-week mouse IVD demonstrates both early (i) and intermediate (ii) stages of excessive tissue formation using H&E stain. Inflammatory infiltrate (yellow arrow) surrounds the affected joint, while fibroblast-like cells (arrowheads) and chondrocyte-like cells (black arrows) are located adjacently to the residual disc (asterisks). **(B)** Excessive tissue at the periphery of the joint is greatly increased in more advanced disease (arrows). Representative image was taken from a 24-week mouse. **(C)** In addition to excess tissue (arrow), columnar chondrocytes expand ectopically along the cortical bone between affected joints (yellow arrowheads). Representative image from a 24-week mouse. **(D)** Representative images taken from 24-week mice show an unaffected IVD and affected joints with excessive or ectopic chondrocyte formation. Cartilaginous tissue (arrows) is positive for toluidine blue (PG content) and type II collagen. Type X collagen stains for hypertrophic chondrocytes while type I collagen delineates mature bone. **(E)** Spinal gene expression profile of cartilage markers *Col2a1*, *Comp* and *Sox9* were analysed by qPCR and normalized to β-actin. Black bars represent naïve and open bars represent PGISp mice. Expression levels are presented as mean ± SD. ***p<0.0001, **p<0.001, *p<0.01 compared to naïve at the same time point, Mann-Whitney test. Scale bars: (A) 300μm, (i) and (ii) 200 μm, (B) 400μm, (C) 300μm and (D) 100μm.

Mature osteophyte formation, defined as aberrant bone formation adjacent to cortical bone (Figure 2.4A), was apparent. Osteophytes showed a variable collagen distribution with different areas containing collagen I-, II- or X-positive and osterix-positive cells (Figure 2.4B). None of the weeks 6 and 8 PGISp mice developed osteophytes whilst 28.6% of mice at week 10 had osteophytes and the percentage increased to 71.4%, 66.7% and 75% at weeks 12, 16 and 24, respectively. A noteworthy observation is that pathological tissue formation was only observed with vertebral joints that exhibited disc damage/destruction.

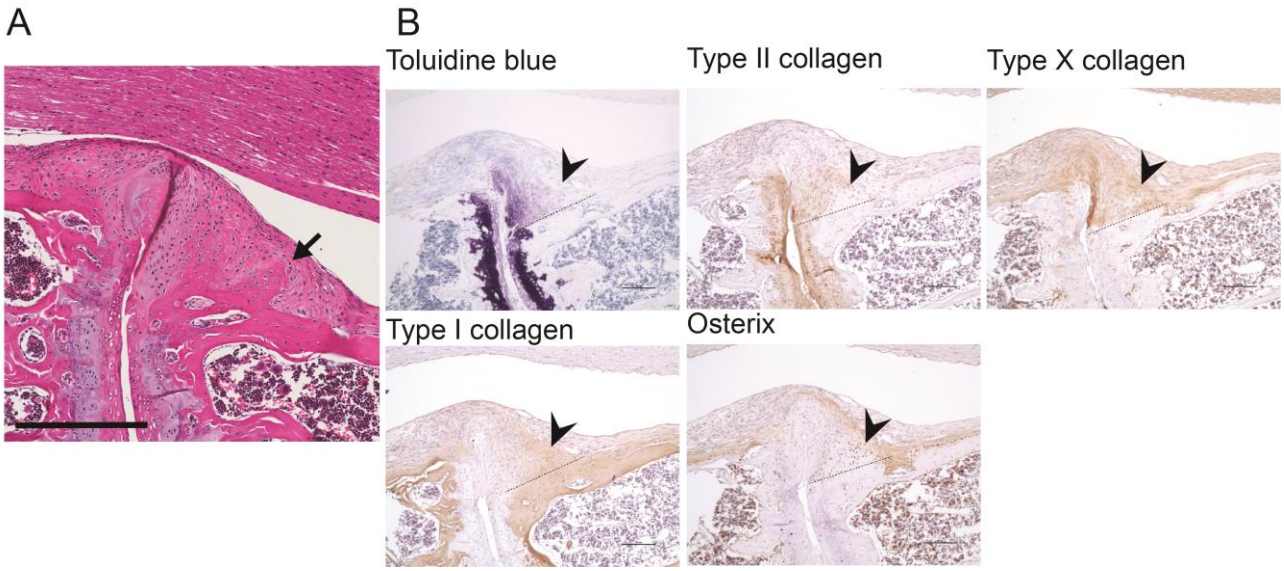

Figure 2.4: New bone and osteophyte formation

(A) Representative image of an osteophyte (arrow) in an affected joint of a 12-week PGISp mouse. (B) Recently formed bone tissue (arrowheads) is characterised by a transition from PG and type II collagen-enriched matrix to type X and type I collagen positive matrix. Osterix positive osteoblasts are embedded in type I collagen positive bone matrix. The dashed line represents the boundary between the original cortical bone and the excessive matrix above showing a reduction of cartilaginous matrix, toluidine blue staining and type II collagen accompanied with an increase of type I collagen and osterix-expressing osteoblasts. Arrowheads indicate cartilage tissue that is strongly positive for type I, X collagen and osterix but weakly for toluidine blue and type II collagen. Scale bar (A) 300 μm and (B) 100 μm.

2-5.4 Modelling of disease

To better model the interdependence of the different scoring criteria irrespective of time post-PG priming, we developed an algorithm to define different disease stages. This algorithm utilised an unsupervised clustering approach based purely on average affected vertebral joint scores across all the criteria measured. This clustering defined three disease stages which interestingly corresponded broadly to the time point post-priming; Stage 1 - early (mainly week 6-8, Figure 2.5A, left box), Stage 2 - intermediate (mainly weeks 10-12, Figure 2.5A, middle box) and Stage 3 - advanced (mainly weeks 16-24, Figure 2.5A, right box). We then further dissected the data to identify the scoring metrics that best delineated each stage. The scores for inflammation (Figure 2.5B), excessive tissue formation (Figure 2.5C) and ectopic chondrocyte formation (Figure 2.5D) strongly differentiated between these three groups. The early stage showed mild to moderate inflammation, low excessive tissue and low ectopic chondrocyte formation. The intermediate stage displayed severe inflammation and moderate excessive tissue and ectopic chondrocyte formation. The advanced stage showed decreased inflammation but pronounced excess tissue and ectopic chondrocyte formation.

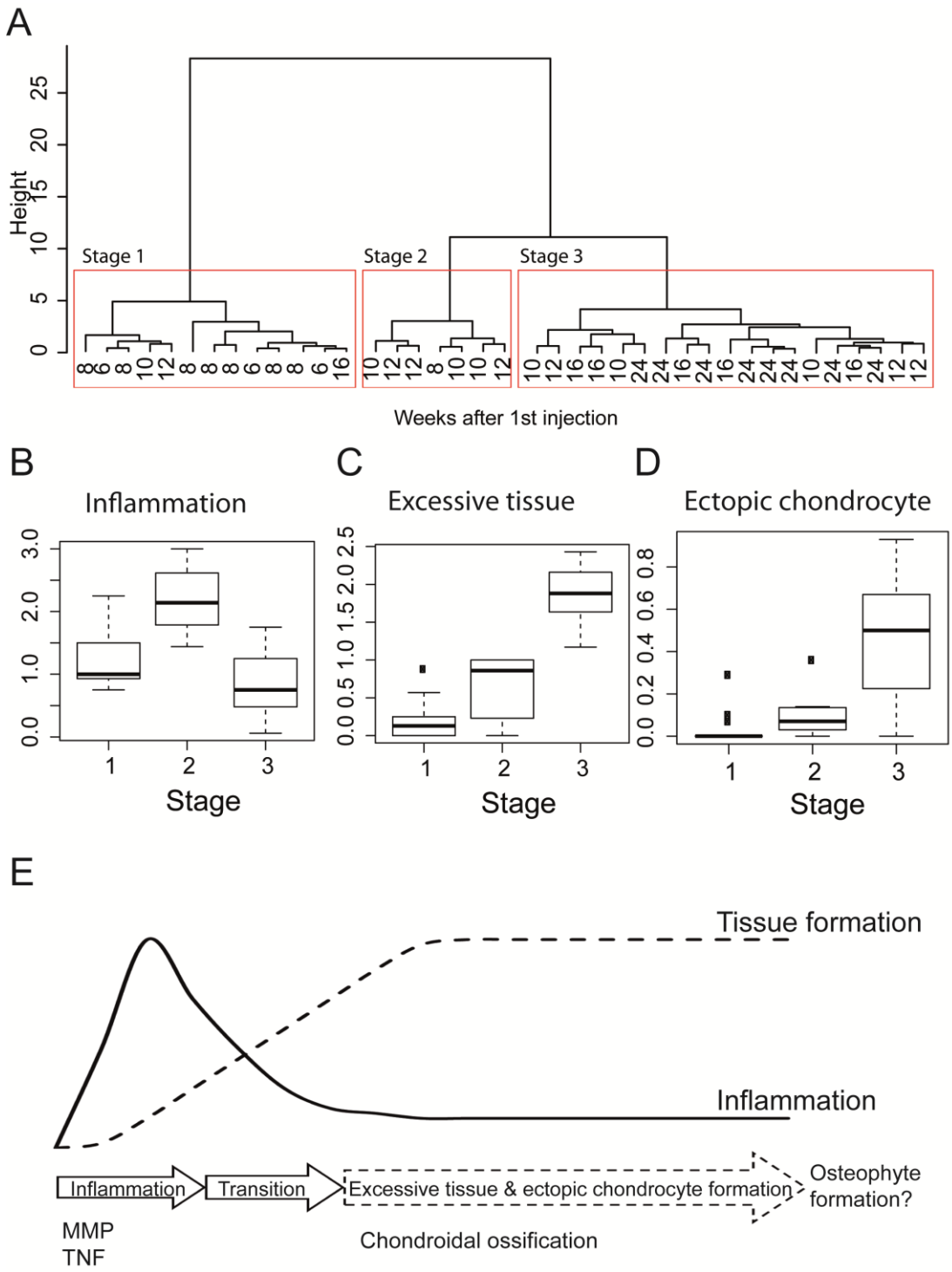

Figure 2.5: Early, intermediate and late phases of disease progression are delineated by inflammation, excessive tissue and ectopic chondrocyte formation.

(A) Unsupervised clustering differentiates the model into 3 stages corresponding with disease duration. The x-axis depicts the time points of the mice. The left box (Stage 1), middle (Stage 2) and right box (Stage 3) represent early, intermediate and advanced

stages of disease development respectively. Scores for **(B)** inflammation **(C)** excessive tissue formation and **(D)** ectopic chondrocyte formation are distinct between these 3 groups. **(E)** Axial disease was initially characterised by transient inflammation that included vertebral joint infiltration by monocular cells, activation of tissue remodelling (MMPs) and pro-arthritic inflammatory pathways (TNF). Vertebral joint inflammation culminated in destructive changes, including destruction of the IVD, the latter of which was irreparable and would have considerable impact on joint biomechanics. In advanced disease, inflammation is decreased; however, excessive tissue and ectopic chondrocyte formation driven by chondroidal ossification was the predominant feature and only occurred in joints in which the IVD had been severely compromised.

2-6 Discussion

Inflammation and syndesmophyte formation are two defining hallmarks in AS. However, the relationship between these features, as well as the underlying controlling factors, is poorly understood. Key questions that remain to be answered are whether the enthesis is the site of disease initiation, if the inflammation is necessary for radiographic disease progression, and what is the nature of the pathological osseous tissue laid down. By detailed analysis of disease progression in the PGISp mouse model of AS, we have provided some insights into these questions.

Entheses, categorized as fibrocartilaginous or fibrous entheses, are traditionally just seen as focal interfaces between ligament and bone. The spine possesses abundant ligaments including IVD, anterior/posterior longitudinal ligaments, ligamenta flava, and interspinous/supraspinous ligaments [70]. It is hypothesized that entheses are prone to microdamage, which allows immune cells from the synovium and bone marrow to enter entheses and interact with the potential autoantigen in the entheses, such as aggrecan [74, 75]. The presence of HLA-B27 molecules might augment the immune responses [76]. Peripheral enthesitis has been described in other spondyloarthropathy (SpA) animal models, such as HLA-B27 transgenic rats [138], TNFΔARE mice [168], grouped DBA/1 male mice [154] and curdlan-treated SKG mice [160]. Disease in the PGISp mouse model is induced by autoimmunity against PG [216]; therefore, we examined whether entheses are the primary sites of disease initiation.

The detailed histology analysis in the present study revealed that the inflammatory invasion started at the periphery of the annulus fibrosus. Further inflammatory infiltrate and ectopic chondrocytes were also shown to expand along the inter-IVD cortical bone surfaces. Although we do not show definitive proof of entheses in these regions, it is well established that the longitudinal spinal ligaments has frequent attachment points in this area [217, 218]. Spinal enthesitis presenting as pannus formation outside of the annulus fibrosus was also reported in HLA-B27 transgenic rats [138] and curdlan-treated SKG mice [160]. Our result supports the hypothesis that enthesial inflammation is the primary site and mode of disease in the PGISp mouse model.

The limited effects of anti-TNF therapies on radiographic progression raise the question as to whether inflammation is required for osteoproliferation in AS. Our detailed histological examination suggests inflammation, excessive tissue formation and ectopic chondrocyte formation typify early, intermediate and late disease stages, respectively. We demonstrated that early mesenchymal expansion initiated before resolution of inflammation; however, severe inflammation was never found simultaneously with severe excessive tissue formation within the same joint supporting sequential rather than parallel progression of these disease features. Therefore, our model predicts that inflammatory lesions are likely to have decreased, if not resolved, in the later disease stages typified by syndesmophyte formation. This prediction is supported by MRI studies in AS patients that have shown: 1) new syndesmophytes are seen more frequently in vertebral corners with resolved inflammation [188]; 2) 68% of syndesmophytes developed from vertebral corners without active inflammation during the 2-year observation period [190]. Although, some consideration needs to be given to the sensitivity limits of MRI for detecting mild inflammation [192].

Excessive tissue formation only occurred at vertebral joints in which the IVD itself had been destroyed. This implies that the sequence of PGISp disease progression is initiation with inflammation leading to disc destruction. IVD spaces are generally preserved in the presence of syndesmophytes in AS patients [219] although there is some degree of disc degeneration degree which is higher than that seen in non-rheumatoid disease control patients and the severity was associated with duration of disease and BASFI index [220]. However, the results were unable to delineate the cause-effect relationship between disc degeneration and syndesmophyte formation. The association between disc degeneration and syndesmophyte formation had not been studied yet.

Axial disease presented in the PGISp model is distinct from other rheumatoid arthritis rodent models. Severe cartilage destruction, proteoglycan depletion and bone erosion observed in collagen-induced arthritis (CIA) [221], collagen type II antibody-induced arthritis (CAIA) [222] and antigen-induced arthritis models [222] are often accompanied with inflammatory pannus. Nevertheless, inflammation in PGISp mice was not the leading cause of endplate cartilage damage even after inflammation destroyed the disc. Other typical features of rheumatoid arthritis mouse models were not evident in the PGISp mice,

such as bone marrow oedema in the rat adjuvant-induced arthritis (AIA) [223] or angiogenesis in the CIA mouse model [224]. These might be due to different animal models, but it also suggests that the mechanisms behind peripheral arthritis might not be applicable to spondylitis.

In the PGISp mouse model, as inflammation decreases, excessive tissue formation commences with ectopic chondrocyte formation occurring late. Such a progression concurs with the “TNF-brake hypothesis” previously proposed by Maksymowych *et al.,* [225] which suggests high level of inflammatory TNF inhibits osteoproliferation and this inhibition is eased as TNF levels drop with resolution of inflammation .This also matches data from rheumatoid arthritis models in which osteoblast function was inhibited in the presence of inflammation [226] and induced after inflammation resolution [227].

Enthesitis and osteoproliferation have also been reported in DBA/1 mice [153], HLA-B27/hβ2m transgenic rats [139] and curdlan-treated SKG mice [160]. However, the relationship between the processes is not well-defined. In the DBA/1 mouse model of ankylosing enthesitis, chondrocyte proliferation was the leading cause of ankle ankylosis [152, 153]. The entheseal proliferation and inflammatory infiltrate were minor in this model and treatment with glucocorticoids [156], but not etanercept [157], did ameliorate inflammation somewhat but had no effect on the ankylosis. In a longitudinal study in HLA-B27/hβ2m transgenic rats, osteoproliferation was found external to the joint space separate from inflammatory infiltrates [139]. However, osteoproliferation and inflammation in HLA-B27/hβ2m transgenic rats were presented simultaneously suggesting distinct but parallel processes. Interestingly, although blocking TNF signalling before or after onset prevented or reduced arthritis respectively, chondroproliferation and its activation of relevant bone morphogenetic protein (BMP) signalling were only prevented by early treatment [114]. In the SKG mouse model, bone formation and erosion were shown to be adjacent to inflammation although it is not clear if there is a progression through these different features as a detailed longitudinal study was not undertaken [160]. So while evidences from other animal models are not clear as to the relationship between inflammation and osteoproliferation, our extensive analysis in the PGISp model clearly supports a direct progression from inflammation to bone formation.

Direct connection of the ectopic chondrocytes and cartilage to the vertebral cartilaginous endplate or growth plate was not a consistent histological feature, indicating that these ectopic tissues were not due to expansion of existing cartilage structures. The annulus fibrosus [228], periosteum [229] and ligament [230] all contain potential chondrocyte precursors. Therefore, it is possible the chondrogenesis is initiated from progenitors located within these disease-affected tissues without direct involvement of pre-existing cartilage. Several features of the excessive tissue in the advanced disease resembled endochondral ossification, such as cartilage formation and chondrocyte hypertrophy. Hypertrophic chondrocytes have been shown to be able to transform directly into osteoblasts and osteocytes subsequently becoming embedded in mature bone [83]. Bleil *et al.,* recently demonstrated zygapophyseal joint ankylosis was caused by direct transformation from cartilage to bone without chondrocyte hypertrophy [79]. The direct transformation/ossification from chondrocytes represents chondroidal ossification [73] and might be the primary mechanism of excessive tissue formation in this model. Examples of mature osteophyte were rare in this study but more evident in later disease stages. This finding suggests the transformation of cartilage to bone in PGISp mice is a slow process modelling the prolonged window between disease onset and radiographic change in AS patients [2].

Our results suggest that if inflammation is not treated early enough to prevent irreparable structural damage, further chondro/osteoproliferation at that location may progress even if the inflammatory process is resolved. The benefits of early intervention regarding both spondylitis and radiographic progression have been demonstrated with different treatments. After treatment with infliximab for 16 weeks, 61% of patients with short disease duration (13.4 months) had 40% improvement from baseline [119] whilst only 47% of patients with long disease duration (7.7 years) reached the same criteria after 24 weeks of treatment [118]. Delaying TNF intervention therapy for 10 years was related to faster radiographic progression compared to those who started treatment within 10 years of disease onset [206]. The benefit of early intervention was also seen using NSAID. AS patients with short disease duration (< 5 years) had less radiographic progression [96] compared to those with long disease duration (11.9 years) [97] following chronic high dose NSAIDs treatment. These studies suggest that anti-inflammatory therapies exert better

clinical outcome in early AS/SpA patients compared to those whose disease is established.

Taken together, our study indicates inflammation leads to IVD destruction in the PGISp mouse AS model. The latter is a prerequisite for induction of excessive tissue formation, with chondroidal ossification rather than endochondral or intramembranous ossification appearing to be the most likely mechanism. This study emphasises the advisability of intervening early in AS patients with more potent anti-inflammatory therapeutic regimens in order to prevent inflammation-induced destructive changes and consequently reduce the frequency of osteoproliferative events.

3 Chapter 3: Extended time course to characterise ongoing disease progression in the PGISp mouse model

3-1 Aim of the long-time course study

In Chapter 2, we demonstrated that the PGISp mouse model mimics many features in AS patients and is a good model for studying the inflammation-osteoproliferation transition. Our results suggested that the mechanism behind the pathologic bone formation is chondroidal ossification. However, a number of issues require further clarification. Firstly, at 24 weeks post the first PG injection, the extensive excessive tissues that were observed in effected joints were mainly composed of cartilaginous matrix but we had no data regarding the mineralisation status of this matrix. Consequently it was not clear whether this cartilaginous matrix directly mineralised or, if given sufficient time, progressed to bone formation by a more traditional endochondral ossification-like mechanism. Secondly, the histology analysis only examined excessive tissue formation in two dimensional (2D) sagittal planes; whether osteophytes developed in other planes was not investigated. We therefore investigated whether the excessive tissue transformed into bone or mineralised cartilage over a longer time course of the disease using 3D computed tomography (CT). CT and histological observations were correlated. In this extended time course study, we anticipated formation of osteophytes either due to bony conversion or direct mineralisation of the cartilaginous excessive tissue evident at 24 weeks.

3-2 Materials and methods

3-2.1 Animal experiments

The induction of axial disease was performed as described in the manuscript presented in Chapter 2. A total of 15 PGISp mice were collected at 38-43 weeks after the first injection. Three age-matched DDA alone-treated and 4 age-matched naïve mice were used as control. Skeletons were fixed in 4% paraformaldehyde for 48 hours. The skeletons were either processed immediately for histological analysis only or stored in PBS for 1-2 weeks before *ex vivo* CT imaging. A subset of the CT-imaged samples was subsequently processed for histology. Mouse numbers in each outcome assay stream are specified in Table 3-1.

Table 3-1: Mouse numbers applied to the specific analysis streams

	Histological analysis only	CT analysis only	Both Histological and CT analysis
PGISp	6	6	3
Naïve or DDA alone-treated IL-4$^{-/-}$ mice	1	4	2

3-2.2 CT imaging

The bone micro-architecture of the spine was imaged *ex vivo* using a Siemens Inveon positron emission tomography–computed tomography (PET-CT) multimodality system (Siemens Medical Solutions Inc., Knoxville, TN, USA). Parameters were as follows: 360° rotation, 360 projections, 80kV voltage, 270μA current, and effective pixel size 27.5μm. All images were reconstructed with a down sampling factor of 1, using Cobra Reconstruction software (Exxim 6.3.39 Computing Corp).

3-2.3 Histology

Skeletons were decalcified, processed and sectioned at 4 μm as described in the manuscript presented in Chapter 2. After deparaffinization and rehydration, sections were

processed for basic histology staining. For H&E staining sections were immersed in Mayer's haematoxylin (Sigma-Aldrich) for 2 minutes, rinsed in tap water for 5 minutes and then stained with eosin (Sigma-Aldrich) for 1.5 minutes. Safranin O/fast green staining was performed to study PG content in the cartilage. In brief, rehydrated sections were stained with Mayer's haematoxylin (Sigma-Aldrich) for 2 minutes, rinsed with tap water for 5 minutes followed by staining with 0.02% fast green (Sigma-Aldrich) in 1% acetic acid for one minute, rinsed in 1%acetic acid/70%EtOH for 30 seconds and 1% safranin O for 10 minutes. Protocol for toluidine blue stain was the same as described in Chapter 2. After H&E, toluidine blue and safranin O/fast green staining, the sections were quickly rinsed in 95% and 100% ethanol followed xylene and mounted in mounting medium (COPD).

3-2.4 Immunohistochemistry

Type I and II collagen and isotype control staining protocol was the same as described in the manuscript presented in Chapter 2.

3-3 Results

3-3.1 3D assessment of spine morphology demonstrated osteophyte orientation varied with spine localisation

To characterise pathologic mineralisation in 3D, axial skeletons were scanned by CT. Seven out of 9 mice scanned using CT had severe disc space narrowing and presented a variety of CT spinal abnormalities suggestive of abnormal bone formation or mineralisation features compared to healthy controls. These two outlier mice had no evident IVD space narrowing or bone erosion, implying they only had mild disease, an anticipated outcome given disease variability demonstrated in Chapter 2. Most of the abnormalities, which are outlined in detail within this Chapter, were simultaneously observed in all but two mice.

In anteroposterior (Figure 3.1A, green, red and blue arrows) and transverse (Figure 3.1B-D) views of CT scans, hyperdense projections, presumably osteophytes, extended perpendicularly from the vertebral bodies were more common in the middle and lower thoracic spine compared to other regions. These osteophytes were not visible in most lateral views (Figure 3.1E). Hyperdense CT signal with structural appearance resembling ectopic bone (defined as abnormal bone formation including psuedo bone marrow cavity

and trabecular structures) was an additional minor feature observed in the lower thoracic spine of the PGISp mice (Figure 3.1A and D, arrowheads). None of these features were observed in the middle-lower thoracic spine of control mice (Figure 3.1F-J).

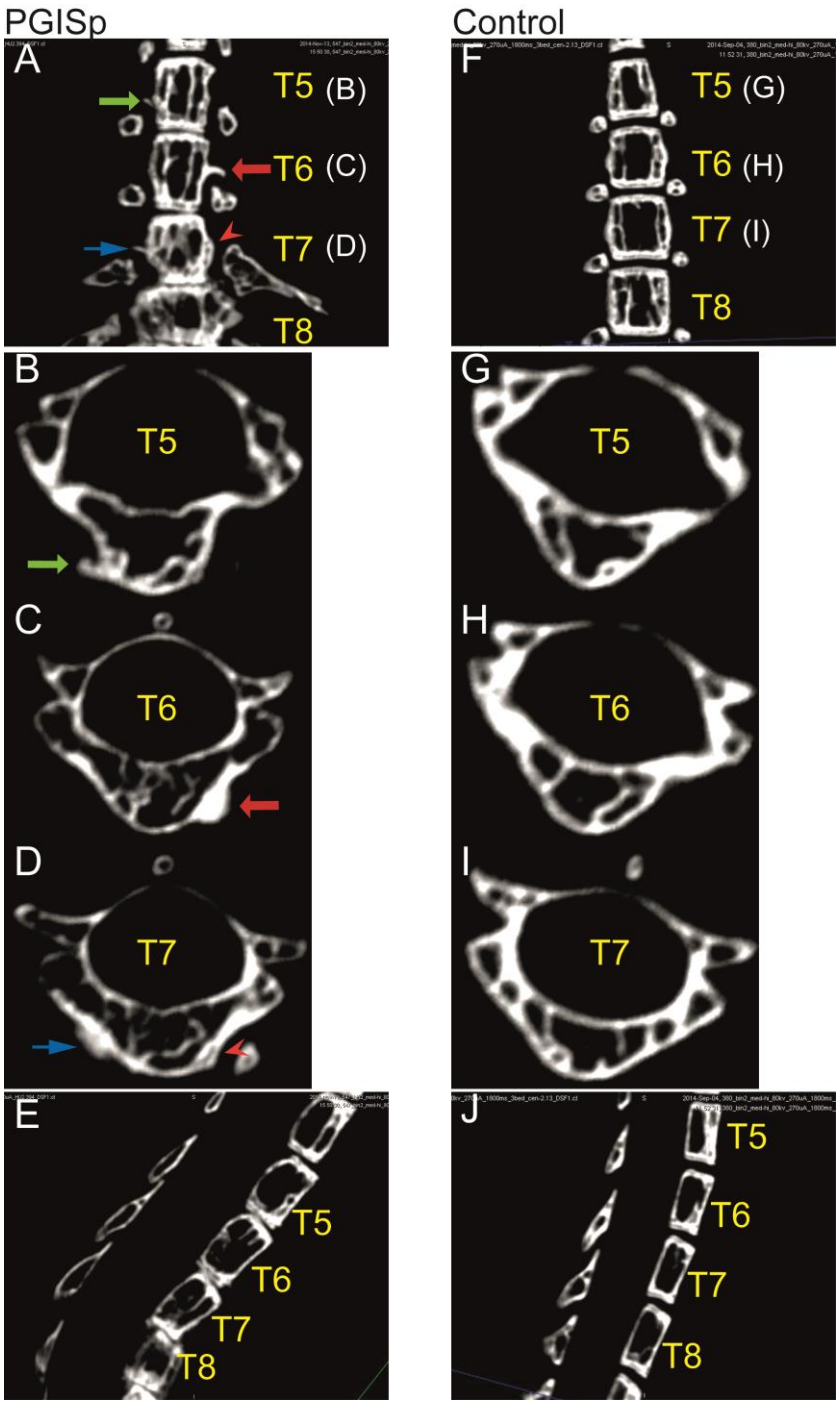

Figure 3.1: Osteophyte formation of the PGISp mice.

CT images were taken from the eighth to eleventh thoracic vertebrae (T5-T8) of a PGISp

mouse at time point 40 weeks on **(A)** anteroposterior view, **(B-D)** transverse sections on **(B)** T5, **(C)** T6 **(D)** T7, and **(E)** lateral view. Osteophytes are indicated by green, red and blue arrows while red arrowheads indicate ectopic bone formation. **(F-J)** The thoracic spine (T5-T8) of an age-matched healthy control IL-$4^{-/-}$ mouse on **(F)** anteroposterior view, transverse sections of **(G)** T5, **(H)** T6, **(I)** T7 and **(J)** lateral view.

Most PGISp mice at 38-43 weeks developed extensive ectopic hyperdense mineralised structures that led to ragged bone surface and widening of almost every vertebral body above the third thoracic vertebrae (T3) (Figure 3.2). These mineralised structures in the upper thoracic spine were seen on the lateral view (Figure 3.2A-D, red arrows) but not the anteroposterior view (Figure 3.2E). Histological assessment of the same samples, with section orientation and depth matching CT plane and depth, showed that these mineralised structures lacked safranin O positive PG (Figure 3.2C, red arrows) but contained high type I collagen positive matrix (Figure 3.2D, red arrows). These observations indicate that these are areas of ectopic mature bone formation. Most excess tissues at the edge of vertebrae contained high PG (Figure 3.2C, asterisk) in the absence of type I collagen (Figure 3.2D, asterisk). Some PG-expressing chondrocytes were embedded in the matrix that contained very low PG (Figure 3.2C, black arrowheads) and no type I collagen expression (Figure 3.2D, black arrowheads). Compared to diseased mice, healthy aged IL-$4^{-/-}$ mice showed a normal appearance with a smooth cortical surface of vertebral bodies (Figure 3.2F, G).

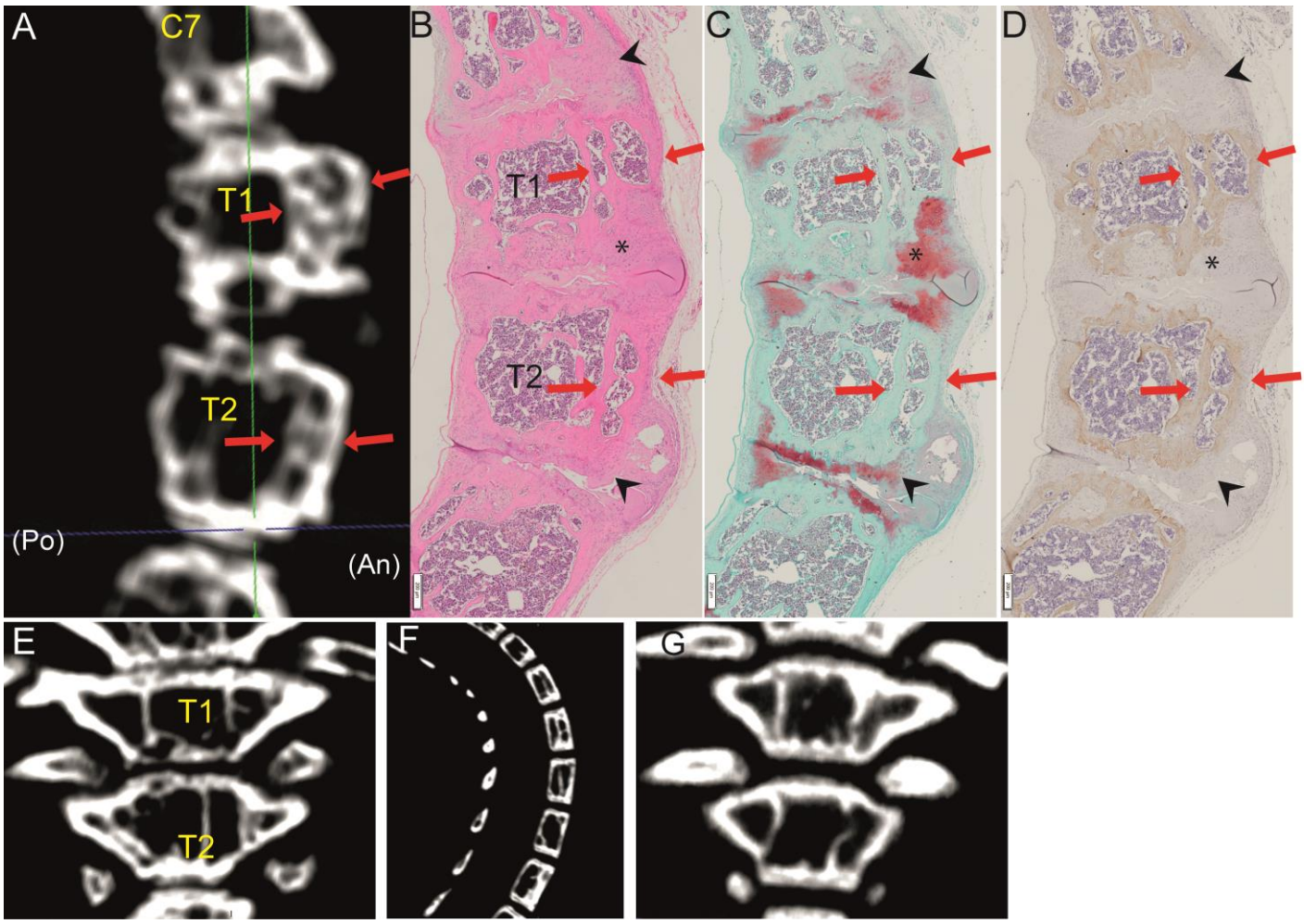

Figure 3.2: Ectopic bone formation of the PGISp mice.

(A-G) Extensive ectopic bone formation in T1-T2 of a PGISp mouse at 40 weeks. **(A)** Lateral view of CT image, **(B)** H&E stain **(C)** safranin O/fast green stain and **(D**) type I collagen IHC. **(E)** Anteroposterior view in matched joints. Ectopic bone formation is shown between red arrows. Asterisk indicates high PG cartilaginous excessive tissues. Arrow heads indicates transition from cartilage to chondroidal bone. **(F-G)** CT images of upper thoracic spine of an age-matched healthy control on **(F)** lateral and **(G)** anteroposterior view. Scale bar in (B-D): 200 μm. An: anterior. Po: posterior.

3-3.2 Fusion of vertebral bodies and zygapophysial joints in PGISp mice

Hyperdense CT signal was observed between vertebral bodies and zygapophysial joints indicating bony fusion. Complete vertebral fusion was only seen in the cervical spine

(Figure 3.3A-D). The cartilaginous endplate and growth plate remnants had fused with the adjacent trabeculae (Figure 3.3 A-E, yellow arrows). To demonstrate that transformation from cartilaginous excessive tissue (Figure 3.3F-H, black arrows and asterisks) to chondroidal bone (Figure 3.3F-H, black arrowheads) have occurred, serial sections were stained for both cartilaginous and bone components. Cartilaginous excessive tissue expressed high PG and, variable type II collagen without type I collagen (Figure 3.3F-H, black arrows and asteriks). In contrast, the periphery of excessive tissue near the fused IVD (Figure 3.3C, boxed area and Figure 3.3 F, black arrow heads) gradually lost PG (Figure 3.3F, black arrowhead) and type II collagen (Figure 3.3G, black arrowhead) but showed increased type I collagen expression indicating chondroidal bone formation rather than merely fibrocartilage or PG-depleted cartilage (Figure 3.3H, black arrowhead).

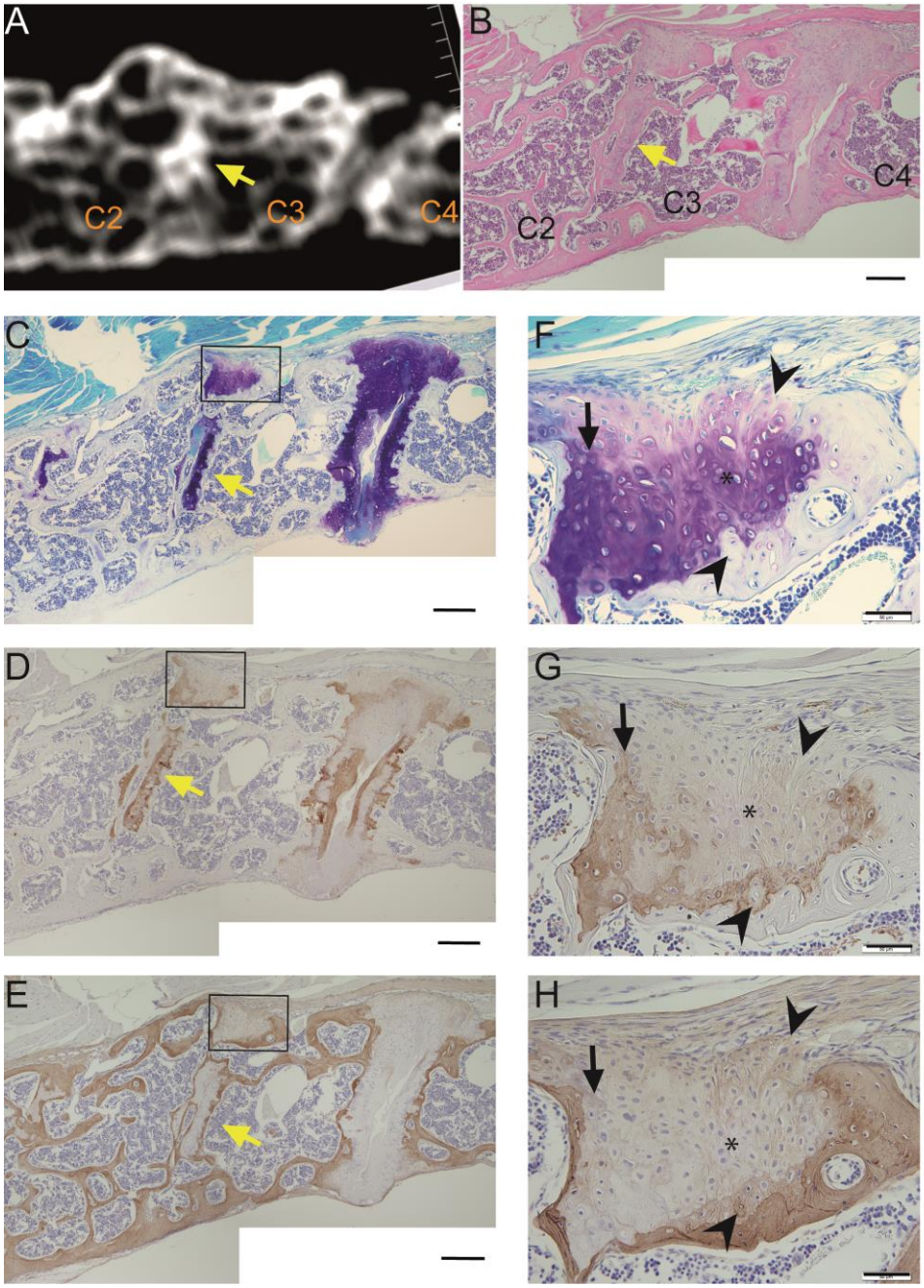

Figure 3.3: Vertebral body fusion in the PGISp mice.

Fusion of the second and third cervical vertebrae (C2-C3) on the **(A)** CT image, **(B)** H&E stain, **(C)** toluidine blue stain, **(D)** type II collagen and **(E)** type I collagen IHC. Yellow arrows indicate remnant endplate and growth plate. The black box delineates the region shown in **(F-H)**. Black arrows identify areas with high PG and high type II collagen content but no type I collagen; while asterisks represent cartilaginous tissues with high PG content but low type II collagen expression. Black arrowheads show chondroidal bone that expresses type I collagen but low cartilaginous matrix. Scale bar: (B-E) 200 μm, (F-H) 50 μm.

The zygapophysial joints have been suggested to be involved in AS [79, 231]. In the PGISp mouse model, a number of zygapophysial joints were fused (Figure 3.4, red arrows). Zygapophysial joint fusion did not show preference in a specific spinal region and the presence of other abnormal mineralisation features in the vertebral bodies was not predictive for zygapophysial joint fusion.

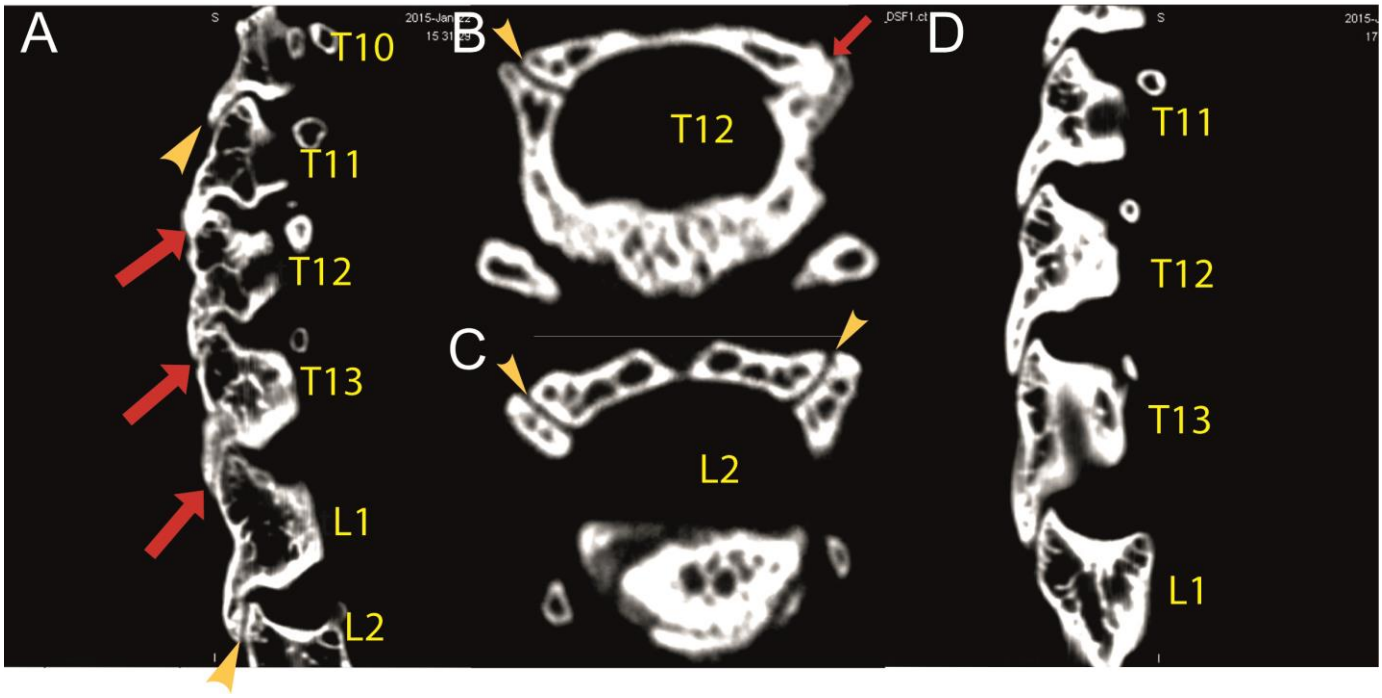

Figure 3.4: Zygapophysial joint fusion in the PGISp mice.

CT images on **(A)** lateral view of the spine from the 10th thoracic vertebrae (T10) to the second lumbar vertebrae (L2). Yellow arrowheads identify unfused zygapophysial joints showing clear hypodense CT signal gaps between joints. Red arrows highlight fused joints. **(B)** Transversal sections of one unfused (yellow arrowhead) and one fused zygapophysial joint (red arrow) **(C)** An affected vertebrae with both zygapophysial joints unfused. **(D)** CT images of T11-L1 of an age-matched healthy control on lateral view.

3-3.3 Mineralisation of the cartilaginous excessive tissue

To study whether excessive tissues progressed to bone or mineralised cartilage, CT images were aligned with the H&E, safranin O/fast green and type I collagen stained sections from the same bones. This approach facilitated delineation of exactly which tissues were mineralised in the CT images.

The normal IVD structure had a hypodense gap between adjacent vertebral bodies with CT imaging (Figure 3.5A) with the mineralised endplate (yellow arrowheads) and subchondral bone separated by un-mineralised growth plates (red arrows). Histology analysis confirmed the IVD had normal appearance on H&E stain (Figure 3.5B) with expected PG distribution in safranin O/fast green staining (Figure 3.5C) and expected type I collagen distribution by IHC (Figure 3.5D).

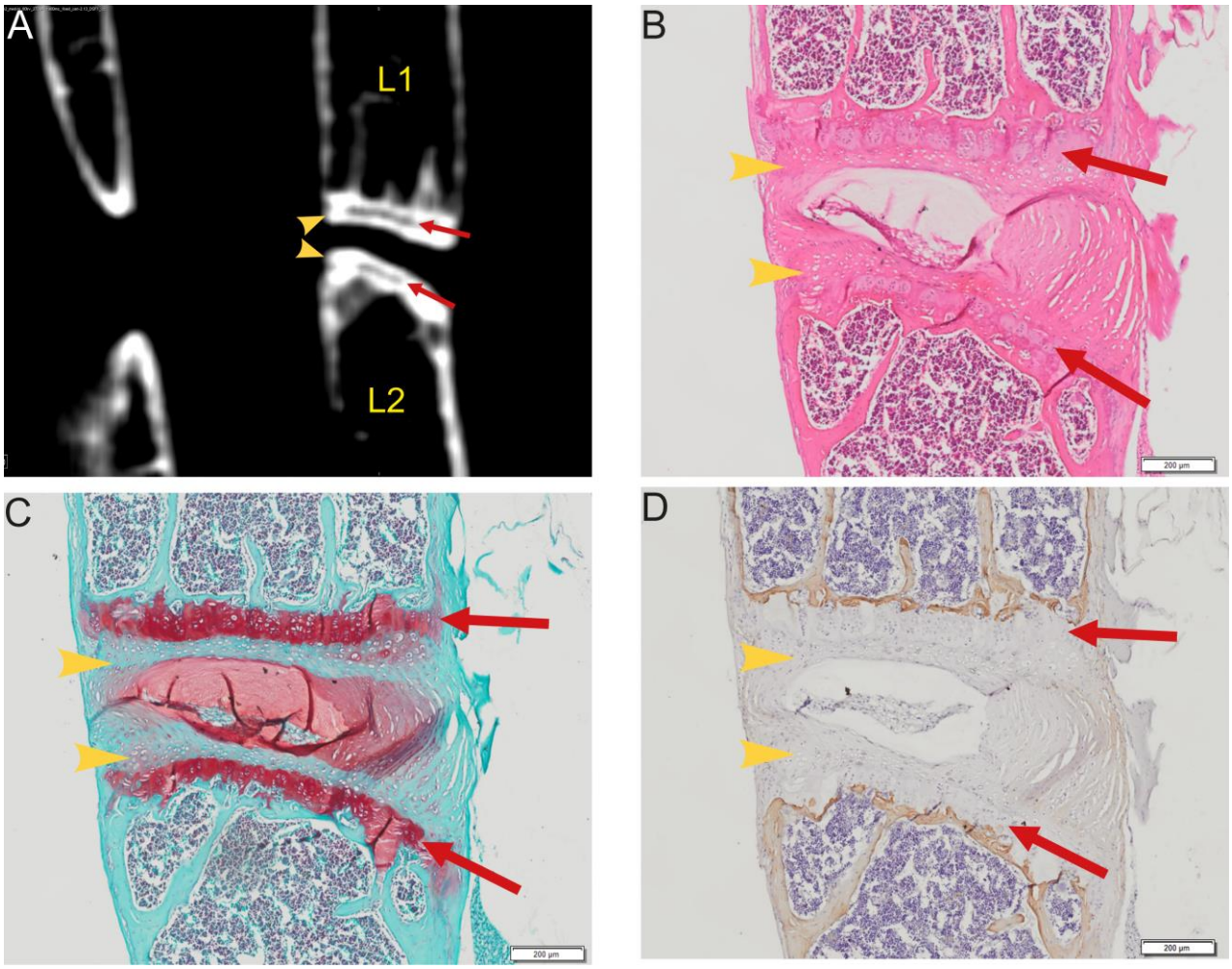

Figure 3.5: An unaffected IVD on lateral view

(A) CT image, **(B)** H&E stain **(C)** safranin O/fast green stain and **(D)** type I collagen of an unaffected IVD (between L1-L2) of a PGISp mouse at 40 weeks. Yellow arrowheads indicate cartilage endplates. Red arrows indicate growth plates. Scale bar: (B-D) 200 μm.

Histological analysis in PGISP mice showed that the excess tissue in mice collected 38-43 weeks after priming had cartilage morphology similar to that observed at 24 weeks and reported in Chapter 2. These excessive tissue deposits were often associated with foci of hyperdense mineralised material on CT images (Figure 3.6, yellow arrowheads). These mineralised foci were always observed near the vertebral corners without direct connection with cortical bone. The excessive tissues in the same region of the CT foci were abundant in chondrocytes (Figure 3.6B, yellow arrowhead) and PG-enriched matrix (Figure 3.6C, yellow arrowhead) but not type I collagen positive matrix (Figure 3.6D, yellow arrowhead). The hyperdense CT signal of these mineralised foci (Figure 3.7A, yellow arrowhead) could also be associated with necrotic disc that still contained remnant annulus fibrosus (Figure 3.7B, yellow arrowheads) and low PG (Figure 3.7C, yellow arrowheads). These mineralised foci were frequently observed along the spine; however, it required histology analysis to differentiate whether theses hyperdense CT signals located in excessive tissue or necrotic disc.

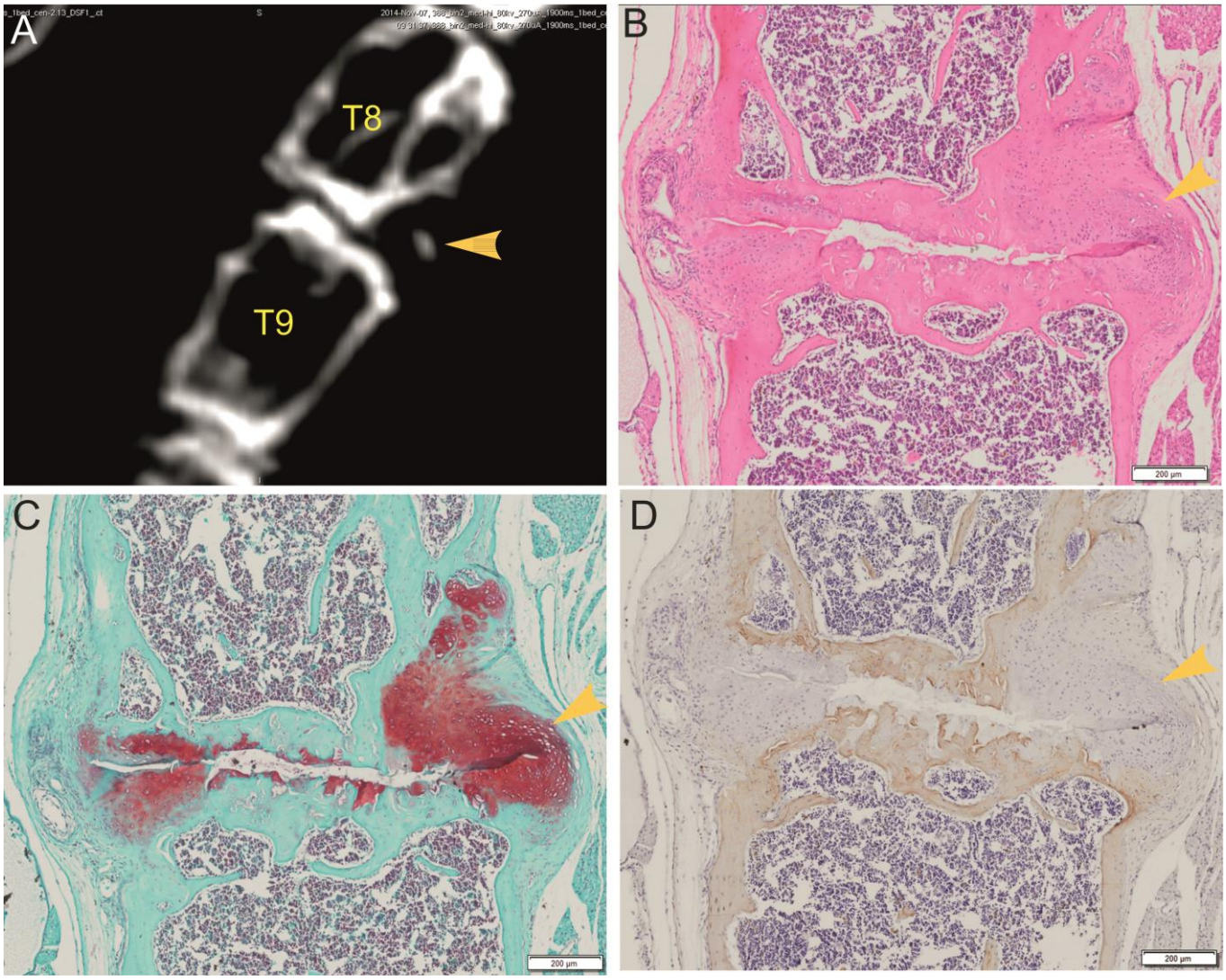

Figure 3.6: Calcification of cartilaginous excessive tissue.

(A) CT image of an IVD between T8 and T9 taken from a PGISp mouse at 40-weeks. **(B)** H&E stain, **(C)** safranin O/fast green stain and **(D)** type I collagen of matched IVD on CT images. Yellow arrowhead indicates mineralised tissue. Scale bar: (B-D) 200 µm.

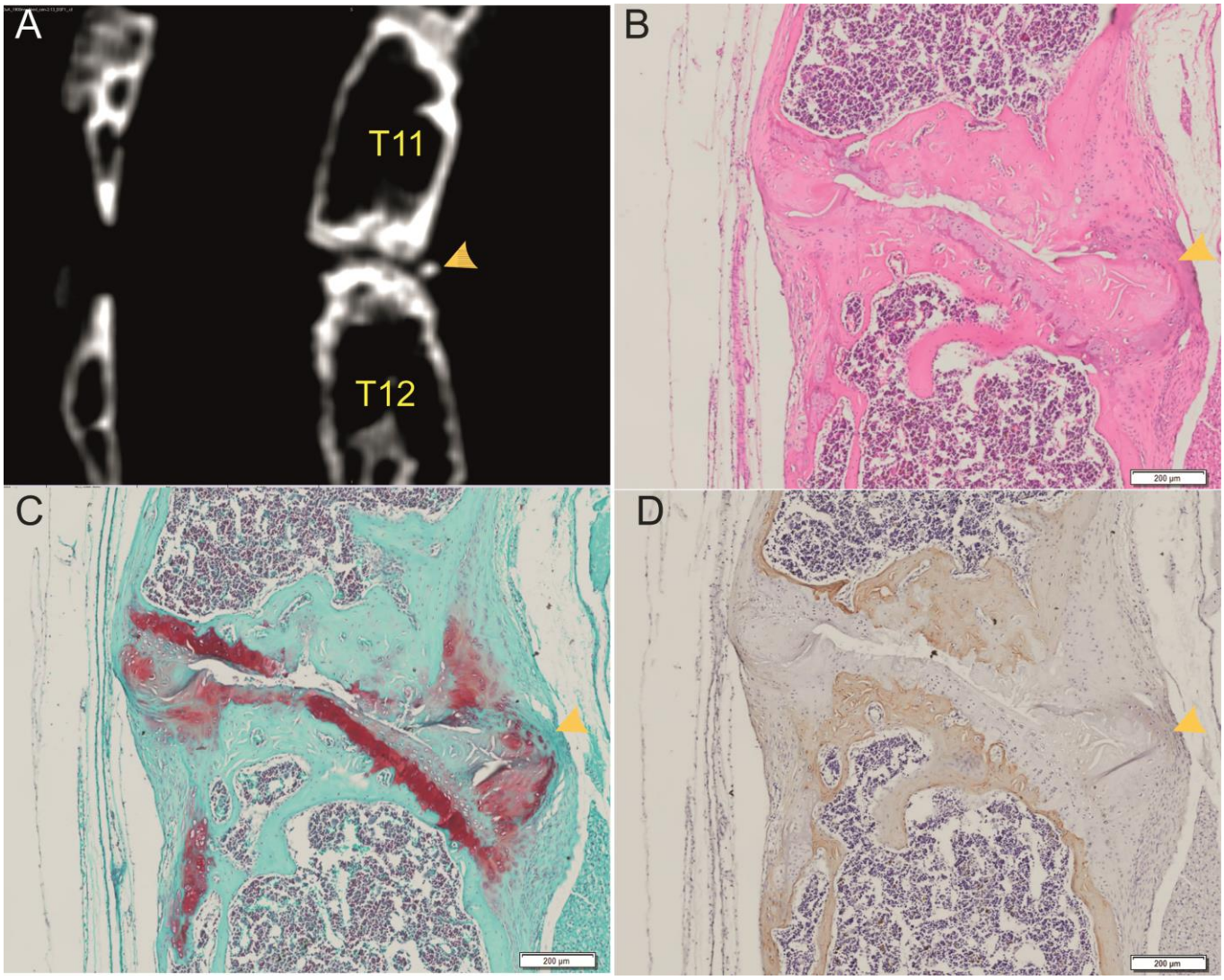

Figure 3.7: Mineralisation of necrotic disc remnants.

(A) CT image of an IVD between T11-T12 taken from a PGISp mouse at 40-weeks. Yellow arrowhead indicates the mineralised disc. **(B)** H&E stain, **(C)** safranin O /fast green stain and **(D)** type I collagen of the same IVD. Scale bar: (B-D) 200 µm.

3-3.4 Mineralisation in IVD of PGISp mice

Extremely hyperdense CT signal areas were frequently noted filling in the IVD space, particularly in the lumbar or lower thoracic spine (Figure 8A, asterisks). All mice had 1-3 IVDs showing this feature in the present study. Histology analysis demonstrated that these mineralised areas had cracked, acellular appearance (Figure 3.8B, asterisks), lacked PG

(Figure 8C, asterisks) and type I collagen expression (Figure 3.8D, asterisks), again suggestive of necrotic disk remnants. However, not all regions of observed necrotic tissue (Figure 3.9, red asterisks) and cartilaginous excessive tissue (Figure 3.9, blue arrow) were mineralised based on CT imaging (Figure 3.9A and B).

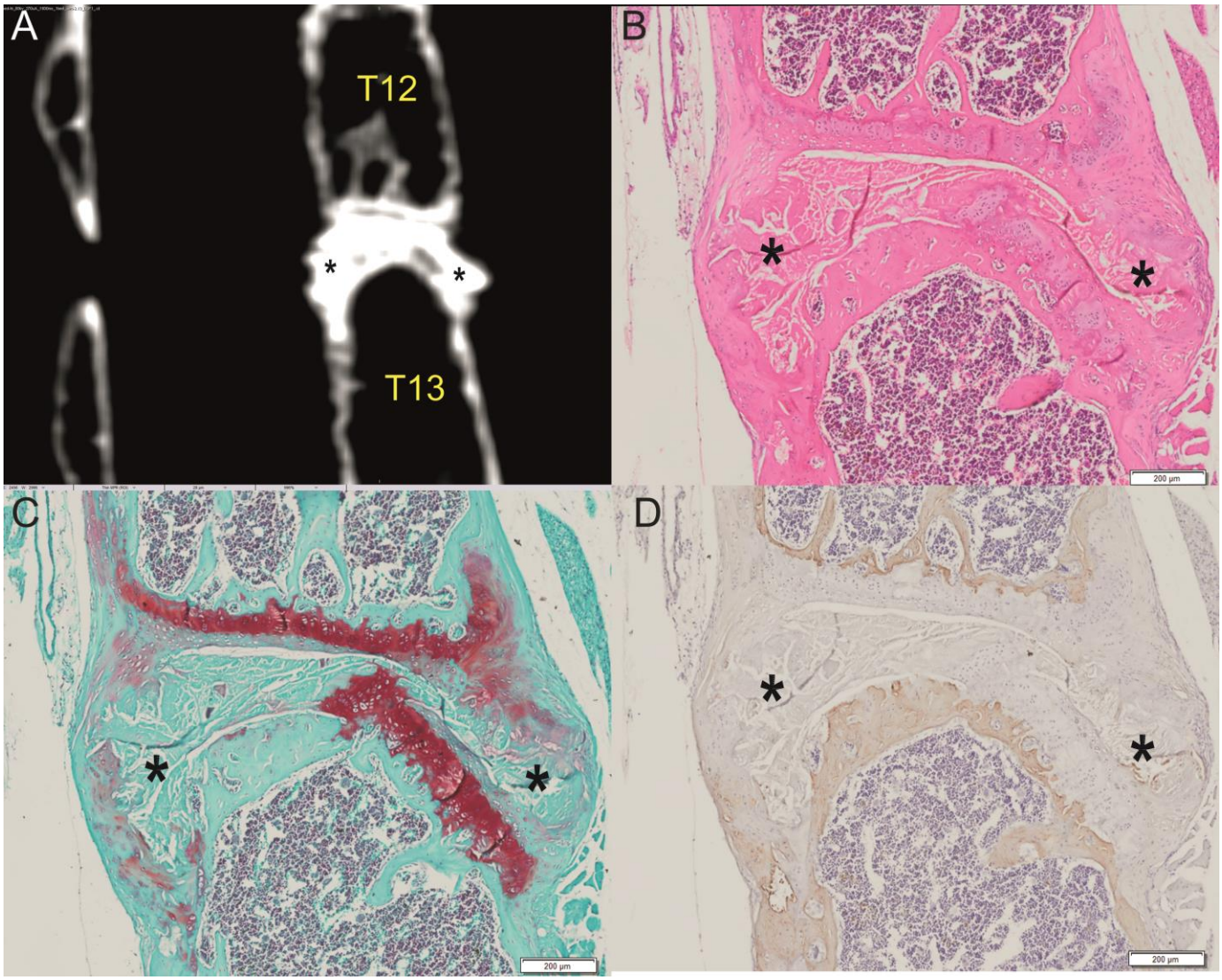

Figure 3.8: Mineral deposition within the IVD space.

(A) CT image of an IVD between T12-T13 taken from a PGISp mouse at 40-weeks. Asterisk indicates the mineralised tissue. **(B)** H&E stain, **(C)** safranin O/fast green stain and **(D)** type I collagen IHC in serial sections of matched IVD. Scale bar in (B-D): 200 µm.

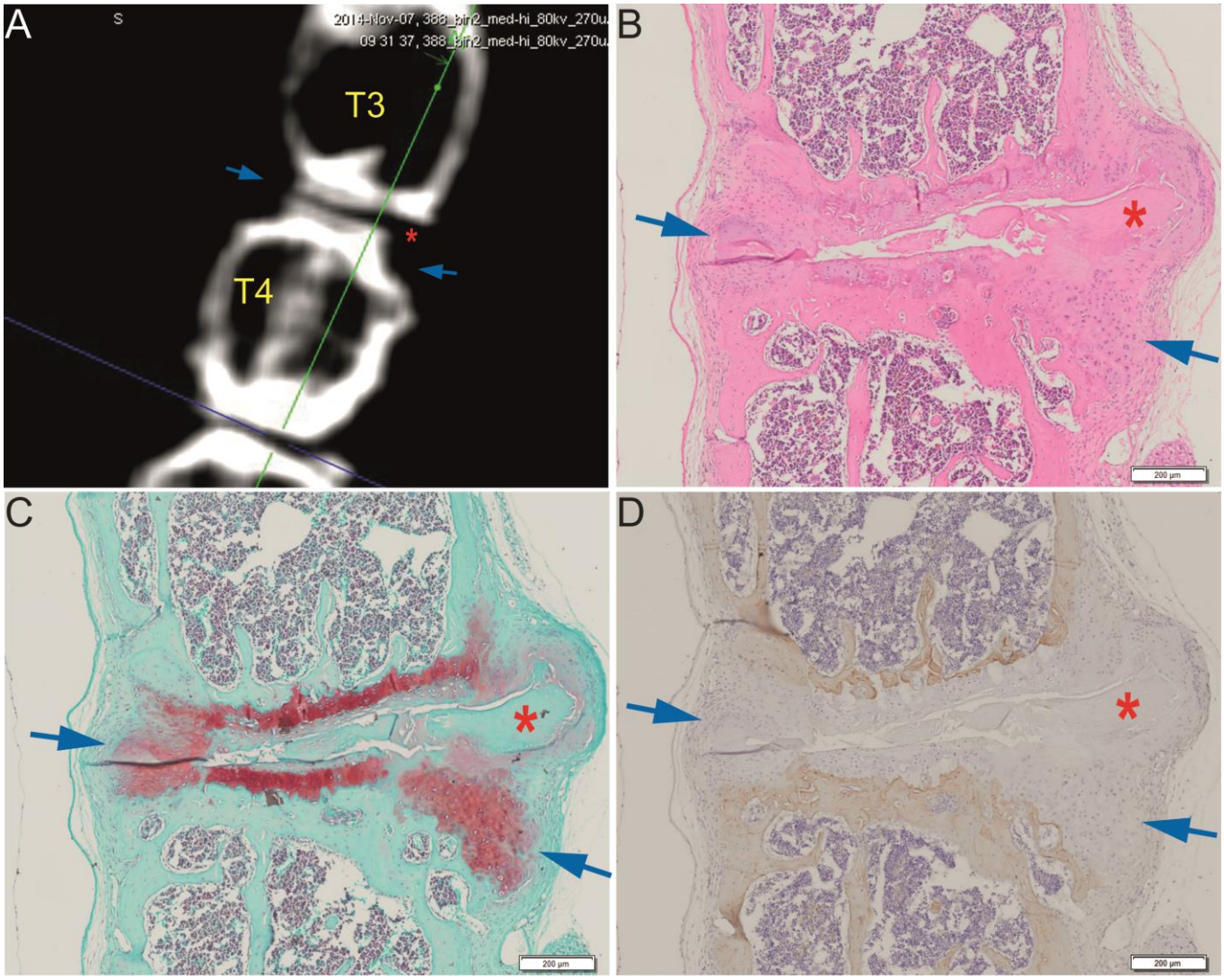

Figure 3.9: Unmineralised excessive tissue formation and necrotic tissue.

CT image of an IVD between T3-T4 taken from a PGISp mouse at 40-week time point. **(B)** H&E stain, **(C)** safranin O/fast green stain and **(D)** type I collagen IHC in serial sections of the matched IVD. Red asterisk indicate necrotic disc while blue arrows indicate non-mineralised excessive tissue that can only be seen by histology but not on CT scan. Scale bar: (B-D) 200 μm.

3-3.5 Mapping aberrant mineralisation in the PGISp mice

The most frequency and anatomical distribution of each of the CT exposed features was mapped schematically in Figure 3.10. Features distributed all along the spine were mineralised foci and zygapophysial joint fusion. Extensive ectopic bone developed on

almost every cervical and upper thoracic spine above T3, while osteophyte formation was the major feature in the lower thoracic spine. Ectopic bone and osteophytes were found in other regions but at lower frequency, and ectopic bone formation in the lower thoracic spine was usually smaller than the ones on the upper spine. Mineral deposition was only present in 1-3 IVD in the lower thoracic or lumbar spine in any of the mice analysed.

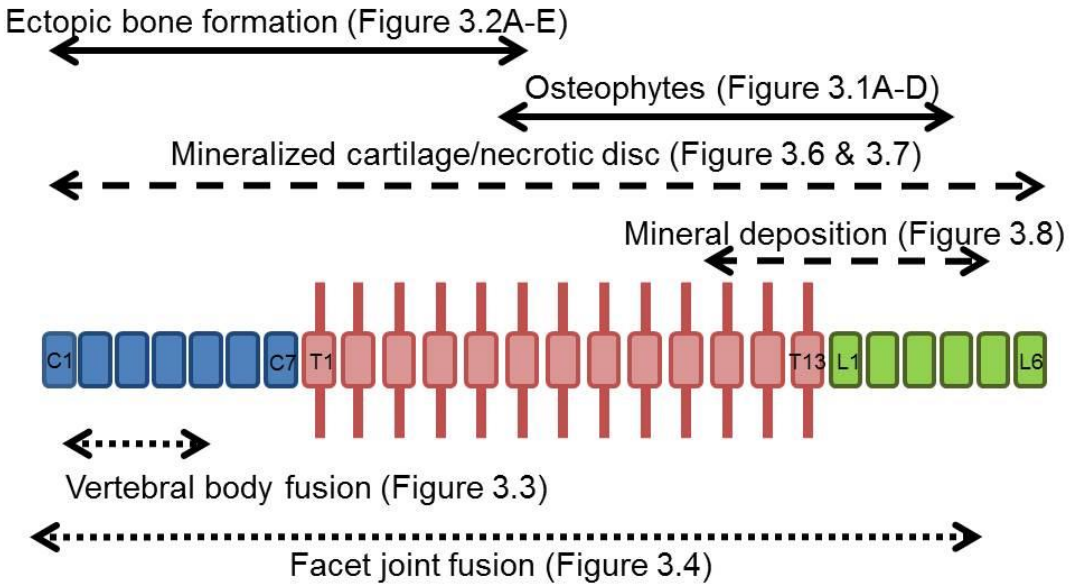

Figure 3.10: Distribution of abnormal bone formation, mineralisation and fusion features in the PGISp mice.

The schematic map is based on CT images of PGISp mice at 38-43 weeks post priming (n=7). Solid lines are features of abnormal bone formation; dashed lines are features of mineralisation related to IVD or cartilage; dotted lines are fusion of joints. C: cervical vertebrae. T: thoracic vertebrae. L: lumbar vertebrae.

3-4 Discussion

In the studies reported in Chapter 3 we anticipated observation of more osteophyte formation in mice with advanced disease compared to Chapter 2. The observations reported in this chapter showed that extensive mineralisation of this tissue did occur in the PGISp model but progression required an extended time period. This kinetics of progression is not dissimilar to AS which often has a protracted disease course [232]. Our assessment of mineralised pathological tissue patterns presented as several interesting abnormal bone formation and mineralisation features: osteophyte, ectopic bone, mineralised cartilage, mineralised IVD, vertebral body and zygapophysial joint fusion.

There are some discrepancies between abnormal bone formation in the PGISp mice and the syndesmophytes in AS patients. The syndesmophytes of AS patients usually develop from the vertebral corners at an angle <45° and bridge two adjacent vertebral bodies [233]. However, the osteophytes of PGISp mice grew outwards, and mineralised cartilage in the excessive tissue did not bridge the vertebral bodies. The upright/bipedal posture, anatomical structure and less severe IVD destruction in AS patients might generate distinct mechanical stress that acts upon the spine thus explaining the variation is osteophyte distribution and angle. Despite this variation, in comparison with other SpA animal models, discussed in detail within the literature review presented in Chapter 1, the PGISp mouse model still presents the most similar spinal disease progression to that seen in AS patients. Due to this we believe it is currently the best animal model to study how inflammation and structural damage can induce excessive bone formation and abnormal mineralisation in the spine.

In the end of Chapter 2, we hypothesized that inflammation-derived IVD destruction altered mechanical stress, which subsequently activated osteoproliferation and result in excessive tissue formation. In the extended time course study, all the abnormal bone formation features were observed in affected vertebral joints. Hence, the current results still support our earlier conclusion. The various morphologies, orientation and frequency of these features might be due to the crouched/quadrapedal posture of mice that results in differences in the mechanical stresses acting on the spine.

Biomechanical stress has been suggested to be associated with enthesitis in the TNFΔARE mice and osteophyte formation in the CAIA [169]. In the 24-week time course study, we suggested that entheses at the interface between anterior/posterior longitudinal ligaments were potentially involved in the disease initiation and development. If this was the case, it would be expected that most ectopic bone and osteophytes formation would develop near the anterior/posterior longitudinal ligament entheses. However, much of the osteoproliferation was not associated with entheses in the present study. CT quantitative analyses in AS patients also showed that syndesmophytes developing from vertebral rim were not always related to anterior/posterior longitudinal ligament entheses [219]. These suggest that entheseal mechanical stress might not be the only factor influencing this pathologic outcome.

It is noteworthy that the abnormal bone formation reported in this Chapter occurred in a similar anatomical position to the severe inflammatory infiltrates (Chapter 2, Figure 2.2E) and ectopic chondrocytes (Chapter 2, Figure 2.3C) that were observed adjacent to the periosteum during 24-week time course study. The ectopic chondrocytes that presented with a columnar distribution similar to growth plate might contribute to abnormal bone formation through an endochondral ossification-like mechanism. The periosteal layer is known to contain osteo-chondroprogenitors that can give rise to either cartilage or bone under the right conditions through either endochondral or intramembranous bone formation [234, 235]. Filling the sub-periosteal space with osteo- or chondro-inducing biomaterials led to *in situ* woven bone or cartilage formation without supplementing with growth factors or additional progenitor cells [236]. Periosteal osteophyte formation is also a feature of a number of arthritic animal models, such as the AIA, CIA rat models [237], K/BxN serum transfer mouse model [238, 239] and the DBA mouse model of SpA [240]. Therefore, periosteal reaction might contribute to ectopic chondrocyte and abnormal bone formation in inflammatory arthritis. Further histological analyses across the time course or dynamic histomorphometric analysis are required to determine when and how the ectopic bone develops.

Large anterior osteophytes have been known to result in dysphagia and airway obstruction in AS patients [241, 242].The cervical and upper thoracic vertebrae in this model presented the least well preserved vertebral structure with CT images showing

extensive erosion, ectopic bone, excessive tissue formation and vertebrae fusion (Figure 3.2 and 3.3). Ectopic bone and the adjacent excessive tissues appeared like a disorganized expansion of the vertebral body and cartilaginous endplate/growth plate.

The histology showed that the majority of excessive tissues near the vertebral corners in the PGISp mouse model retained cartilage morphology even 43 weeks post priming. Mineralisation assessed through CT images suggests the presence of mineralised cartilage. Direct transformation from chondrocytes to osteoblasts have been suggested in normal bone development [83] as well as in the zygapophyseal joints of AS patients [79]. Direct Von kossa and masson trichrome stains would be more appropriate for studying calcification than H&E stain in the present study. Un-decalcified sections stained with a nonaqueous alcoholic eosin staining method [243] or alizarin red [244] under polarizing microscopy compared with an immediate section stained with H&E and collagen type II would help to clarify the components of calcified materials.

IVD calcification has been reported in fused spines in AS [245]. Altered calcium metabolism has been suggested to contribute to AS, such as increased carbonic anhydrase I (CAI), an enzyme that catalyses the hydration of CO_2 to H_2CO_3 and participates in calcium deposition [246, 247]. ANK a transmembrane protein that exports inorganic pyrophosphate (ppi) and maintains the ratio of intracellular to extracellular ppi concentration [248], is increased in the progressive ankylosis (ank) model [7]. Loss-of-function mutation [249] and deletion of *ank* [40] leads to ectopic bone formation in almost all joints in these mice. The spinal disease of the *ank/ank* mouse model, which carries loss-function mutant *ank*, displayed mineral deposition and chondrocyte hypertrophy in the annulus fibrosus by the age of 8 weeks, and complete ankylosis by syndesmophytes by 18 weeks [39]. However, the important element of AS, inflammation, is absent in the disease development of *ank/ank* mouse model. Therefore, altered calcium metabolism might be a second co-trigger of osteoproliferation. IVD calcification is found in other degeneration-related disc pathological conditions, such as disc degeneration disease [250] and protruding disc [251], suggesting it might be associated with mechanical force.

The location and orientation of osteophytes might explain why these features were rarely seen in the earlier 24-week time course histological analysis, even though these mice

might have already developed osteophytes. The tissue collected in the previous 24-week time course experiment only included middle-lower thoracic to upper lumbar spine. Histological analysis focused on the sagittal sections (equivalent to the lateral view of CT images) of the centre of the vertebral bodies. This method allows clear images of most IVD and is ideal for scoring other features that are not region- and orientation- specific. However, most osteophytes were small and developed on the lateral sides of the vertebral bodies, implying our histological analysis was not ideal for detecting osteophytes. However, the upper thoracic spine, on which osteophytes should be clearly seen on the lateral view as Figure 3, was not collected in the 24-week time course experiment. Therefore, the better protocol to study abnormal bone formation in PGISp mice is to perform *in vivo* CT assessment during the time course to follow the progression of osteophyte/ectopic bone formation, and before processing for histological analysis and decide the orientation of histological analysis based on CT images.

Taken together, we have demonstrated a number of interesting anabolic features in the PGISp mouse model, including abnormal cartilage and bone formation features. We suggested that chondroidal ossification is involved in the excessive tissue formation near destroyed IVDs. Also the excessive cartilaginous tissue reported at 24 weeks might be transformed into mineralised cartilage over an extended time period. Finally, periosteal reactions might be involved in the formation of multiple osteophytes and ectopic bones adjacent to periosteum in the middle of the vertebral bodies.

4 Chapter 4: Targeting PTGER4 as a potential therapeutic approach in AS

4-1 Introduction

A single nucleotide polymorphism (SNP) near *PTGER4* that increases the risk of AS was identified in genome-wide association studies (GWAS) [51]. *PTGER4* encodes one of the prostaglandin E2 (PGE2) receptors, PGE2 receptor subtype 4 (EP4). EP2 and EP4 are the predominant PGE2 receptors expressed on cells involved in inflammation and bone formation [252, 253] which are features of early and late stage AS respectively.

PGE2 has both pro-inflammatory and anti-inflammatory roles. Its immune suppressive functions include down-regulating IFN-γ production by macrophages [254] and inhibiting neutrophil recruitment to the inflamed intestine [255]. Recent studies indicate that the pro-inflammatory roles of this PGE2/EP2/EP4 axis are mainly through regulating Th1/Th17 cell development. Low PGE2 levels assist Th1 differentiation while high levels induce Th17 differentiation [256]. This pathway also facilitates IL-23-induced Th17 development by increasing IL-23 expression in dendritic cells [256, 257]. Misoprostol, a non-selective EP agonist, has been shown to augment arthritic symptoms in the CAIA model and increase inflammatory cytokine expression in the joints, including IL-23, IL-17, TNF and IL-6 [258]. Non-steroidal anti-inflammatory drugs (NSAIDs) are non-selective cyclooxygenase inhibitors that exert anti-inflammatory effects by blocking PGE2 synthesis (Figure 1.2). NSAIDs have been recommended as the first-line therapy for AS [115].

The pro-inflammatory role of PGE2/EP4 signalling in arthritis has been studied using gene knockout mice, as well as with receptor subtype-specific agonists and antagonists. EP4 deficiency [259] and ER-886046, an EP4 antagonist [260], significantly reduced the incidence and severity of CAIA. Prophylactic or therapeutic administration of ER-819762, an EP4 antagonist, improved the clinical symptoms of both CIA and glucose-6-phosphate isomerase (GPI)-induced arthritis mouse model [257]. Prophylactic administration of CJ-023,423 [261] or therapeutic administration of MF498 [262], two different EP4 antagonists, significantly reduced paw swelling in the AIA rat model. The above studies suggest that EP4 specific antagonists might be potential anti-inflammatory therapies in arthritis.

PGE2 also plays important roles in bone anabolism mainly through EP2 and EP4. PGE2 mediates mechanical stress-induced bone formation [263]. It up-regulates the expression and activity of a gap junction protein, connexion 43, which is a gap junctional intercellular communication subunit important in bone cell communication [264]. Deficiency of EP4 led to decreased osteoblastogenesis and osteopenia [88, 265], whereas ONO-4819, an EP4 agonist, enhanced osteoblasts differentiation in animal models [266]. Administration of ONO-AE1-329, an EP4-specific agonist, increased osteoblast number and bone mineral density in ovariectomised rats [88]. CP-734432, another EP4 agonist, rescued the delayed and impaired fracture healing responses in COX-2 knockout mice [87]. In opposition to its anabolic effects, PGE2 also exerts catabolic effects through up-regulating osteoclastogenesis via EP2 and EP4 [267, 268]. An *in vitro* study showed that PGE2 induced osteoclast differentiation in mouse bone marrow culture; the effect was partially replicated by ONO-AE1-259 (EP2 agonist) or ONO-AE1-329 (EP4 agonists) alone, while the synergistic effect of these two agonists was similar to PGE2 stimulation [269]. PGE2 signalling regulates both anabolic and catabolic process during bone remodelling, while the overall effects of activation of PGE2 signalling dominates anabolic effects *in vivo* [266, 270].

NSAIDs have been reported to retard radiographic progression at high dose [96] and continuous use [97, 271] compared to low dose treatment. However, it is not yet clear whether decreased radiographic progression is due to inhibition of bone formation or through inhibiting inflammation.

Based on the following rationale, we hypothesized that activation of PGE2/EP4 signalling plays an important role in AS pathogenesis: 1) *PTGER4* is associated with AS, 2) AS is characterised by both inflammation and ectopic osteoproliferation and 3) PGE2/EP2/EP4 signalling can promote both inflammation and bone formation. Therefore, the PGE2/EP4 axis may be a common signalling pathway that drives both inflammation and the progression to osteoproliferation in AS. To test this hypothesis, PGISp mice were treated with an EP4 antagonist, ONO-AE2-227, or an agonist, ONO-AE1-329. To differentiate the effects of EP4 from other EPs, indomethacin, a non-selective COX inhibitor which blocks PGE2 production and the downstream EP1-4 signalling, was used in the study as a positive control. Intermittent human parathyroid hormone peptide 1-34 (hPTH 1-34)

treatment served as a positive control for bone anabolism as it has been shown to increase osteoblastogenesis [272]. Treatment with hPTH 1-34 had been widely used in clinic to prevent fracture and improve bone mineral density (BMD) [273-275]. We predicted that ONO-AE2-227 and indomethacin would reduce the severity of inflammation and excessive tissue formation whereas ONO-AE1-329 would exacerbate disease.

4-2 Materials and methods

4-2.1 Treatment

The disease induction was conducted as previously detailed in Chapter 2. PGISp mice were treated with ONO-AE1-329 (EP4 agonist), ONO-AE2-227 (EP4 antagonist) [276] or an NSAID, indomethacin, from the first day of immunisation until the day of sacrifice (3-6 mice/group). Table 4-1 lists the details of all treatments and the suppliers of the reagents. All mice were sacrificed 16-20 weeks after the commencement of treatments (Figure 4.1A). IL-$4^{-/-}$ mice used in this study were sourced form an internal breeding colony housed within The University of Queensland Biological Resource Facilities (Princess Alexandra Hospital (PAH) and Australian Institute for Bioengineering and Nanotechnology (AIBN) facilities). All experiments were approved by the University of Queensland animal ethics committee.

Table 4-1: Details of treatments

Drug	Function	Administration	Company	Dosage	Mouse number
ONO-AE1-329	EP4 agonist	Subcutaneous injection	Ono Pharmaceutical, Osaka, Japan	0.05 mg/kg/daily	5
				0.1 mg/kg/daily	5
				0.3 mg/kg/daily	6
ONO-AE2-227	EP4 antagonist	Oral gavage	Ono Pharmaceutical,	10 mg/kg/daily	5
				20 mg/kg/daily	5
				30 mg/kg/daily	5
hPTH 1-34	Bone anabolism	Subcutaneous injection	H-4835, Bachem	30 μg/kg/daily,	4

			Bubendorf, Switzerland	5 days/week,	
indomethacin	Non-steroid inflammatory drug	Oral gavage	I8280, Sigma-Aldrich	2 mg/kg/daily	3

4-2.2 Clinical peripheral arthritis score

The peripheral arthritis symptoms of all mice were scored daily. Score criteria are described in Table 4-2. The peripheral scores are presented as the sum of four paws in the following contents and figures.

Table 4-2 Clinical score

Hind limbs	
0	Normal
0.5	Minimal inflammation in only ankle or toe
1	Mild swelling of ankle and tarsal
1.5	Inflammation spreads to metatarsal and toes
2	Severe inflammation from ankle to toes
3	Very severe inflammation from ankle to toes
Front paws	
0	Normal
0.5	Mild swelling in carpal or digits
1	Moderate swelling in the carpal and digits
2	Severe swelling in the carpal and digits

4-2.3 Histology and scoring regimen

The histology and scoring regimens used were the same as in Chapter 2 of this thesis.

4-2.4 Serum cytokine measurement

Anaesthesia was induced by methoxyflurane before cardiac bleeding at sacrifice. Blood samples were clotted at room temperature (RT) for 3 hours and centrifuged at 1000xg for

15 minutes. Serum was separated and stored at -80℃. Serum IL-17 was measured using the IL-17A ELISA MAX™ Deluxe set (BioLegend) following the manufacturer's instructions. Ninety-six well plates were coated with anti-IL-17 antibody overnight at 4℃ and washed in wash buffer (phosphate-Buffered Saline (PBS) plus 0.05% Tween-20, pH7.4). After blocking with assay diluent at RT for one hours, five-fold diluted serum samples and standards were added to the wells and incubated at RT for two hours. All samples and standards were assayed in triplicate. Plates were washed and incubated with biotinylated detection antibody at RT for one hour. Avidin-horseradish peroxidase (HRP) was added and incubated at RT for 30 minutes followed by a 20 minutes reaction in 3, 3′,5,5′-Tetramethylbenzidine substrate in dark. The enzymatic reaction was stopped with 2N H_2SO_4 and the absorbance at 450 and 540 nm was read using a Synergy MX multi-mode reader (Biotek). A standard curve, which included the following concentrations; 1000, 500, 250, 125, 62.5, 31.25, 15.6 and 0 pg/ml, was used to calculate serum IL-17 concentration.

Serum CRP level was measured using mouse CRP ELISA DuoSet kit (R&D system, DY1829, Minneapolis, Minn., USA). The procedure was the similar to the IL-17 ELISA with the following modifications. The serum samples were diluted 15,000 fold in 10% fetal bovine serum (FBS). Plates were coated with capture antibody overnight at RT. The incubation time with biotinylated detection antibody and avidin-HRP was 2 hours and 20 minutes respectively. The standard curve included the following concentrations 1500, 750, 375, 187.5, 93.75, 46.88, 23.44 and 0 pg/ml.

4-2.5 Bone mineral density

BMD and bone mineral content (BMC) were measured by dual x-ray absorptiometry (DXA) using a Piximus (GE Lunar) before and after treatment *in vivo*. Mice were anesthetized by intraperitoneal injection of zoletil (40mg/kg) and xylazine (10mg/kg) before the scan.

4-2.6 CT image

Pelvis bone micro-architecture was imaged using the same acquisition protocol described in Chapter 3. All ONO-AE1-329 and ONO-AE2-227-treated PGISp mice were imaged *in vivo.* Anaesthesia was induced using 1-2% of isoflurane with air-oxygen mixture. The

imaging system was non-functional at the scheduled collection time points for DDA alone-treated mice, hPTH 1-34 and indomethacin-treated PGISp mice. Consequently, no CT data was obtained for indomethacin and hPTH 1-34-treated mice but skeletons of DDA-treated mice were fixed in 4% paraformaldehyde and stored in 70% ethanol until the Inveon had been repaired.

4-2.7 Statistical analyses

The statistical significance of data was analysed by Mann-Whitney analysis. *P* value less than 0.05 was considered as a significant difference. The relationship between two data outputs were determined by Spearman correlation. Above statistical analyses were performed using PRISM 6 (GraphPad Software, La Jolla, CA).

Sample size calculation was conducted using a power calculator (http://powerandsamplesize.com/) with a significance α of 0.05 and power of 1-β=0.8. Sample size was calculated through 2-tailed distribution calculation.

4-3 Results

4-3.1 Peripheral arthritis was not affected by either an EP4 agonist or antagonist

Clinical arthritic scores were used to monitor the development of peripheral arthritis. There was large score variation within groups, which greatly restricted the ability to perform meaningful between-group comparisons with the current sample size. All dosages of ONO-AE1-329 (an EP4 agonist) and 10 and 20 mg/kg/day of ONO-AE2-227 (an EP4 antagonist) resulted in a non-significant trend of reduction in the mean arthritic scores up to 70 days post commencing treatment (Figure 4.1B and C). The small peak of peripheral arthritis scores in the ONO-AE2-227 30 mg/kg/day group between days 30-35 days after treatment was due to extremely severe disease progression in two mice (Figure 4.1C). The onset of peripheral arthritis, defined as the day when any paw reached score one, was delayed in the ONO-AE1-329 0.1 mg/kg/day group (Figure 4.1D). Overall, the EP4 agonist and antagonist did not have a significant impact on peripheral arthritis.

The hPTH 1-34 and indomethacin-treated mice all developed arthritis. However, the symptoms were scored by multiple technicians during a period when I was absent. The data exhibited significant scorer-dependent variation (data not shown). Therefore, the data was deemed to be compromised and was not included in Figure 4.1.

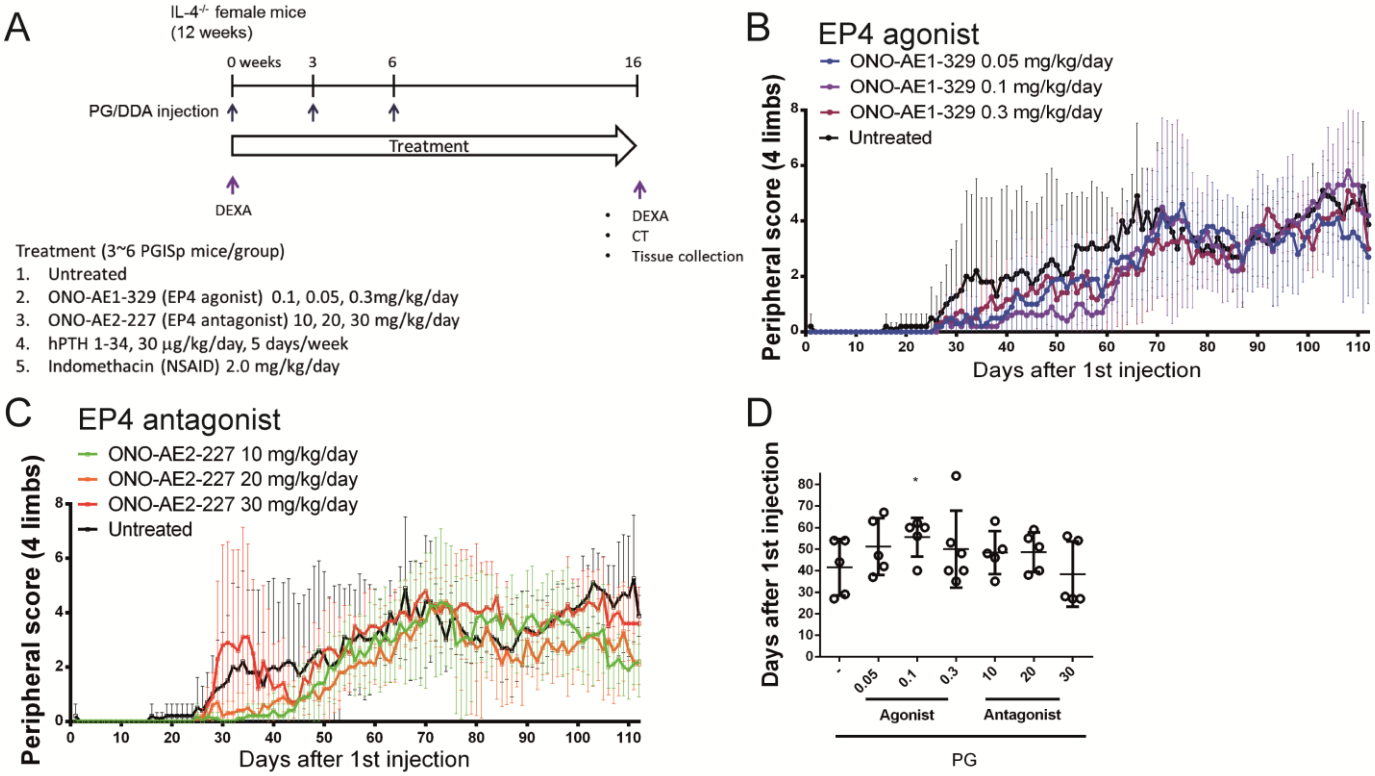

Figure 4.1: Peripheral arthritis was not affected by either an EP4 agonist or antagonist.

(A) PGISp mice were treated with ONO-AE1-329 (EP4 agonist), ONO-AE2-227 (EP4 antagonist), hPTH 1-34 or indomethacin (IND) for 16 weeks from the first day of immunisation. **(B-C)** Peripheral disease development was scored visually and presented by the sum arthritic scores of all four paws across the time course. Agonist and antagonist-treated mice are compared with the same untreated mouse cohort but presented in (B) and (C) respectively**. (D)** The graph shows the disease onset after the first immunisation. Disease onset was determined as the first day of peripheral arthritis score of 1 reached. Data is presented by mean ± SD. The statistical significance of data was analysed by Mann-Whitney analysis. *p<0.05 compared to untreated PGISp mice.

4-3.2 Targeting EP4 did not affect axial disease development

The percentage of affected IVD (Figure 4.2A) and inflammation scores (Figure 4.2B) were not significantly different across all the treatment groups. Only a trend of reduced bone erosion (Figure 4.2C), disc destruction (Figure 4.2D), cartilage damage (Figure 4.2E), and excessive tissue formation (Figure 4.2F), and ectopic chondrocyte formation (Figure 4.2G,)

was noted in the group treated with low dose 0.05mg/kg/day of EP4 agonist. Overall, there were no significant effects on histological scores compared to untreated PGISp mice (Table 4-3, end of Chapter 4).

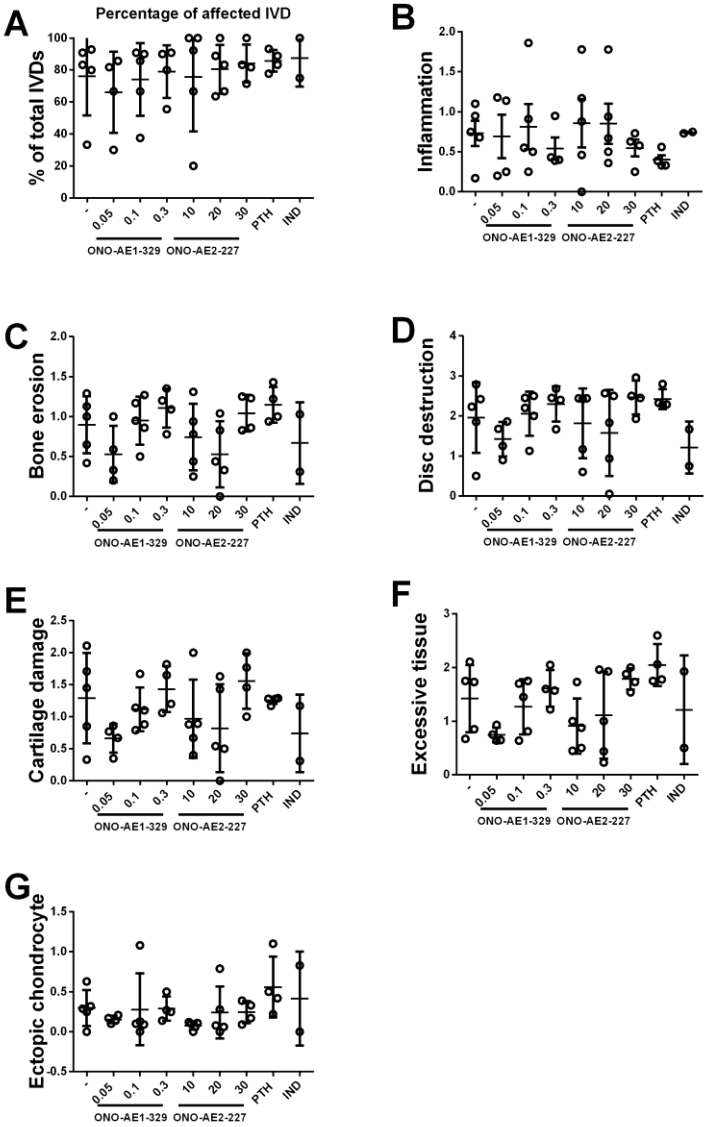

Figure 4.2: Targeting EP4 did not affect axial disease development.

Spinal disease progression scored on H&E staining are described by **(A)** the percentage of affected vertebral joints in one mouse. Histological features include **(B)** inflammation, **(C)** disc destruction, **(D)** bone erosion, **(E)** cartilage damage, **(F)** excessive tissue formation and **(G)** ectopic chondrocyte formation. Data was presented by mean ± SD. Each point represents the average scores of all vertebral joints of one mouse.

4-3.3 Targeting EP4 did not affect serum inflammatory markers

PGE2/EP4 is known to regulate inflammation and Th17 cell in vivo [256]; hence serum IL-17 and CRP levels were used to examine the systemic inflammatory status. Serum IL-17 (Figure 4.3A, p=0.4430) and CRP levels (Figure 4.3B, p=0.4134) did not differ between any of the treatment groups. Final peripheral inflammation scores did not correlate with either serum IL-17 (r=-0.0075, p=0.6703) or CRP (r=-0.1118, p=0.4596). Histological scores did not correlate with serum IL-17 (r=0.1840, p=0.2784) CRP (r=-0.0066, p=0.9688).

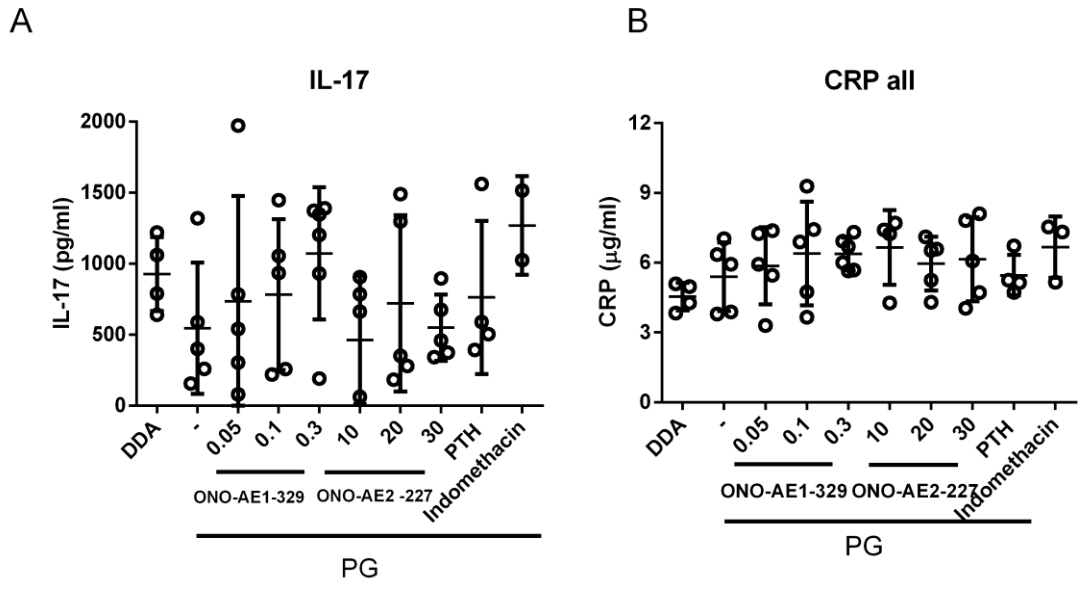

Figure 4.3: Targeting EP4 did not affect serum inflammatory markers.

(A) Serum IL-17 and **(B)** CRP level of DDA control and PGISp mice treated with ONO-AE1-329 (agonist), ONO-AE2-227 (antagonist), hPTH 1-34 and indomethacin for 16 weeks were was measured using ELISA. Data is presented by mean ± SD. The statistical significance of data was analysed by Mann-Whitney analysis. Difference is considered significant when $p<0.05$.

4-3.4 Targeting EP4did not have significant influence on bone

To examine whether ONO-AE1-329 and ONO-AE2-227 exerted any systemic effects on bone, we measured BMD and BMC using DEXA before treatment and upon experiment completion and calculated the percent change in bone paramters. The BMD and BMC were increased in the lower spine, pelvis and femur of the PGIS mice treated with hPTH 1-34 (Figure 4.4 B-G). However, among all the treatments tested, only ONO-AE1-329 at 0.1 mg/kg/day and indomethacin increased pelvis BMC when compared to untreated PGISp mice (Figure 4.4 E); while all other treatments had no significant effects on BMD and BMC (Table 4-3).

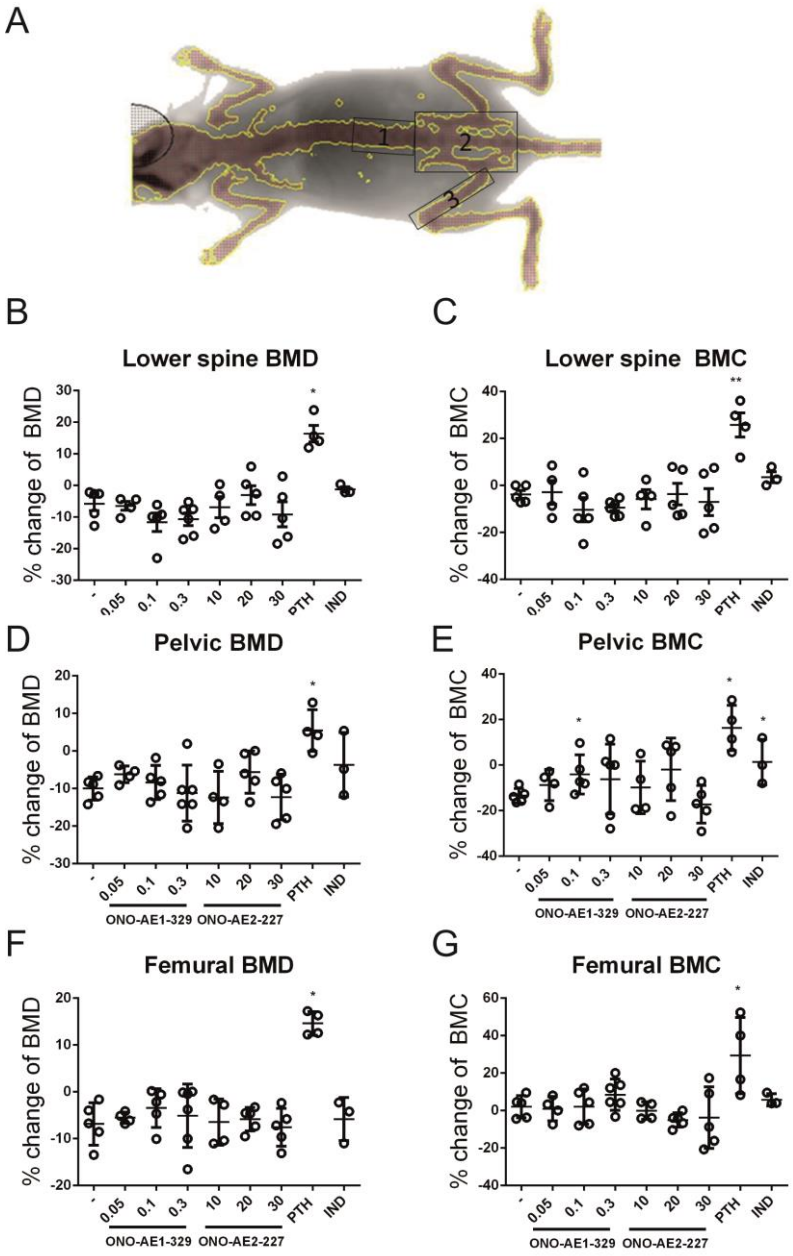

Figure 4.4: Targeting EP4 did not affect BMD and BMC of lower spine, pelvis and femur.

The BMD and BMC of PGISp mice treated with ONO-AE1-329 (EP4 agonist), ONO-AE2-227 (EP4 antagonist), hPTH 1-34 and indomethacin were measured using dual x-ray absorptiometry. **(A)** The representative image of region analysed. Boxed area indicated the (1) lower spine, (2) pelvis and (3) femur. Lower spine was determined by drawing a rectangle (99x30 pixels) parallel to the spine and above the pelvis. The pelvis analysed included sacrum and both iliac bones. The left femur was analysed in a rectangle with length from knee joint to iliac bone and width by 16 pixels. All mice were scanned before and after 16-week treatment, and the increase or decrease of **(B)** lower spine BMD, **(C)** lower spine BMC, **(D)** pelvic BMD, **(E)** pelvic BMC, **(F)** femoral BMD and **(G)** femoral BMC

was presented as the percentage change compared to baseline. Data is presented by mean ± SD. **p<0.01, *p<0.05 compared to untreated PGISp mice, with statistically significant differences determined using a Mann-Whitney test.

Bone morphometry was also analysed by CT to determine the localized effects of the EP4 agonist and antagonist on bone. The total bone volume of the 6th lumbar vertebrae, including calcified cartilage, cortical bone and trabecular bone (Figure 4.5A), was not different between all treatments (Figure 4.5B, Table 4-3). Since disease severity might affect bone structure, the vertebral body analysed was grouped according to IVD destruction, which was defined by the presence (Figure 4.5C, yellow arrowheads) or absence of space between the adjacent vertebrae (Figure 4.5D, red arrowheads). The severity of IVD destruction did not affect the mineralised tissue volume (Figure 4.5E). The cortical bone thickness was neither changed by treatments (Figure 4.5F, Table 4-3) nor by IVD destruction (Figure 4.5G, Table 4-4, end of Chapter 4). There were no CT images of hPTH 1-34-treated mice due to technical problems.

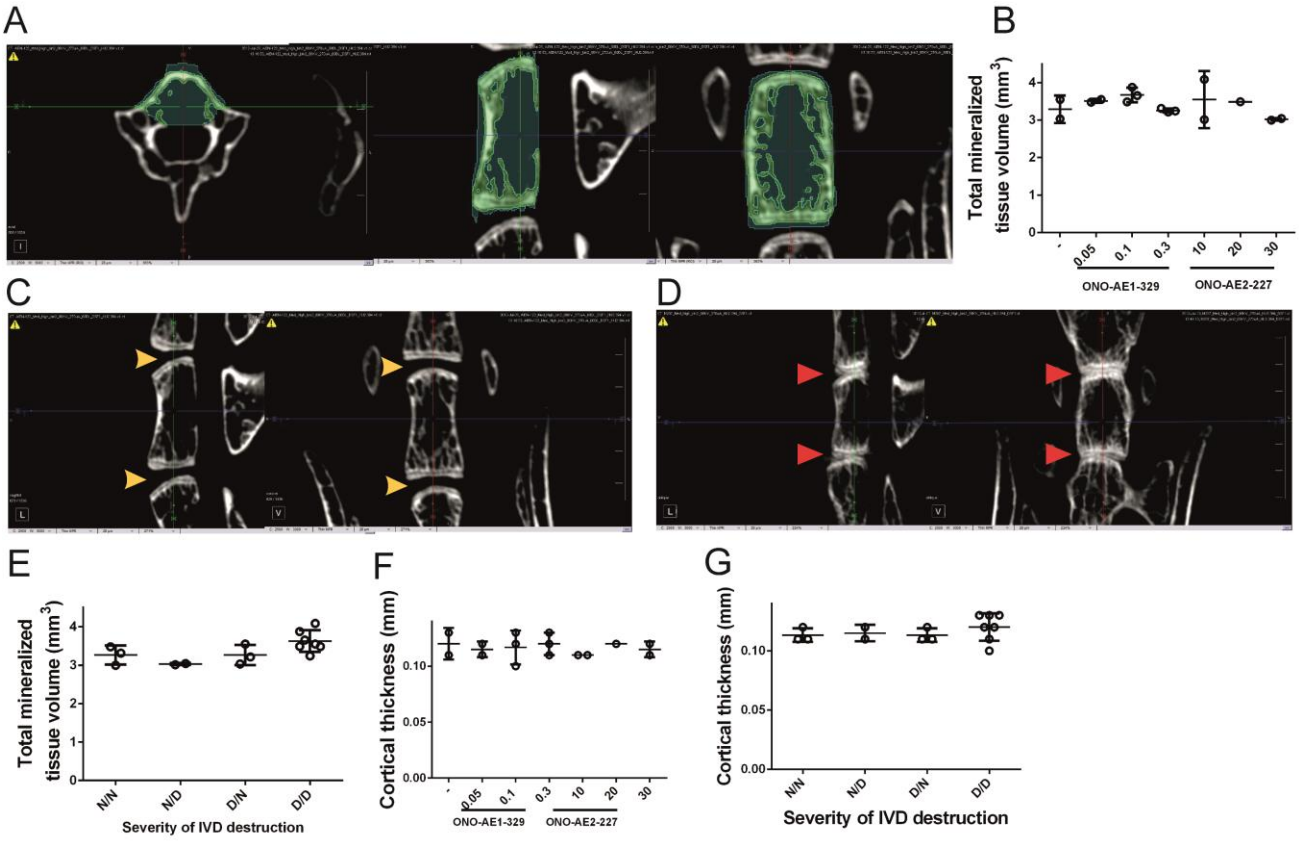

Figure 4.5: Mineralised tissue volume and cortical bone thickness were not changed by an EP4 agonist and antagonist.

(A) The cortical bone, trabecular bone and mineralised cartilage were analysed with CT images. The region of interest (green area) in the 6th lumbar vertebrae is shown in three planes. Left to right: transversal, lateral and anteroposterior. **(B)** The total mineralised tissue volumes are not different between all treatments. The space between two vertebral bodies indicates the severity of destruction: **(C)** The presence of inter-vertebrae spaces (yellow arrowheads) and **(D)** the absence of space indicates destroyed IVD (red arrowheads). **(E)** The mice are further grouped according to the severity of IVD destruction. N: no significant narrowing of IVD space as the example in (C); D: complete destroyed IVD as the example in (D). The features above IVD/below IVD were indicated as label. The cortical bone thickness was measured and grouped according to **(F)** the treatments and **(G)** the severity of IVD destruction. Data is presented by mean ± SD. The statistical significance of data was analysed by Mann-Whitney analysis. Difference is considered significant when $p<0.05$.

4-4 Discussion

4-4.1 EP4 in inflammation- peripheral, axial inflammation and serum inflammatory markers

We hypothesized that blocking EP4 using the antagonist would reduce inflammation. However, only daily administration of a low dose of ONO-AE2-227 showed a non-significant trend towards delaying peripheral disease onset compared to untreated mice. Power calculations suggested a sample size of 55, 59 and 263 mice was required for 10 20 and 30 mg/kg/day respectively indicating the anti-inflammatory effects are not significant (Table 4-5, end of Chapter 4).

It is known that Th17 are the primary cell type mediating EP4-related auto-immune diseases. EP4 antagonists have demonstrated promising inflammatory suppression in contact hypersensitivity, autoimmune encephalomyelitis (EAE) and CIA mouse models, which are all known as Th17-mediated diseases [256, 257, 277]. EP4 has disparate roles in Th17 development. PGE2 inhibits naïve T cells from differentiating into Th17 *in vitro*, while it enhances IL-17 production by matured Th17 and memory T cells [278, 279]. The dual effects have been proved using the EAE mouse model, in which EP4 enhances inflammation in the immunization phase, but then switches to anti-inflammation during the elicitation phase [277]. Therefore, administration of EP4 antagonist at different stages might lead to different therapeutic outcomes. However, the PG immunisation route in the present study was intraperitoneal injection, which was recently reported to induce arthritis predominately through Th1 instead of Th17 cells [280]. This may explain why blocking EP4 signalling showed no effects in this experiment.

Overall, the effects on peripheral arthritis in this study do not support our original hypothesis. The time point in our study had already passed the peak of axial inflammation; therefore, whether EP4 blockade had any effects on the initial spinal inflammatory phase cannot be determined from the current study. An earlier time point with larger group numbers would be required to further establish whether EP4 plays a role in PGISp axial inflammation.

4-4.2 EP4 in bone formation

We hypothesized that excessive tissue formation in the PGISp mice is associated with PGE2/EP4 signalling. Therefore, an EP4 agonist was expected to increase bone formation while antagonists would suppress bone formation. Subcutaneous injection of hPTH 1-34 increased spinal BMD and BMC suggesting that PGISp mice can respond to systemically administered bone anabolic agents. However, neither an EP4 agonist nor EP4 antagonist significantly effected BMD, BMC, mineralised tissue volume and cortical bone thickness of PGISp mice.

EP4 agonists have been suggested to increase bone anabolism; however, it might be dependent on the animal strains and disease models. EP4 agonists have been proven to rescue osteoporosis in ovariectomised rats [89, 270, 281]. However, the anabolic effect of ONO-AE1-329 on vertebrae was insignificant and only augmented by osteopontin deficiency [282]. Subcutaneous injection of ONO-4819, an EP4 agonist, enhanced ectopic bone formation in collagen pellets containing recombinant BMP-2 implanted on mouse back; however, systemic delivery of EP4 agonist in the same study did not affect tibial BMD and BMC [283]. Similarly, L-161982, an EP4 antagonist, inhibited PGE2-induced increase of tibial cancellous bone area without affecting basal level [284]. The above studies suggest that EP4 signalling might only be effective in certain pathological conditions, such as osteoporosis. Moreover, EP4 signalling might need to work synergistically with other signalling pathways to exert an effect on bone, such as BMP-2.

Another factor causing the discrepancy between our study and the literature might be the region analysed. Most regions analysed in the literature are the tibia, femur and lumbar spine; however, different bone regions might have different sensitivity to EP4 signalling. Lumbar and caudal vertebrae have different responses to ONO-4819, an EP4 agonist, even though they are both parts of the axial skeleton [270]. Similarly, administration of ONO-AE1-329 at 30μg/kg three times daily for three weeks significantly increased bone volume to total volume ratio in femora but not vertebrae [282]. Moreover, CP-734432, an EP4 agonist, has been shown to increase osteoid volume and osteogenesis marker expression without changing cancellous bone volume [89]. Taken together, the effects of EP4 agonists and antagonists appear to be skeletal site-dependent.

4-4.3 EP4 in excessive tissue formation

The results of Chapter 2 suggest excessive tissue was mainly cartilage, which might be laid down through chondroidal ossification. Cartilage formation is initiated as mesenchymal condensation followed by chondrocyte proliferation, hypertrophy and eventually mineralisation. Several *in vitro* studies suggest that PGE2 is not critical in regulating the initial mesenchymal condensation and proliferation in primary mouse limb bud [285] and human mesenchymal stem cells [286]. PGE2 might be more important in the later stage of chondrogenesis since *in vitro* stimulation of limb bud mesenchymal stem cells with PGE2 reduced the hypertrophy and calcification without affecting chondrocyte differentiation [287]. These studies suggest that PGE2 may have more important roles in terminal chondrocyte differentiation and ossification. Therefore, blocking EP4 signalling may only prolong the process of chondroidal ossification but not prevent the initiation of excessive tissue formation.

4-4.4 Treatment outcome is influenced by drug delivery

The lack of efficacy in the current study might be due to failed drug delivery; however, we did not include a positive control to demonstrate the activity of compounds. The drug preparation and dosage were according to the manufacturer's instruction. Therapeutic efficacy of these compounds at these doses via these delivery routes has been observed in models of inflammatory disease (personal communication). Diet containing 400 ppm of ONO-AE2-227 has been shown to reduce the aberrant crypt foci formation [276, 288]. Oral gavage in this experiment should allow more consistent drug intake compared to diet; however, this compound has not been extensively studied *in vivo*. Moreover, the volume of gavage had been shown to increase serum corticosteroid levels compared to sham gavage [289]. Therefore, although the control PGISp mice were handled and scored daily, treatments with daily placebo by gavage or subcutaneous injection should be performed in an ideal experimental design.

The efficacy of EP4 agonist and antagonist could have been specifically measured by assaying changes in tissue cAMP levels by ELISA [290] or the phosphorylation of PKA, PI3K and AKT using Western blotting of joint tissue extracts. Unfortunately, neither axial

skeleton nor peripheral joints were collected for such assays. Indomethacin has been shown to down-regulate PGE2 expression in paws [291] and plasma [292] at lower doses and in a shorter treatment duration compared to the present study; therefore efficacy was anticipated. Measuring PGE2 level in either plasma or joints would have provided proof of NSAIDs efficacy, a control measure that would be undertaken in future studies.

4-4.5 Mouse strain might affect treatment outcome

It is known that BALB/c mice have Th2-polarised immune responses because of higher production and sensitivity to PGE2, which decreases the production of Th1 cytokine, IFN-γ and IL-12 [254, 293]. IL-4 is known to be protective in PGISp mouse model and the lack of IL-4 increases arthritis penetrance and accelerates disease progression [183]. This somewhat overcomes the protective nature of the pro-Th2 background. However, if IL-4 is involved in the protection elicited by the treatments, the absence of IL-4 in our model would have diminished the effects. Although IL-4 expression is not the primary target of PGE2/EP4 signalling, how PGE2/EP4 signalling affects immune responses in the absence of IL-4 remains unknown.

4-4.6 Conclusion

An EP4 agonist and antagonist did not have any significant impact on disease progression in the PGISp mice. However, without confirmation of successful drug delivery no definitive conclusions could be drawn from the current study. This study also revealed that the large degree of inter- and even intra-mouse disease variability of the PGISp model raises concerns regarding its usefulness for therapeutic testing. This contrasts with the appropriateness of this model with respect to recapitulation of AS disease feature and progression patterns (Chapter 2). Therefore, confirmation of the role of EP4 in inflammatory processes contributing to AS remains unknown although it seems evident there are no strong protective effects of this treatment approach.

4-5 Tables

Table 4-3: *p* values compared to untreated mice (Mann-Whitney analysis)

Treatment	**ONO-AE1-329 (mg/kg/day)**			**ONO-AE2-227 (mg/kg/day)**			**hPTH 1-34 (μg/kg/5 days/ week)**	**IND (mg/kg/day)**
Dosage	**0.05**	**0.1**	**0.3**	**10**	**20**	**30**	**30**	**2**
Day of disease onset	0.3889	0.0397	0.7511	0.5000	0.3889	0.8333	-	-
Incidence	0.3968	0.8889	0.8413	0.6349	> 0.9999	0.9524	0.7778	0.8571
Inflammation	0.7143	0.8016	0.4603	0.8016	0.8016	0.2857	0.1667	0.9048
Disc destruction	0.2857	0.9444	0.7143	0.8968	0.6667	0.2857	0.4127	0.2857
Bone erosion	0.127	0.9444	0.4127	0.6667	0.2222	0.7143	0.4524	0.381
Cartilage damage	0.2857	0.6667	0.873	0.6667	0.3095	0.5556	0.6825	0.2857
Excessive tissue formation	0.1111	0.4524	> 0.9999	0.246	0.6667	0.6032	0.127	0.6667

Treatment	**ONO-AE1-329 (mg/kg/day)**			**ONO-AE2-227 (mg/kg/day)**			**hPTH 1-34 (μg/kg/5 days/ week)**	**IND (mg/kg/day)**
Dosage	**0.05**	**0.1**	**0.3**	**10**	**20**	**30**	**30**	**2**
Ectopic chondrocyte formation	0.1905	0.4603	0.7857	0.1032	0.5873	> 0.9999	0.4127	0.9524
Serum IL-17	0.7429	0.4000	0.1429	0.6786	0.5714	0.2500	0.2286	-
Serum CRP	0.7302	0.5317	0.4156	0.1111	0.4127	0.4127	> 0.9999	0.2500
Lumbar BMD	0.8750	0.0625	0.0625	0.4375	> 0.9999	0.6250	0.0159	0.2500
Lumbar BMC	0.6250	0.3125	0.0625	0.8750	> 0.9999	0.6250	0.0079*	0.2500

Treatment	**ONO-AE1-329 (mg/kg/day)**			**ONO-AE2-227 (mg/kg/day)**			**hPTH 1-34 (μg/kg/5 days/ week)**	**IND (mg/kg/day)**
Dosage	**0.05**	**0.1**	**0.3**	**10**	**20**	**30**	**30**	**2**
Pelvic BMD	0.1905	0.5317	0.5065	0.5238	0.1508	0.8016	0.0159*	0.2500
Pelvic BMC	0.2857	0.0317*	0.4004	> 0.9999	0.2222	0.4127	0.0159*	0.0357*
Femoral BMD	0.8730	0.3095	0.4156	> 0.9999	0.9444	0.8016	0.0159*	> 0.9999
Femoral BMC	0.6825	> 0.9999	0.1623	0.6032	0.0952	0.5317	0.0317*	0.7143
Mineralised tissue	0.6667	0.4000	> 0.9999	> 0.9999	Insufficient number.	0.6667	No images	No images
Cortical bone thickness	> 0.9999	> 0.9999	> 0.9999	> 0.9999	Insufficient number	> 0.9999	No image	No image

Table 4-4: *p* values compared to N/N (Mann-Whitney analysis)

	N/D	D/N	D/D
Mineralised tissue	0.6000	0.9000	0.0667
Cortical bone thickness	> 0.9999	> 0.9999	0.4167

Table 4-5: Sample size required to reaching significant difference

Treatment	**Untreated**	**ONO-AE1-329 (mg/kg/day)**			**ONO-AE2-227 (mg/kg/day)**			**hPTH 1-34 (μg/kg/5 days/ week)**	**IND mg/kg/day)**
Dosage	**-**	**0.05**	**0.1**	**0.3**	**10**	**20**	**30**	**30**	**2**
Day of disease onset(Mean ± SD)	41.60±13.09	51.20±13.16	55.60±8.989	50.00±17.85	48.40±10.01	48.60±9.236	38.40±15.18	-	-
Sample size	-	30	14	39	59	55	263	-	-
Disc destruction (Mean ± SD)	1.958±0.8828	1.423±0.4322	2.056±0.5554	2.300±0.4373	1.814±0.8717	1.578±1.077	2.460±0.4213	2.425±0.2509	1.210±0.6505

Treatment	**Untreated**	**ONO-AE1-329 (mg/kg/day)**			**ONO-AE2-227 (mg/kg/day)**			**hPTH 1-34 (μg/kg/5 days/ week)**	**IND mg/kg/day)**
Dosage	**-**	**0.05**	**0.1**	**0.3**	**10**	**20**	**30**	**30**	**2**
Sample size	-	43	1272	105	589	85	49	56	22
Excessive tissue formation (Mean ± SD)	1.422±0.6262	0.7425±0.1345	1.270±0.5139	1.610±0.3403	0.9120±0.5150	1.112±0.8109	1.788±0.1986	2.048±0.3939	1.215±1.011
Sample size	-	14	266	174	24	64	46	16	144

5 Chapter5: Early intervention ameliorates axial disease progression in the PGISp mouse model of AS

5-1 Introduction

The results of Chapter 2 suggest that inflammatory infiltrate initiates disc destruction, which might increase mechanical stress, destabilise the vertebral joints and lead to severe cartilaginous endplate damage. The subsequent excessive tissue formation, including the formation of bone, might be an aberrant repair response to disc destruction. Hence, we hypothesised that inflammation-derived disc destruction is a prerequisite of excessive tissue formation. Suppressing inflammation before leading to irreparable tissue damage might be an effective therapeutic approach for preventing or at least ameliorating progression of AS.

Shorter disease duration is associated with better improvement in inflammatory symptoms and disease activity after anti-TNF treatment (Chapter 1, Table1-3). However, absolute disease diagnosis, fulfilling the modified New York criteria for AS, requires for diagnosis that the patient develops radiographic evidence of sacroiliac disease including erosions and sclerosis [294]. Due to this criterion, diagnosis is not confirmed until disease is well established, and consequently appropriate treatment is frequently delayed until significant damage has already occurred. Moreover, it is also difficult to unequivocally prove the absolute benefit of therapeutic approaches in AS as it is unethical to prescribe placebos to patients for long-term studies to observe the nature of disease progression. Therefore, there is potentially great value in AS animal models for testing the benefits of early treatment interventions.

TNF blockers are used as the “gold-standard” therapy in AS patients. Etanercept (ETN) is a commercial TNF blocker synthesised as a fusion of the soluble TNF receptor 2 and the constant region of human IgG1. The efficacy of ETN is well-established [295] and has shown in non-radiographic axial spondyloarthritis patients with disease duration shorter than five years [130], which represents a patient group with earlier disease.

Local injection of glucocorticoid to inflamed joints, such as the sacroiliac joints, effectively reduces local inflammation in AS patients [115, 296]. Intravenous methylprednisolone

pulse injection significantly improves clinical symptoms, pain, stiffness, serum ESR and CRP within one week in established AS patients, and the effects last for an average of 12 weeks [297]. Only one pulse of methylprednisolone at 1 mg significantly reduced pain and improved spinal mobility in AS patients with severe pain within 24 hours, and four pulses prolonged the improvement up to ten months [298]. Oral prednisolone (PRD) treatment at 50 mg/day reduced serum CRP level and improved the clinical outcomes of AS patients in a two-week clinical study [299]. These studies showed favourable results of local as well as systemic glucocorticoid treatment in AS patients.

The combination of these two effective anti-inflammatory drugs, TNF inhibitors and glucocorticoids, was selected to achieve strong anti-inflammatory effects in the present study. A prophylactic treatment is not practical in the clinic, and it cannot differentiate whether the efficacy is due to blockade of disease onset or inflammation-induced disc destruction. The goal of the present study was not to prevent inflammation but to prevent the subsequent disc destruction. Hence, we chose an early intervention approach rather than a prophylactic treatment regimen. Since there are no reliable methods or markers to detect spinal inflammation *in vivo*, the timing of treatment commencement was selected according to the findings of Chapter 2. We allowed mice to develop inflammatory responses and started intervention at the point where we predict mild spondylitis will have developed without pronounced tissue erosion or excessive tissue formation. We hypothesized that early intervention with potent anti-inflammatory therapy would inhibit or slow down disease progression.

5-2 Materials and methods

5-2.1 Animal experiments

IL-4$^{-/-}$ females with body weights 17-20.6g were included in this study. Protocol for disease induction was the same as Chapter 2. PGISp mice were treated with vehicle, ETN alone or ETN plus PRD (ETN+PRD). ETN (kindly provided by Pfizer, NY, USA) was administered at 2 mg/kg by subcutaneous injection 3 times a week. PRD was administered at 1.5 mg/kg/day by a slow-release pellet (Innovative Research of America, Sarasota, FL, USA) implanted subcutaneously. Vehicle group were treated with PBS by subcutaneous injection with or without placebo pellets. All treatments started 3 days after the third PG injection and continued for 2 or 6 weeks as described in Figure 5. 1A.

5-2.2 Peripheral arthritis

The peripheral scoring regimens used were the same as in Chapter 4 of this thesis.

5-2.3 Histology

The histology and scoring regimens used were the same as in Chapter 2 of this thesis.

5-2.4 Statistics and sample size calculation

Mann-Whitney analysis was used to test statistically significant differences. *P* values less than 0.05 were considered significant differences. The relationships between two data outputs were determined by Spearman correlation. All the statistical analyses were performed using PRISM 6 (GraphPad Software, La Jolla, CA). The significant differences between the proportions of treatments were determined by Z-test (http://epitools.ausvet.com.au/content.php?page=home) through one-tailed distribution calculation with the significance level 0.05. Sample size calculation was conducted using a power calculator (http://powerandsamplesize.com/) with a significance α of 0.05 and power of 1-β=0.8.

5-3 Results

5-3.1 ETN+PRD delayed symptom onset and suppressed peripheral arthritis

In the PGISp AS model, clinical scores fluctuate; hence the onset of disease was defined as when single paw recorded a positive score three consecutive scores (scored every other day). As reported in early chapters, the onset of peripheral arthritis varied between individual mice, with the earliest onset observed from 4 weeks post priming (Figure 5.1B). In vehicle-treated mice, peripheral arthritis score steadily increased from 4 weeks followed by an accelerated exacerbation from 6.5-8 weeks and then stabilization of peripheral score from 8 weeks post priming onwards (Figure 5.1B, black line). The mice treated with the ETN+PRD treatment had similar peripheral arthritis onset and progression until 6 weeks post-priming (Figure 5.1B, red), which was the treatment initiation point (Figure 5.1A). When compared to vehicle-treated mice, ETN+PRD-treated mice had significantly lower peripheral scores from week 7 to 9 post priming (Figure 5.1B, red, $p<0.05$). From 9 weeks onwards, peripheral disease appeared to escape drug-induced suppression, as peripheral scores of ETN+PRD-treated mice increased steadily and equalized with vehicle-treated mice at approximately 10.5 weeks post priming (Figure 5.1B, red and black lines). The mice in the ETN alone group all had onset prior to treatment initiation and more severe peripheral arthritis from week 5 (Figure 5.1B, blue lines). Surprisingly, ETN alone did not suppress clinical scores immediately; however, it seemed to retard disease progression as the peripheral arthritis score from approximately 8 weeks post priming showed a declining trend when compared with the vehicle-treated group (Figure 5.1 B, blue line).

The variation in disease onset characteristic to this model (see Chapter 2) and the arbitrary treatment initiation point may have influenced treatment impacts. To more specifically investigate whether ETN+PRD delayed PGISp disease onset and/or suppressed inflammatory symptoms, we grouped mice based on whether definite peripheral disease symptoms were detected prior to treatment (onset Pre-RX) or if peripheral arthritis was only detected after treatment was initiated (onset post-RX) (Table 5-1). Mice with no peripheral arthritis before the end of this study might develop peripheral symptoms if the time course was prolonged. Conservatively, these mice were grouped in onset post-RX group during analysis. In onset pre-RX mice, average peripheral arthritis

scores did not reveal consistent significant suppression of disease, likely due to the broad variance in rate of disease progression between mice in this AS model (Figure 5.1C, red). A treatment effect of ETN+PRD was more evident when the difference in peripheral arthritis scores before and after treatments in individual mice were examined (Figure 5.1D). Progression of arthritic symptoms was significantly suppressed across the majority of the treatment period by ETN+PRD treatment (Figure 5.1D, red). ETN alone neither dramatically decreased peripheral disease nor altered disease progression (Figure 5.1D, blue). The peripheral disease in this group was stable for four weeks before a slowly increasing.

Within the onset post-RX group, all vehicle-treated mice developed peripheral arthritis within 2 weeks after the third PG immunization (Figure 5.1E, F. Black line), whereas ETN+PRD treatment significantly delayed disease onset for 3 weeks (Figure 5.1E. Redline). This was verified by stable arthritis scores in ETN+PRD treated mice over the same period (Figure 5.1F, red line). However, from 9 weeks post priming, there was no significant difference in peripheral arthritis score between vehicle and ETN+PRD treated mice within the onset post-RX group (Figure 5.1E) and the "change in arthritis" score suggested similar disease severity once the initial onset delay was overcome (Figure 5.1F). The results suggest that while ETN+PRD treatment delayed peripheral disease onset and suppressed the severity of arthritic symptoms, and that it did so more effectively than ETN alone, the combined treatment did not completely inhibit inflammation.

Table 5-1: Percentage of mice in Pre-RX and onset post-RX groups

	6-12 weeks			6-8 weeks	
	Vehicle (N=7)	ETN+PRD (N=8)	ETN (N=5)	Vehicle (N=5)	ETN+PRD (N=7)
Onset pre-RX	57.1%	62.5%	100% *	40%	28.6%
Onset post-RX	42.9%	25%	0	40%	0*
No peripheral	0	12.5%	0	20%	71.4% *

	6-12 weeks			6-8 weeks	
disease					
Total	7	8	5	5	7

*p<0.05 compared to vehicle at the same time point

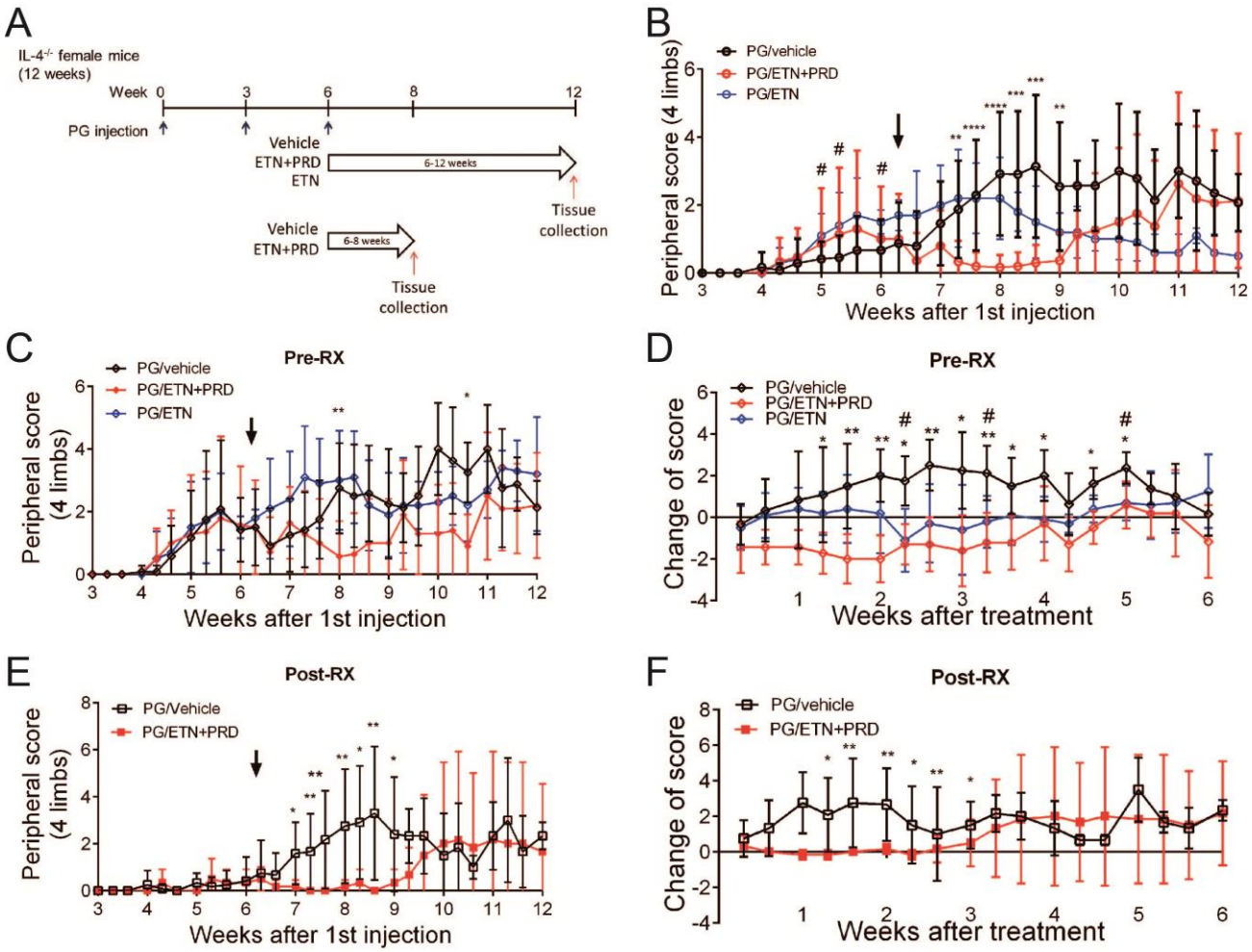

Figure 5.1: Combination of ETN and PRD suppressed peripheral arthritis.

(A) Axial disease was induced by intraperitoneal injection of PG as described in the Materials and Methods. PGISp mice were treated with vehicle, etanercept (ETN) (2mg/kg, 3 times a week, subcutaneous injection) plus prednisolone (PRD) (1.5mg/kg/day, slow released pellet) or ETN alone (n=5-8/group). Treatment started 3 days after the third PG injection at week 6 and was continued until either week 8 or 12 post priming. **(B)** Peripheral arthritis progression of mice receiving vehicle (black), ETN+PRD (red) and ETN

(blue) represented as the sum of all four limbs scores per mouse. Arrow indicates the initiation of treatment. PGISp mice were divided into **(C, D)** onset pre-RX **(E, F)** and onset post-RX according to the sequence of treatment commencement and the onset of peripheral arthritis. **(C)** The raw peripheral scores as per in (A) and **(D)** change of peripheral score after treatment of onset pre-RX group mice. **(E)** The raw peripheral scores as per in (A) and **(F)** change of peripheral scores after treatment of onset post-RX group mice. Data was presented by mean ± SD. The statistical significance of data was analysed by Mann-Whitney analysis. ****p<0.0001, ***p<0.001, **p<0.01, *p<0.05 ETN+PRD treatment compared with vehicle. # p<0.05 ETN alone compared with vehicle.

5-3.2 ETN+PRD ameliorated axial disease

We next examined whether the anti-inflammatory treatments, as per Figure 5.1A, can suppress axial disease progression. The average percentage of affected IVDs in ETN+PRD treatment groups (52.17% and 50.0% at week 8 and 12 respectively), were not significantly different between the vehicle groups (50.85% and 60.25% at week 8 and 12 respectively, Figure 5.2A). However, only the ETN+PRD treatment group contained animals with no evidence of axial disease (3/7 at 8 weeks and 2/6 at 12 weeks). ETN+PRD treatment significantly suppressed inflammation at both time points (Figure 5.2B). All vehicle-treated mice had either peripheral or axial disease after treatment for 6-8 week, while 40% of ETN+PRD-treated mice still had no detectable peripheral and axial disease (Table 5-2). Trends towards reductions in disc destruction (Figure 5.2C), bone erosion (Figure 5.2D), cartilage damage (Figure 5.2E) and excessive tissue formation (Figure 5.2F) were also seen in the ETN+PRD treatment group, although the differences were not significant compared to vehicle-treated mice. However, mice treated with ETN alone displayed similar axial disease progression compared to vehicle and significantly more severe disease in all outcomes compared to ETN-PRD treated mice (Figure 5.2 B-E).

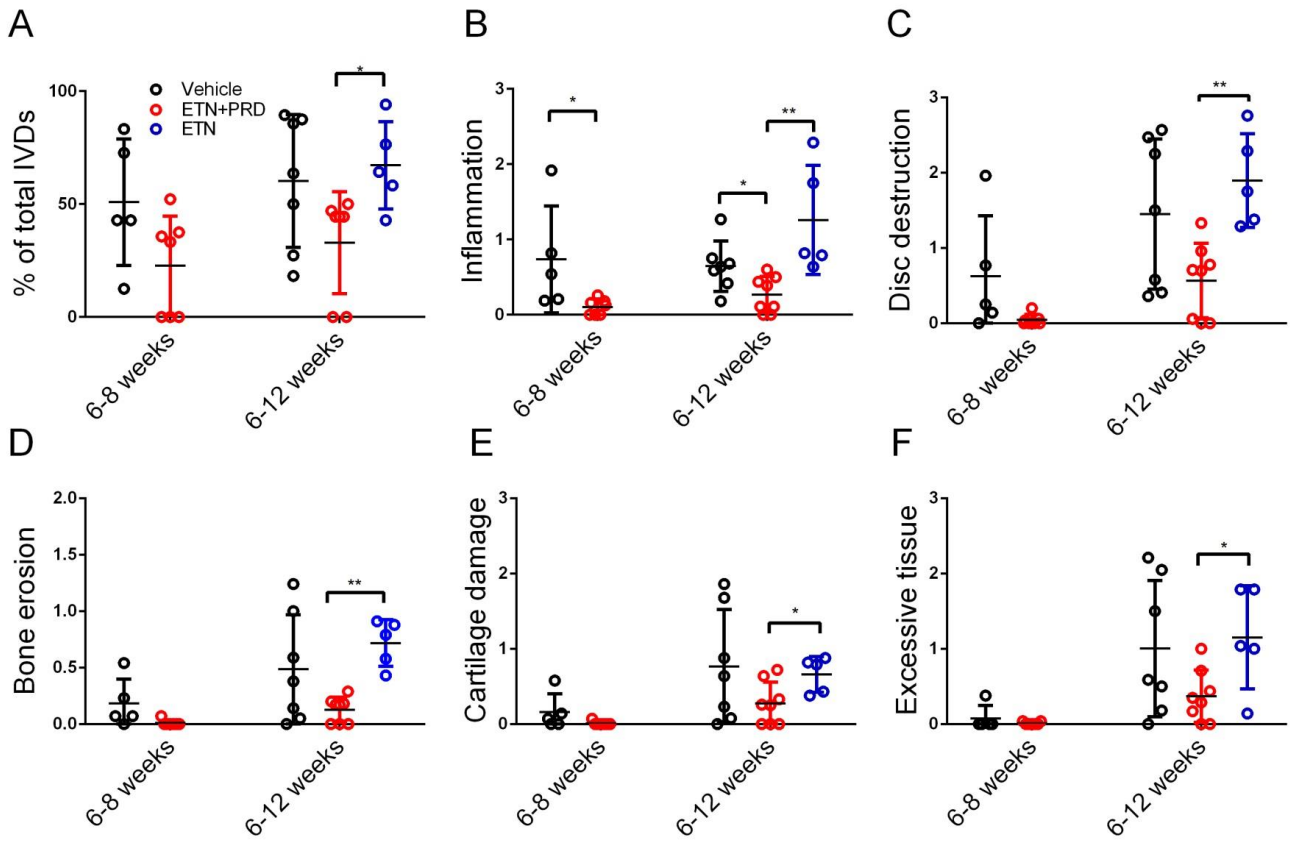

Figure 5.2: Combination of ETN and PRD suppressed spinal inflammation.

(A) The percentage of affected joints in individual mice. Semi-quantitative histological scoring of the following disease features: **(B)** inflammation, **(C)** disc destruction, **(D)** bone erosion, **(E)** cartilage damage and **(F)** excessive tissue formation. Each point represents the average score of all IVD within a mouse. The results are presented as mean ± SD. The statistical significance of data was analysed by Mann-Whitney analysis. **p<0.01, *p<0.05 compared with indicated groups.

Table 5-2: Percentage of mice developing peripheral and/or axial disease

Treatment duration	**6-12 weeks**			**6-8 weeks**	
Treatment (mouse number)	**Vehicle (N=7)**	**ETN+PRD (N=8)**	**ETN (N=5)**	**Vehicle (N=5)**	**ETN+PRD (N=7)**
Both peripheral and axial	100%	62.5%	100%	60%	42.85%
Peripheral disease only	0	25%	0	0	0
Axial disease only	0	12.5%	0	40%	14.3%
No disease	0	0	0	0	42.85%*
Total mouse number	7	8	5	5	7

*p<0.05 compared to vehicle at the same time point

5-3.3 Axial disease is independent of peripheral arthritis

According to our hypothesis, treatment should be more effective for preventing osteoproliferative spinal disease when commenced early in disease evolution. As the point of onset of axial disease could not be determined without sacrificing mice, we used the peripheral arthritis score as a surrogate of disease evolution to determine when to initiate treatment. Mice were sub-grouped according to the onset of peripheral disease. Early onset of peripheral disease did not lead to more severe axial disease in either vehicle or ETN+PRD treatment group (Figure 5.3A-F, pre versus post). In both pre-RX and post-RX groups, ETN+PRD therapy demonstrated a trend toward reduced incidence, inflammation, disc destruction, bone erosion, cartilage damage and excessive tissue formation compared to vehicle (Figure 5.3A-F, red) with non-significant differences. As this sub-grouping resulted in smaller group sizes, this greatly reduced statistical power of the

experiment. Although most diseased mice presented with both peripheral and axial disease, there were individual mice that developed either only peripheral or only axial disease (Table 5-2), indicating independent involvement of the different disease sites, and that peripheral disease is not a totally reliable predictor of axial disease.

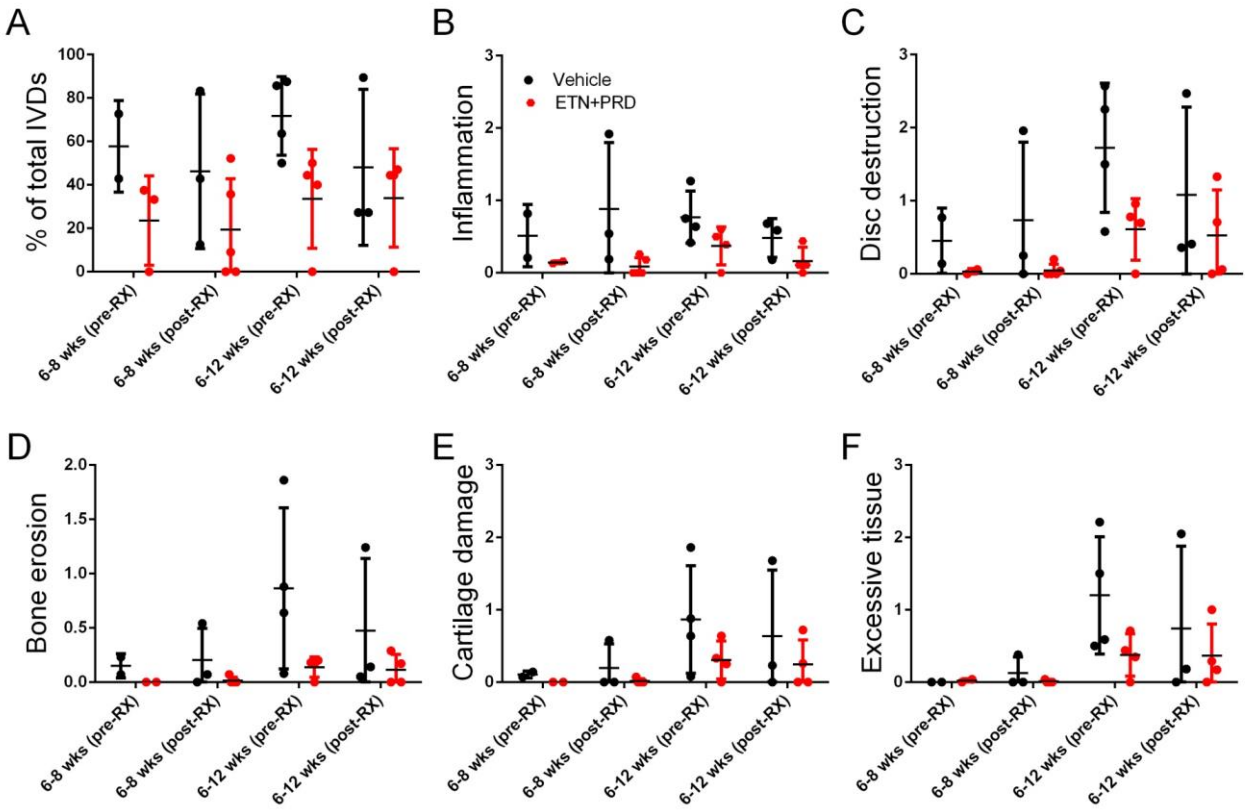

Figure 5.3: Early intervention showed a trend toward reduction of axial disease independent of whether peripheral disease had early or late onset.

PGISp mice receiving vehicle (black) and ETN+PRD treatment (red) were grouped according to the onset of peripheral arthritis. **(A)** Incidence of affected IVDs, and histological features of the following disease features: **(B)** inflammation, **(C)** disc destruction, **(D)** bone erosion, **(E)** cartilage damage and **(F)** excessive tissue formation were presented as mean ± SD. The statistical significance of data was analysed by Mann-Whitney analysis.

5-3.4 Disc destruction is associated with disease severity

Prevention of disc destruction was the main goal of the chosen anti-inflammatory treatments in the present study. However, Figure 5.2C shows that reduction of disc destruction score in ETN+PRD treatment did not reach significance. This was likely due to the presence of high and low disc destruction subgroups in both vehicle and ETN+PRD treatment groups (Figure 5.2C) and overall relatively small sample size. Disc destruction was strongly and positively correlated with inflammation, bone erosion, cartilage damage and excessive tissue formation in all PGISp mice treated for 6-12 weeks (Figure 5.4A). This was similar to both vehicle (Figure 5.4B) and ETN+PRD-treated mice (Figure 5.4C), but inflammation was not significantly correlated with disc destruction in either group. The correlation between disc destruction and bone erosion was less significant in the vehicle-treated group (p=0.048) and became non-significant (p=0.15) in ETN+PRD treatment group (Figure 5.4C).

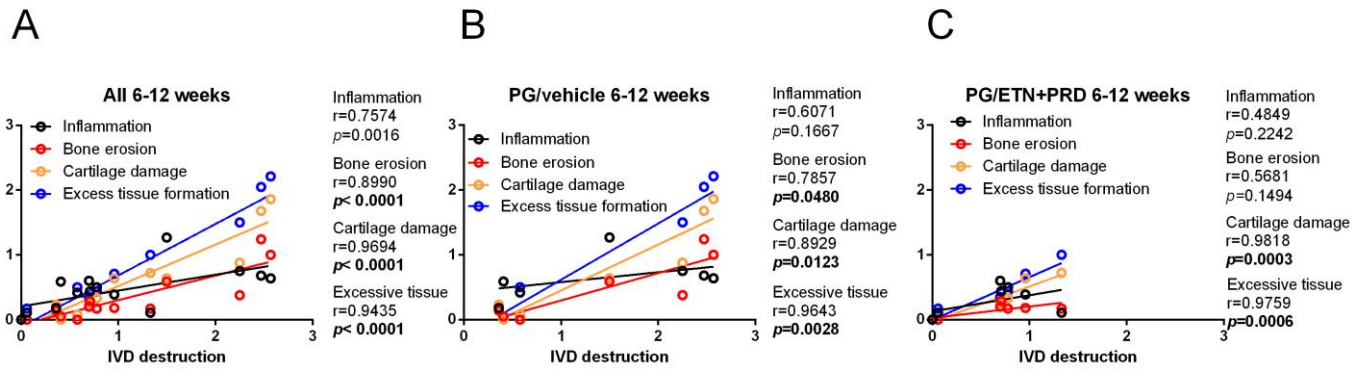

Figure 5.4: Disc destruction is strongly associated with bone erosion, cartilage and excessive tissue formation.

Correlation between disc destruction with Inflammation (black), bone erosion (red), cartilage damage (orange) and excessive tissue formation (blue) of **(A)** all PGISp mice treated with vehicle and ETN+PRD treatment from week 6 to 12, **(B)** only vehicle group, and **(C)** only ETN+PRD treatment. Statistical significance was analysed by Spearman correlation.

Since the stage of progression of axial disease at the initiation of therapy also likely effected the treatment outcome [202, 203, 205, 206] and we had shown that peripheral disease was not a full proof surrogate of axial disease (Figure 5.3 and Table 5-2), grouping based on disc destruction severity was then considered in the analysis. The mean disc destruction score in vehicle and ETN+PRD-treated groups,1.45 and 0.57 respectively, was set as the cut-off value to separate mice into low and high disc destruction groups: vehicle(L), vehicle(H), ETN+PRD(L) and ETN+PRD(H) (Figure 5.5).

Analysis of low versus high IVD destruction subgroups within the treatment regimens demonstrated that there was a trend but no statistically significant difference in the average disc destruction score between vehicle (L) and vehicle (H) (Figure 5.5A, orange vs brown, p=0.0571). In contrast, the mean disc destruction score within the ETN+PRD (L) was significantly lower than the ETN+PRD (H) (Figure 5.5A, light green vs dark green, p<0.05). Subgrouping in this manner also showed that in mice with low disc destruction, irrespective of whether they were vehicle (Figure 5.5, orange vs brown) or ETN+PRD treated (Figure 5.5, light green vs dark green), the severity of inflammation (Figure 5.5B), bone erosion (Figure 5.5C), cartilage damage (Figure 5.5D) and excessive tissue formation (Figure 5.5E) tended to be lower. Significant reductions were observed between ETN+PRD (L) (light green) and ETN+PRD (H) (dark green) for all measures (p<0.05) except for inflammation (Figure 5.5B-E, p=0.0536).

When comparing ETN+PRD (H) with vehicle (H) (Figure 5.5A, dark green vs brown, p<0.05), the mean disc destruction score within the ETN+PRD (H) was significantly lower than the vehicle (H). These observations imply that ETN+PRD treatment reduced disc destruction outcomes independent of variation of the disease severity course (mild or robust disease). Furthermore, ETN+PRD (H) was shown to reduce inflammation significantly (Figure 5.5B, dark green vs brown p<0.05) and bone erosion (Figure 5.5C, p<0.05). A trend toward reduced cartilage damage (Figure 5.5D, p=0.064) and excessive tissue formation (Figure 5.5E, p=0.064) was also observed in the ETN+PRD (H). Therefore, in the subgroup of mice that had more robust disease induction, ETN+PRD treatment was able to reduce axial disease and damage considerably.

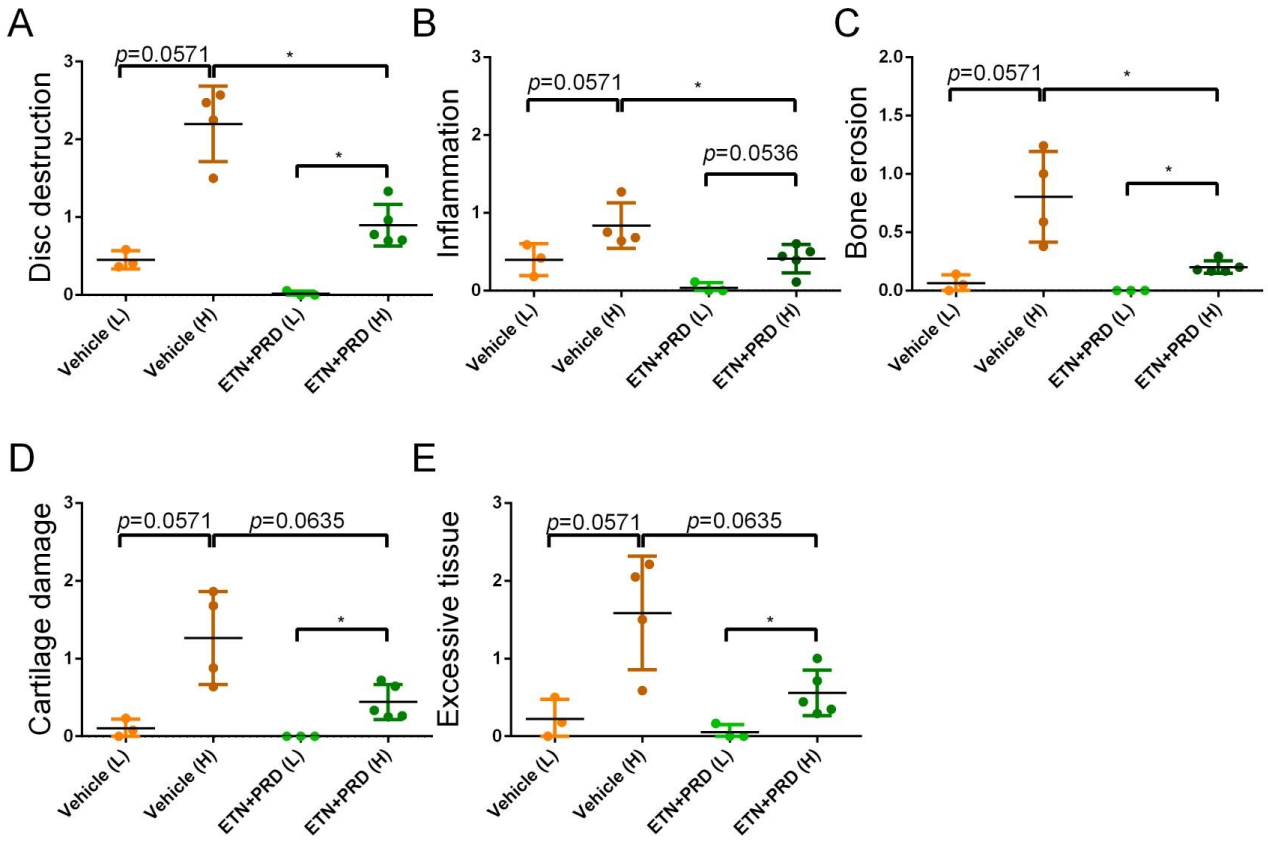

Figure 5.5: Combination of ETN and PRD reduced axial disease in more severely affected mice.

PGISp mice in vehicle group were sub-grouped into low disc destruction (Vehicle (L), orange), and high disc destruction (Vehicle (H), brown) in relation to the average score,1.45. ETN+PRD-treated mice were split into low disc destruction, (ETN+PRD (L), light green), and high disc destruction (ETN+PRD (H) ,dark green) in relation to the average score, 0.57: Semi-quantitative histological scores for (A) disc destruction, (B) inflammation, (C) bone erosion, (E) cartilage damage and (F) excessive tissue formation. The results are presented as mean ± SD. The statistical significance of data was analysed by Mann-Whitney analysis. * $p<0.05$ compared with indicated group.

5-4 Discussion

The aim of this intervention project was to examine whether inflammation-induced disc destruction is the prerequisite for excessive tissue formation in the context of AS and whether interventions to reduce inflammation before it leads to deleterious structural damage would alter disease progression.

The combination of strong anti-inflammatory drugs, ETN and PRD, was commenced 3 days after the third PG injection, when about 50% of mice had developed detectable peripheral arthritis while the other half may be either unaffected or have subclinical inflammation. The early intervention with ETN+PRD treatment significantly delayed disease onset and ameliorated the progression of peripheral arthritis. All the vehicle-treated mice developed either peripheral or axial disease in the 6-12 week group; while 40% of ETN+PRD-treated mice in 6-8 week group did not have detectable peripheral or axial disease suggesting ETN+PRD treatment controlled inflammation for the first 2-3 weeks. The histological analysis demonstrated that this transient suppressive effect in the early phase had led to a significant reduction of inflammation and a declining trend of disc destruction, cartilage damage, bone erosion and excessive tissue formation.

Early diagnosis and initiation of disease prevention strategies have been suggested to retard syndesmophyte formation. Delaying anti-TNF treatment for more than ten years after onset resulted in higher radiographic progression rate than those who started anti-TNF within ten years of onset [206]. The mean changes of mSASSS score after high-dose NSAID treatment for two years were 0.02 and 0.4 in patients with disease duration 5.5 years [96] and 11.9 years [97] respectively. The presence of syndesmophytes when treatment commenced strongly predicted radiographic progression regardless of treatments [202, 203, 205, 206] suggesting that anti-inflammatory therapy is more effective in inhibiting radiographic progression before structural damage has been initiated. The results from HLA-B27/hβ2m transgenic rats also demonstrated that early treatment blocked chondroproliferation and activation of BMP signalling, but not delayed treatment [114]. The above studies and our results all support the concept that early intervention is beneficial for preventing the subsequent osteoproliferation.

Early intervention should have chances to prevent inflammation-derived disc destruction or ameliorate the ongoing process. The therapeutic window was short and varied between individual mice and even individual discs. If the disc was affected by more aggressive disease and destruction was not suppressed in time, it might compromise the treatment efficacy.

Since the treatment and disc destruction both affect the outcome in the present study, subgrouping is required to separate the effects of treatment and disc destruction. We were unable to monitor the axial disease. Chapter 2 showed that the inflammation is upstream of all the following events, but the same inflammatory score might indicate either developing or declining phase of inflammation. Therefore, inflammatory scores were not well correlated with other features in either treatment group and could not be used as good indicator of disease.

Figure 5.3 showed that disc destruction was strongly and positively correlated with cartilage damage and excessive tissue formation in both vehicle and ETN+PRD-treated mice; therefore, it served a better indicator of disease severity in the present study. Presumably, PGISp mice that had more aggressive disease progression before treatment were more likely to develop more severe disc destruction at the end of this study. Subgrouping mice by the severity of disc destruction and comparing those had more robust disease in each treatment group showed that early intervention with ETN+PRD was able to significantly ameliorate inflammation, disc destruction, bone erosion and a trend toward cartilage damage and excessive tissue formation was also observed. It suggests that even in more severe disease, early intervention might still have the potential to ameliorate destruction and retarded excessive tissue formation. Power calculations demonstrated that the current study is underpowered and will require 21 mice to reach a significant difference. Since no study had showed that this dosage of combined ETN+PRD can suppress spondylitis and we can't monitor axial disease *in vivo* for treating axial disease in the PGISp mouse model, a small scale study like the present study is necessary to determine the sample size for future study.

Since disc destruction is more likely to be the direct trigger of repair and subsequent excessive tissue formation, suppressing disc destruction might aid improving anti-

inflammatory treatment outcome. The anti-resorption drugs, bisphosphonates, have been reported to reduce inflammation and improve disease activity in AS patients [232, 300-305]. These studies were shorter than one year, which was not long enough to observe the effect on radiographic progression formation. Alendronate reduced cartilage degeneration and osteophyte formation in the anterior cruciate ligament transection (ACLT) rat model of OA [306]. Osteophyte formation in postmenopausal women was slowed down by alendronate treatment for 3-4 years [307]. Therefore, bisphosphonates might be able to reduce resorption, strengthen the joint structure and reduces osteophyte formation.

Overall, our results support the hypothesis that early intervention with effective anti-inflammatory treatment has the potential to suppress inflammation and reduce the following tissue destruction and excessive tissue formation. Combining anti-resorption agents with anti-inflammatory treatment might be another therapeutic approach for suppressing syndesmophyte formation in AS.

6 Final discussion and future direction

6-1 Final discussion

The association between inflammation and excessive bone formation is of great interest in the context of AS. Therapies aiming to relieve symptoms effectively reduce inflammation; however, their effects on syndesmophyte formation are limited (Table 1-5). The mechanisms triggering inflammation and regulating the inflammation-osteoproliferation transition remain poorly understood, largely due to the lack of relevant bone biopsies. Hence, an animal model is a necessary substitute for understanding the axial disease progression in AS.

The PGISp mouse model is known to develop inflammation, extensive IVD destruction and excessive tissue formation in the axial skeleton [105, 176], but no study had characterised the disease progression or the correlation between inflammation, catabolic and anabolic features in this model.

The in-depth histological analysis, conducted across a 40-week time course study in this thesis, demonstrated that PGISp disease manifests in a heterogeneous fashion at individual vertebral joints and between individual animals, similar to the broad range of disease severity seen in AS patients [212]. The early inflammation and advanced excessive tissue formation mimics the progression of AS in humans (Figure 6.1A). These characteristics support that the PGISp is a good model for understanding disease mechanisms, even though it results in experimental challenges. Overall this thesis achieved unparalleled characterisation of the PGISp mouse model, and provides insight into the mechanisms of disease progression in AS.

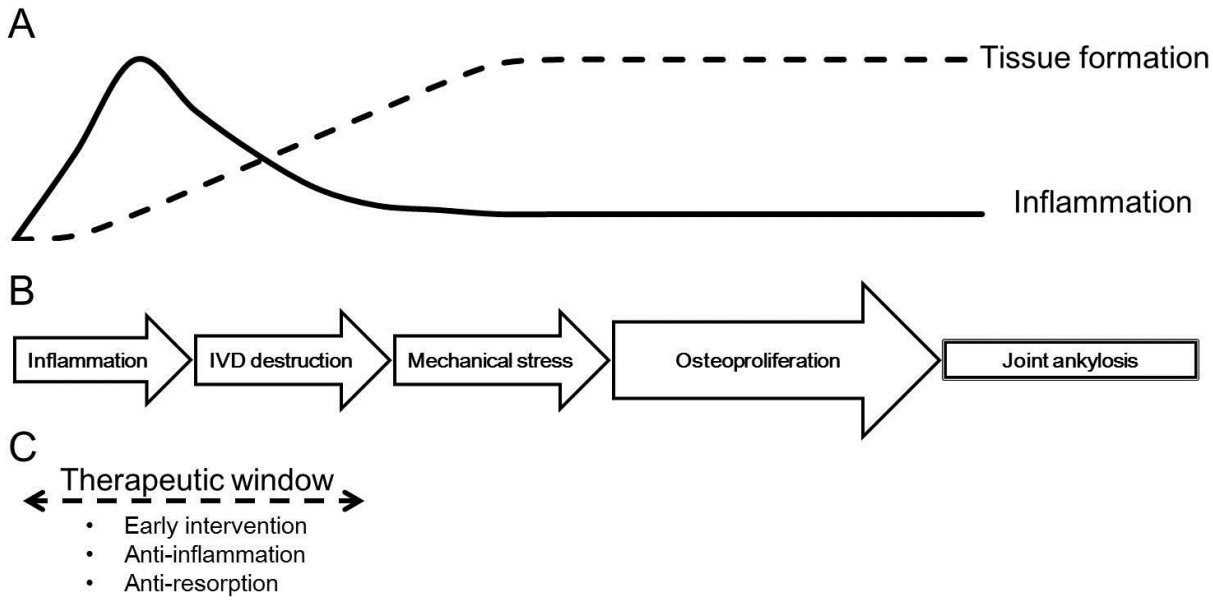

Figure 6.1 The model of disease progression and potential therapeutic strategies.

(A) Inflammation and tissue formation are features of early and advanced stages respectively. **(B)** Proposed pathway mapping how initial inflammation leads to osteoproliferation and ankylosis. **(C)** The therapeutic window is in the inflammatory and IVD destruction phases. Early intervention with anti-inflammatory and anti-resorption treatments are the potential therapeutic strategies for AS.

6-2 Contribution of this thesis

6-2.1 Involvement of enthesis in the disease initiation and development

Entheses are the sites where ligaments attach to bone and bear mechanical stress during movement. Enthesitis, inflammation in the entheses, is a characteristic feature of AS [308]; hence the link between where enthesitis occurs and where disease initiates has been long questioned.

The interfaces between the anterior/posterior longitudinal ligaments and annulus fibrosus, spinal entheses, were sites where inflammatory infiltrates initially appeared in the PGISp model. Spinal inflammation has also been reported in similar regions in the HLA-B27/hβ2m transgenic rats [138] and curdlan-treated SKG mice [160]. In more advanced stages,

excessive tissue, ectopic chondrocyte and bone formation features occurred in similar or adjacent anatomic positions including the enthesis at the anterior/posterior longitudinal ligaments and nearby cortical bone surfaces. These observations provide strong support that spinal enthesis is highly involved in PGISp disease development and infer support for similar pathological mechanisms in AS patients [169].

6-2.2 Mechanisms involved in excessive tissue formation

Endochondral, intramembranous and chondroidal ossification have all been reported in AS sacroiliac joints [73] and SpA biopsies [78]. Direct transformation from cartilage to bone has recently been shown in the fused zygapophysial joints in AS patients [79]. The PGISp mice developed extensive excessive tissue around the destroyed IVD. These pathological tissues were primarily cartilaginous in morphology with high PG content (Chapters 2 and 3) but also included foci of mineralised cartilage (Chapter 3). We also observed chondrocyte-like cells embedded in matrix containing low PG and low/no type I collagen, suggesting this tissue might be transitioning from cartilage to chondroidal bone within PGISp affected joints (Chapters 2 and 3). Other anabolic features, such as ectopic chondrocyte expansion (Chapter 2), osteophytes and ectopic bone (Chapter 3) occurred adjacent to the periosteum, implying the involvement of periosteal cells in PGISp ankylosis (Chapter 3).

The morphology and distribution of ectopic bone and osteophyte imply the contribution of biomechanical input in driving the anabolic process in PGISp disease. Given the severity of disc destruction observed in many PGISp mice (Chapter 2) and other structural changes (Chapter 3), it is obvious that axial skeleton biomechanics would be substantially altered in affected mice. Biomechanical stress has been shown to be associated with enthesitis in TNFΔARE mice and osteophyte formation in the collagen antibody-induced arthritis mouse model (CAIA) [169]. The present study suggests that both entheseal and non-entheseal biomechanical stress might play important roles in progression of spinal disease in PGISp mice, for not all the pathological bone developed from enthesis. More detailed investigation is required to define the specific changes that occur.

6-2.3 The association between inflammation and osteoproliferation

In the PGISp mouse model, mesenchymal cell proliferation initiated when inflammatory infiltrates were still present, but excessive tissue formation continued to progress after inflammation resolution. No colocalisation of severe inflammation and extensive excessive tissue formation was observed. Therefore, it was concluded that these two features do not initiate and progress in parallel in this model (Figure 6.1A).

Severe inflammation was observed associated with IVD destruction (Chapter 2) and was highly suggestive of the inflammatory process mediating disc destruction. The severity of disc destruction was positively correlated with cartilage damage, bone erosion, and excessive tissue formation (Chapter 5). IVDs separate vertebrae and play important roles in bearing compressive loads [309]. As discussed above, IVD destruction would alter mechanical stresses throughout the spine, but particularly at the IV joints, and we propose that these mechanical changes are a major driver of excessive tissue formation. Therefore, vertebral joint inflammation triggers a cascade of events that ultimately causes anabolic changes within the axial skeleton of PGISp mice (Figure 6.1B). Therefore, our characterisation of the PGISp model suggests that inflammation is required for the subsequent excessive tissue formation and eventually spine ankylosis.

This concept was verified in the PGISp mouse model by an early aggressive intervention study conducted in Chapter 5. The PGISp mice were treated with a combination of two strong anti-inflammatory treatments, etanercept and prednisolone (ETN+PRD). Treatment was commenced early in disease, a stage at which we anticipated that mice would have developed axial inflammation but limited disc destruction. The present study showed that early intervention with ETN+PRD significantly suppressed inflammation and demonstrated a trend in the reduction of disc destruction as well as excessive tissue formation (Chapter 5). These results support the hypothesis that inflammation is required for excessive tissue formation.

6-2.4 Clinical implications

Clinical studies have shown that patients with shorter disease duration usually have a greater improvement in disease activity after anti-TNF treatment (Table 1-3). Anti-TNF

treatment might retard radiographic progression in AS (Table 1-6), however AS patients who have already developed syndesmophytes tend to show more radiographic progression regardless of their treatment [202, 203, 205, 206]. The above studies suggest that early intervention can lead to better therapeutic outcomes.

Chapter 5 supports the promise that improved efficacy and outcomes will be achieved by early intervention with inflammation targeted drugs. This early intervention regimen might require changes in AS diagnosis requirements, becoming more aligned with starting treatment in non-radiographic axial SpA patients. Similar to AS patients, greater severity of disease at onset of treatment in PGISp mice compromised the treatment effects (Chapter 5). However, even if mice had more severe disease, early intervention still retarded disease progression when compared to the vehicle treatment. Hence, early intervention strategy show promise for improving treatment efficacy.

Therefore, the short therapeutic window falls between inflammation initiation and disc destruction (Figure 6.1C). However, it could be easily missed in AS patients, especially when there are no sensitive biomarkers or diagnosis criteria currently available. Slowing down disc destruction and joint damage might assist in attenuating excessive tissue formation if destructive processes have already been initiated.

The mRNA expression analysis in Chapter 2 demonstrated that MMP-3 and MMP-13 were both upregulated in the PGISp spine. These enzymes are known to be associated with cartilage and disc degeneration and osteophyte formation in OA [310], and potentially mediated destructive phenotypes in the PGISp mouse model. Therefore, blocking cartilage degrading enzymes might have benefits toward preventing disc damage in AS.

Anti-resorption therapy, bisphosphonates, has been demonstrated to reduce inflammation and decrease disease activity indices significantly in AS patients, although conclusions regarding their effects on syndesmophyte formation could not be drawn due to the short study duration [232, 300-305]. Reduction in osteophyte formation has been reported as a consequence of bisphosphonate treatment in other osteoporosis in postmenopausal women [307], and disease models, for example the anterior cruciate ligament transection rat model of OA [306]. Therefore, considering the observations made within this thesis, incorporating anti-resorption therapy in AS treatment, thereby reducing erosive damage

within effected areas, may alleviate biomechanical changes, strengthen the structure of spine and consequently reduce syndesmophyte formation.

6-2.5 Limitation of the PGISp mouse model

We acknowledge that the PGISp mouse model cannot perfectly replicate the disease symptoms of AS in human, as is the case with any animal model of disease. Female BALB/c mice have been shown to be more susceptible to PGIA/PGISp compared to male mice [311]. Gender effects might be attributed to genetics and interactions with the X chromosome have been shown to control disease susceptibility and onset whereas severity-associated loci were more strongly apparent in males [312]. Gender differences have also been reported in other disease models on the BALB/c background, such as curdlan-induced SpA in SKG mice [160] and ovalbumin-sensitised airway allergenic responses [313]. Difference of immune regulatory mechanisms between BALB/c and other strains and human might partially explain altered susceptibility of these models [313, 314]. IVD destruction in PGISp mice evolved to complete destruction much more rapidly than AS patients [219]. Therefore, the The syndesmophytes of AS patients usually develop from the vertebral corners at an angle <45° [233] and bridge two adjacent vertebral bodies. Osteophytes in PGISp mice grew outwards with morphologies differing from syndesmophyte. Subchondral bone lesions indicated by MRI lesions at vertebral corners in human disease were not seen in the PGISp mouse model. Nevertheless, compared to other current SpA/AS animal models, the data presented in this thesis confirms that the PGISp mouse model is still the best model to study the inflammation-osteoproliferation transition in AS patients.

Shared features with patients is an advantage of this model, however, some of these “advantages” limit its application in testing therapies. Similar to the slow progression in structural change in AS patients [232], it takes at least 24 weeks to establish extensive excess tissue in the PGISp mouse model. The variation caused by heterogeneous disease, which is also similar to what is seen in AS patients [315], greatly reduces the power of obtained data, as seen in Chapter 4 and Chapter 5. Therefore, time restraints and large sample sizes increase the difficulty of conducting experiments using this model.

The inadequate anti-inflammatory effects of ONO-AE1-329, the EP4 antagonist used in Chapter 4, indomethacin (Chapter 4) and etanercept alone (Chapter 5) suggest that very potent and perhaps non-specific anti-inflammatory treatments are required to suppress the inflammation in this model. Thus dissection of minor or partially compensated disease pathways would be extremely difficult to achieve using the PGISp model. Nevertheless, if a treatment successfully suppresses inflammation in this model, it might have a greater chance of suppressing inflammation in patients that are also often refractory to many anti-inflammatory treatment regimens.

6-3 Future directions

6-3.1 Improving methodology

Histological analysis was the main assessment of axial disease in the present study. It is suitable for in-depth analysis, particularly for characterising the inflammation, erosion and cartilaginous tissue formation. However, it is not ideal for studying bone structural change. On the contrary, CT analysis has the advantages of studying changes in bone. In the future experiments, both histology and CT analysis should be performed to provide more information about the mechanisms behind abnormal bone formation. A serial histology and IHC staining analysis could be performed to identify potential signalling pathways. The size of osteophyte and ectopic bone formation using CT imaging could be used to classify stages and detailed histological examination could distinguish types of ossification. Candidate pathways that had been reported in osteophyte formation, such as Wnt and BMP that had been discussed in section 1-3.2, can be tested with IHC especially in samples at the early tissue formation stage.

However, due to highly variable disease progression in this model and multiple factors contributing to disease development (eg, inflammation, mechanical stress, various cell types), targeting a single pathway either by genetically modified animal models or molecules might not be an effective strategy to verify the involvement of any particular signalling pathways.

6-3.2 Incorporating anti-resorption therapies with present early intervention treatment

We and other clinical studies have pointed out that early intervention in AS patients might improve not only inflammatory symptoms, but also excessive tissue formation. It leads to a number of future directions in this field. First of all, developing sensitive diagnostic tools and criteria are required for accurately and early identifying AS patients. Secondly, anti-inflammatory therapies need to be able to suppress inflammation effectively without leaving subclinical inflammation that might continue causing IVD or structural destruction/destabilization. GWAS suggests a long list of candidates that might be important in regulating disease development (Table 1-1). Unfortunately, Chapter 4 did not

provide enough evidence in support of or against whether *PTGER4*, a candidate gene identified by our group [51], is a good therapeutic target. However, there is no doubt that more functional studies are required to evaluate these candidate genes. Finally, preventing structural damage and ankylosis is the ultimate goal; therefore, it is worth testing whether combining anti-inflammatory and anti-resorption therapies, such as bisphosphonates, might enhance the efficacy of anti-inflammatory treatments. These could also be coupled with approaches that provide biomechanical support to a destabilized axial skeleton.

7 Bibliography or List of References

1. Akkoc N. Are spondyloarthropathies as common as rheumatoid arthritis worldwide? A review. Curr Rheumatol Rep. 2008; 10:371-8.

2. van Tubergen A, Weber U. Diagnosis and classification in spondyloarthritis: identifying a chameleon. Nat Rev Rheumatol. 2012; 8:253-61.

3. Thomas GP, Brown MA. Genetics and genomics of ankylosing spondylitis. Immunol Rev. 2010; 233:162-80.

4. Machado P, Landewe R, Braun J, Hermann KG, Baker D, van der Heijde D. Both structural damage and inflammation of the spine contribute to impairment of spinal mobility in patients with ankylosing spondylitis. Ann Rheum Dis. 2010; 69:1465-70.

5. Brown MA, Kennedy LG, MacGregor AJ, Darke C, Duncan E, Shatford JL, Taylor A, Calin A, Wordsworth P. Susceptibility to ankylosing spondylitis in twins: the role of genes, HLA, and the environment. Arthritis Rheum. 1997; 40:1823-8.

6. Cortes A, Hadler J, Pointon JP, Robinson PC, Karaderi T, Leo P, Cremin K, Pryce K, Harris J, Lee S *et al*. Identification of multiple risk variants for ankylosing spondylitis through high-density genotyping of immune-related loci. Nat Genet. 2013; 45:730-8.

7. Cortes A, Maksymowych WP, Wordsworth BP, Inman RD, Danoy P, Rahman P, Stone MA, Corr M, Gensler LS, Gladman D *et al*. Association study of genes related to bone formation and resorption and the extent of radiographic change in ankylosing spondylitis. Ann Rheum Dis. 2014:[Epub ahead of print].

8. Bartolome N, Szczypiorska M, Sanchez A, Sanz J, Juanola-Roura X, Gratacos J, Zarco-Montejo P, Collantes E, Martinez A, Tejedor D *et al*. Genetic polymorphisms inside and outside the MHC improve prediction of AS radiographic severity in addition to clinical variables. Rheumatology (Oxf). 2012; 51:1471-8.

9. Wang CM, Ho HH, Chang SW, Wu YJ, Lin JC, Chang PY, Wu J, Chen JY. ERAP1 genetic variations associated with HLA-B27 interaction and disease severity of syndesmophytes formation in Taiwanese ankylosing spondylitis. Arthritis Res Ther. 2012; 14:R125.

10. Park JH, Adoro S, Guinter T, Erman B, Alag AS, Catalfamo M, Kimura MY, Cui Y, Lucas PJ, Gress RE *et al*. Signaling by intrathymic cytokines, not T cell antigen receptors, specifies CD8 lineage choice and promotes the differentiation of cytotoxic-lineage T cells. Nat Immunol. 2010; 11:257-64.

11. Wang Y, Godec J, Ben-Aissa K, Cui K, Zhao K, Pucsek AB, Lee YK, Weaver CT, Yagi R, Lazarevic V. The transcription factors T-bet and Runx are required for the ontogeny of pathogenic interferon-gamma-producing T helper 17 cells. Immunity. 2014; 40:355-66.

12. Labonte D, Thies E, Kneussel M. The kinesin KIF21B participates in the cell surface delivery of gamma2 subunit-containing GABAA receptors. Eur J Cell Biol. 2014; 93:338-46.

13. Kreft KL, van Meurs M, Wierenga-Wolf AF, Melief MJ, van Strien ME, Hol EM, Oostra BA,

Laman JD, Hintzen RQ. Abundant kif21b is associated with accelerated progression in neurodegenerative diseases. Acta Neuropathol Commun. 2014; 2:144.

14. Boniface K, Bak-Jensen KS, Li Y, Blumenschein WM, McGeachy MJ, McClanahan TK, McKenzie BS, Kastelein RA, Cua DJ, de Waal Malefyt R. Prostaglandin E2 regulates Th17 cell differentiation and function through cyclic AMP and EP2/EP4 receptor signaling. J Exp Med. 2009; 206:535-48.

15. Roth S, Ruland J. Caspase recruitment domain-containing protein 9 signaling in innate immunity and inflammation. Trends Immunol. 2013; 34:243-50.

16. Elewaut D, Ware CF. The unconventional role of LT alpha beta in T cell differentiation. Trends Immunol. 2007; 28:169-75.

17. Puimege L, Libert C, Van Hauwermeiren F. Regulation and dysregulation of tumor necrosis factor receptor-1. Cytokine Growth Factor Rev. 2014; 25:285-300.

18. Lazarevic V, Chen X, Shim JH, Hwang ES, Jang E, Bolm AN, Oukka M, Kuchroo VK, Glimcher LH. T-bet represses T(H)17 differentiation by preventing Runx1-mediated activation of the gene encoding RORgammat. Nat Immunol. 2011; 12:96-104.

19. Nimmerjahn F, Ravetch JV. Fcgamma receptors as regulators of immune responses. Nat Rev Immunol. 2008; 8:34-47.

20. Yamamoto M, Sato S, Saitoh T, Sakurai H, Uematsu S, Kawai T, Ishii KJ, Takeuchi O, Akira S. Cutting Edge: Pivotal function of Ubc13 in thymocyte TCR signaling. J Immunol. 2006; 177:7520-4.

21. Fukushima T, Matsuzawa S, Kress CL, Bruey JM, Krajewska M, Lefebvre S, Zapata JM, Ronai Z, Reed JC. Ubiquitin-conjugating enzyme Ubc13 is a critical component of TNF receptor-associated factor (TRAF)-mediated inflammatory responses. Proc Natl Acad Sci U S A. 2007; 104:6371-6.

22. Thorburn AN, Macia L, Mackay CR. Diet, metabolites, and "western-lifestyle" inflammatory diseases. Immunity. 2014; 40:833-42.

23. Fallarini S, Magliulo L, Paoletti T, de Lalla C, Lombardi G. Expression of functional GPR35 in human iNKT cells. Biochem Biophys Res Commun. 2010; 398:420-5.

24. Roychoudhuri R, Hirahara K, Mousavi K, Clever D, Klebanoff CA, Bonelli M, Sciume G, Zare H, Vahedi G, Dema B *et al*. BACH2 represses effector programs to stabilize T(reg)-mediated immune homeostasis. Nature. 2013; 498:506-10.

25. Lee J, Beliakoff J, Sun Z. The novel PIAS-like protein hZimp10 is a transcriptional co-activator of the p53 tumor suppressor. Nucleic Acids Res. 2007; 35:4523-34.

26. Li X, Thyssen G, Beliakoff J, Sun Z. The novel PIAS-like protein hZimp10 enhances Smad transcriptional activity. J Biol Chem. 2006; 281:23748-56.

27. Pabst O, Forster R, Lipp M, Engel H, Arnold HH. NKX2.3 is required for MAdCAM-1 expression and homing of lymphocytes in spleen and mucosa-associated lymphoid tissue.

EMBO J. 2000; 19:2015-23.

28. Kellermayer Z, Mihalj M, Labadi A, Czompoly T, Lee M, O'Hara E, Butcher EC, Berta G, Balogh A, Arnold HH *et al*. Absence of Nkx2-3 homeodomain transcription factor reprograms the endothelial addressin preference for lymphocyte homing in Peyer's patches. J Immunol. 2014; 193:5284-93.

29. Katayama H, Mori T, Seki Y, Anraku M, Iseki M, Ikutani M, Iwasaki Y, Yoshida N, Takatsu K, Takaki S. Lnk prevents inflammatory CD8(+) T-cell proliferation and contributes to intestinal homeostasis. Eur J Immunol. 2014; 44:1622-32.

30. Okajima F. Regulation of inflammation by extracellular acidification and proton-sensing GPCRs. Cell Signal. 2013; 25:2263-71.

31. Bosmann M, Ward PA. Modulation of inflammation by interleukin-27. J Leukoc Biol. 2013; 94:1159-65.

32. Daniels J, Kadlubar S. Sulfotransferase genetic variation: from cancer risk to treatment response. Drug Metab Rev. 2013; 45:415-22.

33. Bernardeau C, Dernis-Labous E, Blanchard H, Lamarque D, Breban M. Nitric oxide in rheumatology. Joint Bone Spine. 2001; 68:457-62.

34. Liang Y, Zhu Y, Xia Y, Peng H, Yang XK, Liu YY, Xu WD, Pan HF, Ye DQ. Therapeutic potential of tyrosine kinase 2 in autoimmunity. Expert Opin Ther Targets. 2014; 18:571-80.

35. Ishizaki M, Muromoto R, Akimoto T, Ohshiro Y, Takahashi M, Sekine Y, Maeda H, Shimoda K, Oritani K, Matsuda T. Tyk2 deficiency protects joints against destruction in anti-type II collagen antibody-induced arthritis in mice. Int Immunol. 2011; 23:575-82.

36. Hedl M, Lahiri A, Ning K, Cho JH, Abraham C. Pattern recognition receptor signaling in human dendritic cells is enhanced by ICOS ligand and modulated by the Crohn's disease ICOSLG risk allele. Immunity. 2014; 40:734-46.

37. Dong YF, Soung do Y, Schwarz EM, O'Keefe RJ, Drissi H. Wnt induction of chondrocyte hypertrophy through the Runx2 transcription factor. J Cell Physiol. 2006; 208:77-86.

38. Ho AM, Johnson MD, Kingsley DM. Role of the mouse ank gene in control of tissue calcification and arthritis. Science. 2000; 289:265-70.

39. Las Heras F, DaCosta RS, Pritzker KP, Haroon N, Netchev G, Tsui HW, Chiu B, Erwin WM, Tsui FW, Inman RD. Aberrant axial mineralization precedes spinal ankylosis: a molecular imaging study in ank/ank mice. Arthritis Res Ther. 2011; 13:R163.

40. Gurley KA, Chen H, Guenther C, Nguyen ET, Rountree RB, Schoor M, Kingsley DM. Mineral formation in joints caused by complete or joint-specific loss of ANK function. J Bone Miner Res. 2006; 21:1238-47.

41. Ivkovic S, Yoon BS, Popoff SN, Safadi FF, Libuda DE, Stephenson RC, Daluiski A, Lyons KM. Connective tissue growth factor coordinates chondrogenesis and angiogenesis during skeletal development. Development. 2003; 130:2779-91.

42. Nozawa K, Fujishiro M, Kawasaki M, Kaneko H, Iwabuchi K, Yanagida M, Suzuki F, Miyazawa K, Takasaki Y, Ogawa H *et al*. Connective tissue growth factor promotes articular damage by increased osteoclastogenesis in patients with rheumatoid arthritis. Arthritis Res Ther. 2009; 11:R174.

43. Yoshihara Y, Nakamura H, Obata K, Yamada H, Hayakawa T, Fujikawa K, Okada Y. Matrix metalloproteinases and tissue inhibitors of metalloproteinases in synovial fluids from patients with rheumatoid arthritis or osteoarthritis. Ann Rheum Dis. 2000; 59:455-61.

44. Hayami T, Kapila YL, Kapila S. MMP-1 (collagenase-1) and MMP-13 (collagenase-3) differentially regulate markers of osteoblastic differentiation in osteogenic cells. Matrix Biol. 2008; 27:682-92.

45. Bennett CN, Ouyang H, Ma YL, Zeng Q, Gerin I, Sousa KM, Lane TF, Krishnan V, Hankenson KD, MacDougald OA. Wnt10b increases postnatal bone formation by enhancing osteoblast differentiation. J Bone Miner Res. 2007; 22:1924-32.

46. Li X, Zhang Y, Kang H, Liu W, Liu P, Zhang J, Harris SE, Wu D. Sclerostin binds to LRP5/6 and antagonizes canonical Wnt signaling. J Biol Chem. 2005; 280:19883-7.

47. Dougall WC, Glaccum M, Charrier K, Rohrbach K, Brasel K, De Smedt T, Daro E, Smith J, Tometsko ME, Maliszewski CR *et al*. RANK is essential for osteoclast and lymph node development. Genes Dev. 1999; 13:2412-24.

48. Zhang X, Kuroda S, Carpenter D, Nishimura I, Soo C, Moats R, Iida K, Wisner E, Hu FY, Miao S *et al*. Craniosynostosis in transgenic mice overexpressing Nell-1. J Clin Invest. 2002; 110:861-70.

49. Pierroz DD, Bonnet N, Bianchi EN, Bouxsein ML, Baldock PA, Rizzoli R, Ferrari SL. Deletion of beta-adrenergic receptor 1, 2, or both leads to different bone phenotypes and response to mechanical stimulation. J Bone Miner Res. 2012; 27:1252-62.

50. Burton PR, Clayton DG, Cardon LR, Craddock N, Deloukas P, Duncanson A, Kwiatkowski DP, McCarthy MI, Ouwehand WH, Samani NJ *et al*. Association scan of 14,500 nonsynonymous SNPs in four diseases identifies autoimmunity variants. Nat Genet. 2007; 39:1329-37.

51. Evans DM, Spencer CC, Pointon JJ, Su Z, Harvey D, Kochan G, Oppermann U, Dilthey A, Pirinen M, Stone MA *et al*. Interaction between ERAP1 and HLA-B27 in ankylosing spondylitis implicates peptide handling in the mechanism for HLA-B27 in disease susceptibility. Nat Genet. 2011; 43:761-7.

52. Wright C, Sibani S, Trudgian D, Fischer R, Kessler B, LaBaer J, Bowness P. Detection of multiple autoantibodies in patients with ankylosing spondylitis using nucleic acid programmable protein arrays. Mol Cell Proteomics. 2012; 11:M9.00384.

53. Zou J. Predominant cellular immune response to the cartilage autoantigenic G1 aggrecan in ankylosing spondylitis and rheumatoid arthritis. Rheumatology (Oxford). 2003; 42:846-55.

54. Cohen ES, Bodmer HC. Cytotoxic T lymphocytes recognize and lyse chondrocytes under

inflammatory, but not non-inflammatory conditions. Immunology. 2003; 109:8-14.

55. Appel H, Kuhne M, Spiekermann S, Kohler D, Zacher J, Stein H, Sieper J, Loddenkemper C. Immunohistochemical analysis of hip arthritis in ankylosing spondylitis: evaluation of the bone-cartilage interface and subchondral bone marrow. Arthritis Rheum. 2006; 54:1805-13.

56. Haroon N, Inman RD. Endoplasmic reticulum aminopeptidases: biology and pathogenic potential. Nature Reviews Rheumatology. 2010; 6:461-7.

57. Dangoria NS, DeLay ML, Kingsbury DJ, Mear JP, Uchanska-Ziegler B, Ziegler A, Colbert RA. HLA-B27 misfolding is associated with aberrant intermolecular disulfide bond formation (dimerization) in the endoplasmic reticulum. J Biol Chem. 2002; 277:23459-68.

58. Bowness P, Ridley A, Shaw J, Chan AT, Wong-Baeza I, Fleming M, Cummings F, McMichael A, Kollnberger S. Th17 cells expressing KIR3DL2+ and responsive to HLA-B27 homodimers are increased in ankylosing spondylitis. J Immunol. 2011; 186:2672-80.

59. Kenna TJ, Lau MC, Keith P, Ciccia F, Costello ME, Bradbury L, Low PL, Agrawal N, Triolo G, Alessandro R *et al*. Disease-associated polymorphisms in ERAP1 do not alter endoplasmic reticulum stress in patients with ankylosing spondylitis. Genes Immun. 2014.

60. El Maghraoui A. Extra-articular manifestations of ankylosing spondylitis: prevalence, characteristics and therapeutic implications. Eur J Intern Med. 2011; 22:554-60.

61. Costello ME, Ciccia F, Willner D, Warrington N, Robinson PC, Gardiner B, Marshall M, Kenna TJ, Triolo G, Brown MA. Intestinal dysbiosis in ankylosing spondylitis. Arthritis Rheumatol. 2014.

62. Taurog JD, Richardson JA, Croft JT, Simmons WA, Zhou M, Fernandez-Sueiro JL, Balish E, Hammer RE. The germfree state prevents development of gut and joint inflammatory disease in HLA-B27 transgenic rats. J Exp Med. 1994; 180:2359-64.

63. Rehaume LM, Mondot S, Aguirre de Carcer D, Velasco J, Benham H, Hasnain SZ, Bowman J, Ruutu M, Hansbro PM, McGuckin MA *et al*. ZAP-70 genotype disrupts the relationship between microbiota and host, leading to spondyloarthritis and ileitis in SKG mice. Arthritis Rheumatol. 2014; 66:2780-92.

64. Lin P, Bach M, Asquith M, Lee AY, Akileswaran L, Stauffer P, Davin S, Pan Y, Cambronne ED, Dorris M *et al*. HLA-B27 and human beta2-microglobulin affect the gut microbiota of transgenic rats. PLoS ONE. 2014; 9:e105684.

65. Wang X, Lin Z, Wei Q, Jiang Y, Gu J. Expression of IL-23 and IL-17 and effect of IL-23 on IL-17 production in ankylosing spondylitis. Rheumatol Int. 2009; 29:1343-7.

66. Taylan A, Sari I, Kozaci DL, Yuksel A, Bilge S, Yildiz Y, Sop G, Coker I, Gunay N, Akkoc N. Evaluation of the T helper 17 axis in ankylosing spondylitis. Rheumatol Int. 2012; 32:2511-5.

67. Kenna TJ, Davidson SI, Duan R, Bradbury LA, McFarlane J, Smith M, Weedon H, Street S, Thomas R, Thomas GP *et al*. Enrichment of circulating interleukin-17-secreting interleukin-23 receptor-positive γ/δ T cells in patients with active ankylosing spondylitis. Arthritis

Rheum. 2012; 64:1420-9.

68. Shen H, Goodall JC, Hill Gaston JS. Frequency and phenotype of peripheral blood Th17 cells in ankylosing spondylitis and rheumatoid arthritis. Arthritis Rheum. 2009; 60:1647-56.

69. Sherlock JP, Joyce-Shaikh B, Turner SP, Chao CC, Sathe M, Grein J, Gorman DM, Bowman EP, McClanahan TK, Yearley JH *et al*. IL-23 induces spondyloarthropathy by acting on ROR-gammat+ CD3+CD4-CD8- entheseal resident T cells. Nat Med. 2012; 18:1069-76.

70. Benjamin M, McGonagle D. The anatomical basis for disease localisation in seronegative spondyloarthropathy at entheses and related sites. J Anat. 2001; 199:503-26.

71. Braun J, Khan MA, Sieper J. Enthesitis and ankylosis in spondyloarthropathy: what is the target of the immune response? Ann Rheum Dis. 2000; 59:985-94.

72. Sieper J, Rudwaleit M, Baraliakos X, Brandt J, Braun J, Burgos-Vargas R, Dougados M, Hermann KG, Landewe R, Maksymowych W *et al*. The Assessment of SpondyloArthritis international Society (ASAS) handbook: a guide to assess spondyloarthritis. Ann Rheum Dis. 2009; 68 Suppl 2:ii1-44.

73. Francois RJ, Gardner DL, Degrave EJ, Bywaters EG. Histopathologic evidence that sacroiliitis in ankylosing spondylitis is not merely enthesitis. Arthritis Rheum. 2000; 43:2011-24.

74. Benjamin M, McGonagle D. Histopathologic changes at "synovio-entheseal complexes" suggesting a novel mechanism for synovitis in osteoarthritis and spondylarthritis. Arthritis Rheum. 2007; 56:3601-9.

75. Benjamin M, Toumi H, Suzuki D, Redman S, Emery P, McGonagle D. Microdamage and altered vascularity at the enthesis-bone interface provides an anatomic explanation for bone involvement in the HLA-B27-associated spondylarthritides and allied disorders. Arthritis Rheum. 2007; 56:224-33.

76. McGonagle D, Marzo-Ortega H, O'Connor P, Gibbon W, Pease C, Reece R, Emery P. The role of biomechanical factors and HLA-B27 in magnetic resonance imaging-determined bone changes in plantar fascia enthesopathy. Arthritis Rheum. 2002; 46:489-93.

77. Mau W, Zeidler H, Mau R, Majewski A, Freyschmidt J, Stangel W, Deicher H. Clinical features and prognosis of patients with possible ankylosing spondylitis. Results of a 10-year followup. J Rheumatol. 1988; 15:1109-14.

78. Benjamin M, Toumi H, Suzuki D, Hayashi K, McGonagle D. Evidence for a distinctive pattern of bone formation in enthesophytes. Ann Rheum Dis. 2009; 68:1003-10.

79. Bleil J, Sieper J, Maier R, Schlichting U, Hempfing A, Appel H, Syrbe U: *In situ* analysis of mechanisms of new bone formation in zygapophyseal joints from patients with ankylosing spondylitis. In: *American College of Rheumatology annual meeting.* Boston: American College of Rheumatology; 2014.

80. Long F. Building strong bones: molecular regulation of the osteoblast lineage. Nat Rev Mol

Cell Biol. 2011; 13:27-38.

81. Kronenberg HM. Developmental regulation of the growth plate. Nature. 2003; 423:332-6.

82. Roach HI, Erenpreisa J, Aigner T. Osteogenic differentiation of hypertrophic chondrocytes involves asymmetric cell divisions and apoptosis. J Cell Biol. 1995; 131:483-94.

83. Yang L, Tsang KY, Tang HC, Chan D, Cheah KS. Hypertrophic chondrocytes can become osteoblasts and osteocytes in endochondral bone formation. Proc Natl Acad Sci U S A. 2014; 111:12097-102.

84. Konya V, Marsche G, Schuligoi R, Heinemann A. E-type prostanoid receptor 4 (EP4) in disease and therapy. Pharmacol Ther. 2013; 138:485-502.

85. Paralkar VM, Borovecki F, Ke HZ, Cameron KO, Lefker B, Grasser WA, Owen TA, Li M, DaSilva-Jardine P, Zhou M *et al*. An EP2 receptor-selective prostaglandin E2 agonist induces bone healing. Proc Natl Acad Sci U S A. 2003; 100:6736-40.

86. Li M, Ke HZ, Qi H, Healy DR, Li Y, Crawford DT, Paralkar VM, Owen TA, Cameron KO, Lefker BA *et al*. A novel, non-prostanoid EP2 receptor-selective prostaglandin E2 agonist stimulates local bone formation and enhances fracture healing. J Bone Miner Res. 2003; 18:2033-42.

87. Xie C, Liang B, Xue M, Lin AS, Loiselle A, Schwarz EM, Guldberg RE, O'Keefe RJ, Zhang X. Rescue of impaired fracture healing in COX-2-/- mice via activation of prostaglandin E2 receptor subtype 4. Am J Pathol. 2009; 175:772-85.

88. Yoshida K, Oida H, Kobayashi T, Maruyama T, Tanaka M, Katayama T, Yamaguchi K, Segi E, Tsuboyama T, Matsushita M *et al*. Stimulation of bone formation and prevention of bone loss by prostaglandin E EP4 receptor activation. Proc Natl Acad Sci U S A. 2002; 99:4580-5.

89. Iwaniec UT, Moore K, Rivera MF, Myers SE, Vanegas SM, Wronski TJ. A comparative study of the bone-restorative efficacy of anabolic agents in aged ovariectomized rats. Osteoporos Int. 2007; 18:351-62.

90. Suda M, Tanaka K, Natsui K, Usui T, Tanaka I, Fukushima M, Shigeno C, Konishi J, Narumiya S, Ichikawa A *et al*. Prostaglandin E receptor subtypes in mouse osteoblastic cell line. Endocrinology. 1996; 137:1698-705.

91. Miyamoto M, Ito H, Mukai S, Kobayashi T, Yamamoto H, Kobayashi M, Maruyama T, Akiyama H, Nakamura T. Simultaneous stimulation of EP2 and EP4 is essential to the effect of prostaglandin E2 in chondrocyte differentiation. Osteoarthritis Cartilage. 2003; 11:644-52.

92. Zhang M, Ho HC, Sheu TJ, Breyer MD, Flick LM, Jonason JH, Awad HA, Schwarz EM, O'Keefe RJ. EP1(-/-) mice have enhanced osteoblast differentiation and accelerated fracture repair. J Bone Miner Res. 2011; 26:792-802.

93. Cherian PP, Cheng B, Gu S, Sprague E, Bonewald LF, Jiang JX. Effects of mechanical strain on the function of Gap junctions in osteocytes are mediated through the prostaglandin EP2 receptor. J Biol Chem. 2003; 278:43146-56.

94. Siller-Jackson AJ, Burra S, Gu S, Xia X, Bonewald LF, Sprague E, Jiang JX. Adaptation of connexin 43-hemichannel prostaglandin release to mechanical loading. J Biol Chem. 2008; 283:26374-82.

95. Zhang J, Wang JH. Production of PGE(2) increases in tendons subjected to repetitive mechanical loading and induces differentiation of tendon stem cells into non-tenocytes. J Orthop Res. 2010; 28:198-203.

96. Poddubnyy D, Rudwaleit M, Haibel H, Listing J, Marker-Hermann E, Zeidler H, Braun J, Sieper J. Effect of non-steroidal anti-inflammatory drugs on radiographic spinal progression in patients with axial spondyloarthritis: results from the German Spondyloarthritis Inception Cohort. Ann Rheum Dis. 2012.

97. Wanders A, Heijde D, Landewe R, Behier JM, Calin A, Olivieri I, Zeidler H, Dougados M. Nonsteroidal antiinflammatory drugs reduce radiographic progression in patients with ankylosing spondylitis: a randomized clinical trial. Arthritis Rheum. 2005; 52:1756-65.

98. Kubota T, Michigami T, Ozono K. Wnt signaling in bone metabolism. J Bone Miner Metab. 2009; 27:265-71.

99. Brunkow ME, Gardner JC, Van Ness J, Paeper BW, Kovacevich BR, Proll S, Skonier JE, Zhao L, Sabo PJ, Fu Y *et al*. Bone dysplasia sclerosteosis results from loss of the SOST gene product, a novel cystine knot-containing protein. Am J Hum Genet. 2001; 68:577-89.

100. MacDonald BT, Joiner DM, Oyserman SM, Sharma P, Goldstein SA, He X, Hauschka PV. Bone mass is inversely proportional to Dkk1 levels in mice. Bone. 2007; 41:331-9.

101. Klingberg E, Nurkkala M, Carlsten H, Forsblad-d'Elia H. Biomarkers of bone metabolism in ankylosing spondylitis in relation to osteoproliferation and osteoporosis. J Rheumatol. 2014; 41:1349-56.

102. Diarra D, Stolina M, Polzer K, Zwerina J, Ominsky MS, Dwyer D, Korb A, Smolen J, Hoffmann M, Scheinecker C *et al*. Dickkopf-1 is a master regulator of joint remodeling. Nat Med. 2007; 13:156-63.

103. Appel H, Ruiz-Heiland G, Listing J, Zwerina J, Herrmann M, Mueller R, Haibel H, Baraliakos X, Hempfing A, Rudwaleit M *et al*. Altered skeletal expression of sclerostin and its link to radiographic progression in ankylosing spondylitis. Arthritis Rheum. 2009; 60:3257-62.

104. Poole KES. Sclerostin is a delayed secreted product of osteocytes that inhibits bone formation. The FASEB Journal. 2005.

105. Haynes KR, Pettit AR, Duan R, Tseng HW, Glant TT, Brown MA, Thomas GP. Excessive bone formation in a mouse model of ankylosing spondylitis is associated with decreases in Wnt pathway inhibitors. Arthritis Res Ther. 2012; 14:R253.

106. Kamiya N, Mishina Y. New insights on the roles of BMP signaling in bone-A review of recent mouse genetic studies. Biofactors. 2011; 37:75-82.

107. Bandyopadhyay A, Yadav PS, Prashar P. BMP signaling in development and diseases: a pharmacological perspective. Biochem Pharmacol. 2013; 85:857-64.

108. Lories RJ, Derese I, Luyten FP. Modulation of bone morphogenetic protein signaling inhibits the onset and progression of ankylosing enthesitis. J Clin Investig. 2005; 115:1571-9.

109. Bandyopadhyay A, Tsuji K, Cox K, Harfe BD, Rosen V, Tabin CJ. Genetic analysis of the roles of BMP2, BMP4, and BMP7 in limb patterning and skeletogenesis. PLoS Genet. 2006; 2:e216.

110. Pizette S, Niswander L. BMPs are required at two steps of limb chondrogenesis: formation of prechondrogenic condensations and their differentiation into chondrocytes. Dev Biol. 2000; 219:237-49.

111. Shafritz AB, Shore EM, Gannon FH, Zasloff MA, Taub R, Muenke M, Kaplan FS. Overexpression of an osteogenic morphogen in fibrodysplasia ossificans progressiva. N Engl J Med. 1996; 335:555-61.

112. Shore EM, Xu M, Feldman GJ, Fenstermacher DA, Cho TJ, Choi IH, Connor JM, Delai P, Glaser DL, LeMerrer M *et al*. A recurrent mutation in the BMP type I receptor ACVR1 causes inherited and sporadic fibrodysplasia ossificans progressiva. Nat Genet. 2006; 38:525-7.

113. Park MC, Park YB, Lee SK. Relationship of bone morphogenetic proteins to disease activity and radiographic damage in patients with ankylosing spondylitis. Scand J Rheumatol. 2008; 37:200-4.

114. Milia AF, Ibba-Manneschi L, Manetti M, Benelli G, Generini S, Messerini L, Matucci-Cerinic M. Evidence for the prevention of enthesitis in HLA-B27/hbeta(2)m transgenic rats treated with a monoclonal antibody against TNF-alpha. J Cell Mol Med. 2011; 15:270-9.

115. Zochling J, van der Heijde D, Burgos-Vargas R, Collantes E, Davis JC, Jr., Dijkmans B, Dougados M, Geher P, Inman RD, Khan MA *et al*. ASAS/EULAR recommendations for the management of ankylosing spondylitis. Ann Rheum Dis. 2006; 65:442-52.

116. Sieper J. Developments in therapies for spondyloarthritis. Nat Rev Rheumatol. 2012; 8:280-7.

117. Inman RD, Davis JC, Jr., Heijde D, Diekman L, Sieper J, Kim SI, Mack M, Han J, Visvanathan S, Xu Z *et al*. Efficacy and safety of golimumab in patients with ankylosing spondylitis: results of a randomized, double-blind, placebo-controlled, phase III trial. Arthritis Rheum. 2008; 58:3402-12.

118. van der Heijde D, Dijkmans B, Geusens P, Sieper J, DeWoody K, Williamson P, Braun J. Efficacy and safety of infliximab in patients with ankylosing spondylitis: results of a randomized, placebo-controlled trial (ASSERT). Arthritis Rheum. 2005; 52:582-91.

119. Barkham N, Keen HI, Coates LC, O'Connor P, Hensor E, Fraser AD, Cawkwell LS, Bennett A, McGonagle D, Emery P. Clinical and imaging efficacy of infliximab in HLA-B27-Positive patients with magnetic resonance imaging-determined early sacroiliitis. Arthritis Rheum. 2009; 60:946-54.

120. Braun J, Baraliakos X, Hermann KG, van der Heijde D, Inman RD, Deodhar AA, Baratelle A, Xu S, Xu W, Hsu B. Golimumab reduces spinal inflammation in ankylosing spondylitis:

MRI results of the randomised, placebo- controlled GO-RAISE study. Ann Rheum Dis. 2012; 71:878-84.

121. Rudwaleit M, Listing J, Brandt J, Braun J, Sieper J. Prediction of a major clinical response (BASDAI 50) to tumour necrosis factor alpha blockers in ankylosing spondylitis. Ann Rheum Dis. 2004; 63:665-70.

122. Song IH, Hermann K, Haibel H, Althoff CE, Listing J, Burmester G, Krause A, Bohl-Buhler M, Freundlich B, Rudwaleit M *et al*. Effects of etanercept versus sulfasalazine in early axial spondyloarthritis on active inflammatory lesions as detected by whole-body MRI (ESTHER): a 48-week randomised controlled trial. Ann Rheum Dis. 2011; 70:590-6.

123. Sieper J, Landewe R, Rudwaleit M, van der Heijde D, Dougados M, Mease PJ, Braun J, Deodhar A, Kivitz A, Walsh J *et al*. Effect of Certolizumab Pegol over 96 Weeks in Patients with Axial Spondyloarthritis: Results from a Phase 3 Randomized Trial. Arthritis Rheumatol. 2014.

124. van der Heijde D, Landewe R, Einstein S, Ory P, Vosse D, Ni L, Lin SL, Tsuji W, Davis JC, Jr. Radiographic progression of ankylosing spondylitis after up to two years of treatment with etanercept. Arthritis Rheum. 2008; 58:1324-31.

125. Pedersen SJ, Chiowchanwisawakit P, Lambert RG, Ostergaard M, Maksymowych WP. Resolution of inflammation following treatment of ankylosing spondylitis is associated with new bone formation. J Rheumatol. 2011; 38:1349-54.

126. Baraliakos X, Haibel H, Listing J, Sieper J, Braun J. Continuous long-term anti-TNF therapy does not lead to an increase in the rate of new bone formation over 8 years in patients with ankylosing spondylitis. Ann Rheum Dis. 2013.

127. Heijde Dvd, Landewé R, Baraliakos X, Houben H, Tubergen Av, Williamson P, Xu W, Baker D, Goldstein N, Braun J. Radiographic findings following two years of infliximab therapy in patients with ankylosing spondylitis. Arthritis Rheum. 2008; 58:3063-70.

128. Sieper J, Lenaerts J, Wollenhaupt J, Rudwaleit M, Mazurov VI, Myasoutova L, Park S, Song Y, Yao R, Chitkara D *et al*. Efficacy and safety of infliximab plus naproxen versus naproxen alone in patients with early, active axial spondyloarthritis: results from the double-blind, placebo-controlled INFAST study, Part 1. Ann Rheum Dis. 2014; 73:101-7.

129. Braun J, Brandt J, Listing J, Zink A, Alten R, Golder W, Gromnica-Ihle E, Kellner H, Krause A, Schneider M *et al*. Treatment of active ankylosing spondylitis with infliximab: a randomised controlled multicentre trial. Lancet. 2002; 359:1187-93.

130. Dougados M, van der Heijde D, Sieper J, Braun J, Maksymowych WP, Citera G, Miceli-Richard C, Wei JC, Pedersen R, Bonin R *et al*. Symptomatic efficacy of etanercept and its effects on objective signs of inflammation in early nonradiographic axial spondyloarthritis: a multicenter, randomized, double-blind, placebo-controlled trial. Arthritis Rheumatol. 2014; 66:2091-102.

131. Davis JC, Jr., Van Der Heijde D, Braun J, Dougados M, Cush J, Clegg DO, Kivitz A, Fleischmann R, Inman R, Tsuji W. Recombinant human tumor necrosis factor receptor (etanercept) for treating ankylosing spondylitis: a randomized, controlled trial. Arthritis

Rheum. 2003; 48:3230-6.

132. Davis JC, van der Heijde DM, Braun J, Dougados M, Cush J, Clegg D, Inman RD, Kivitz A, Zhou L, Solinger A *et al*. Sustained durability and tolerability of etanercept in ankylosing spondylitis for 96 weeks. Ann Rheum Dis. 2005; 64:1557-62.

133. Haibel H, Rudwaleit M, Listing J, Sieper J. Open label trial of anakinra in active ankylosing spondylitis over 24 weeks. Ann Rheum Dis. 2005; 64:296-8.

134. Wendling D, Dougados M, Berenbaum F, Brocq O, Schaeverbeke T, Mazieres B, Marcelli C, Leparc JM, Bertin P, Robin M *et al*. Rituximab treatment for spondyloarthritis. A nationwide series: data from the AIR registry of the French Society of Rheumatology. J Rheumatol. 2012; 39:2327-31.

135. Sieper J, Porter-Brown B, Thompson L, Harari O, Dougados M. Assessment of short-term symptomatic efficacy of tocilizumab in ankylosing spondylitis: results of randomised, placebo-controlled trials. Ann Rheum Dis. 2014; 73:95-100.

136. Poddubnyy D, Hermann KG, Callhoff J, Listing J, Sieper J. Ustekinumab for the treatment of patients with active ankylosing spondylitis: results of a 28-week, prospective, open-label, proof-of-concept study (TOPAS). Ann Rheum Dis. 2014; 73:817-23.

137. Baeten D, Baraliakos X, Braun J, Sieper J, Emery P, van der Heijde D, McInnes I, van Laar JM, Landewe R, Wordsworth P *et al*. Anti-interleukin-17A monoclonal antibody secukinumab in treatment of ankylosing spondylitis: a randomised, double-blind, placebo-controlled trial. Lancet. 2013; 382:1705-13.

138. Hammer RE, Maika SD, Richardson JA, Tang JP, Taurog JD. Spontaneous inflammatory disease in transgenic rats expressing HLA-B27 and human beta 2m: an animal model of HLA-B27-associated human disorders. Cell. 1990; 63:1099-112.

139. van Duivenvoorde LM, Dorris ML, Satumtira N, van Tok MN, Redlich K, Tak PP, Taurog JD, Baeten DL. Relationship between inflammation, bone destruction, and osteoproliferation in the HLA-B27/human beta(2) -microglobulin-transgenic rat model of spondylarthritis. Arthritis Rheum. 2012; 64:3210-9.

140. Taurog JD, Maika SD, Simmons WA, Breban M, Hammer RE. Susceptibility to inflammatory disease in HLA-B27 transgenic rat lines correlates with the level of B27 expression. J Immunol. 1993; 150:4168-78.

141. Tran TM, Dorris ML, Satumtira N, Richardson JA, Hammer RE, Shang J, Taurog JD. Additional human β2-microglobulin curbs HLA–B27 misfolding and promotes arthritis and spondylitis without colitis in male HLA–B27–transgenic rats. Arthritis Rheum. 2006; 54:1317-27.

142. Breban M, Fernandez-Sueiro JL, Richardson JA, Hadavand RR, Maika SD, Hammer RE, Taurog JD. T cells, but not thymic exposure to HLA-B27, are required for the inflammatory disease of HLA-B27 transgenic rats. J Immunol. 1996; 156:794-803.

143. Breban M, Hammer RE, Richardson JA, Taurog JD. Transfer of the inflammatory disease of HLA-B27 transgenic rats by bone marrow engraftment. J Exp Med. 1993; 178:1607-16.

144. Taurog JD, Dorris ML, Satumtira N, Tran TM, Sharma R, Dressel R, van den Brandt J, Reichardt HM. Spondylarthritis in HLA-B27/human beta2-microglobulin-transgenic rats is not prevented by lack of CD8. Arthritis Rheum. 2009; 60:1977-84.

145. May E, Dorris ML, Satumtira N, Iqbal I, Rehman MI, Lightfoot E, Taurog JD. CD8 alpha beta T cells are not essential to the pathogenesis of arthritis or colitis in HLA-B27 transgenic rats. J Immunol. 2003; 170:1099-105.

146. Glatigny S, Fert I, Blaton MA, Lories RJ, Araujo LM, Chiocchia G, Breban M. Proinflammatory Th17 cells are expanded and induced by dendritic cells in spondylarthritis-prone HLA-B27-transgenic rats. Arthritis Rheum. 2012; 64:110-20.

147. DeLay ML, Turner MJ, Klenk EI, Smith JA, Sowders DP, Colbert RA. HLA-B27 misfolding and the unfolded protein response augment interleukin-23 production and are associated with Th17 activation in transgenic rats. Arthritis Rheum. 2009; 60:2633-43.

148. Turner MJ, DeLay ML, Bai S, Klenk E, Colbert RA. HLA–B27 up-regulation causes accumulation of misfolded heavy chains and correlates with the magnitude of the unfolded protein response in transgenic rats: Implications for the pathogenesis of spondylarthritis-like disease. Arthritis Rheum. 2007; 56:215-23.

149. Utriainen L, Firmin D, Wright P, Cerovic V, Breban M, McInnes I, Milling S. Expression of HLA-B27 causes loss of migratory dendritic cells in a rat model of spondylarthritis. Arthritis Rheum. 2012; 64:3199-209.

150. Milia AF, Manetti M, Generini S, Polidori L, Benelli G, Cinelli M, Messerini L, Ibba-Manneschi L, Matucci-Cerinic M. TNFalpha blockade prevents the development of inflammatory bowel disease in HLA-B27 transgenic rats. J Cell Mol Med. 2009; 13:164-76.

151. Nordling C, Karlsson-Parra A, Jansson L, Holmdahl R, Klareskog L. Characterization of a spontaneously occurring arthritis in male DBA/1 mice. Arthritis Rheum. 1992; 35:717-22.

152. Lories RJ, Matthys P, de Vlam K, Derese I, Luyten FP. Ankylosing enthesitis, dactylitis, and onychoperiostitis in male DBA/1 mice: a model of psoriatic arthritis. Ann Rheum Dis. 2004; 63:595-8.

153. Corthay A, Hansson AS, Holmdahl R. T lymphocytes are not required for the spontaneous development of entheseal ossification leading to marginal ankylosis in the DBA/1 mouse. Arthritis Rheum. 2000; 43:844-51.

154. Matthys P, Lories RJ, Bert De K, Heremans H, Luyten FP, Billiau A. Dependence on interferon-gamma for the spontaneous occurrence of arthritis in DBA/1 mice. Arthritis Rheum. 2003; 48:2983-8.

155. Ebihara S, Date F, Dong Y, Ono M. Interleukin-17 is a critical target for the treatment of ankylosing enthesitis and psoriasis-like dermatitis in mice. Autoimmunity. 2014:1-8.

156. Braem K, Deroose CM, Luyten FP, Lories RJ. Inhibition of inflammation but not ankylosis by glucocorticoids in mice: further evidence for the entheseal stress hypothesis. Arthritis Res Ther. 2012; 14:R59.

157. Lories RJ, Derese I, de Bari C, Luyten FP. Evidence for uncoupling of inflammation and joint remodeling in a mouse model of spondylarthritis. Arthritis Rheum. 2007; 56:489-97.

158. Sakaguchi N, Takahashi T, Hata H, Nomura T, Tagami T, Yamazaki S, Sakihama T, Matsutani T, Negishi I, Nakatsuru S *et al*. Altered thymic T-cell selection due to a mutation of the ZAP-70 gene causes autoimmune arthritis in mice. Nature. 2003; 426:454-60.

159. Negishi I, Motoyama N, Nakayama K, Nakayama K, Senju S, Hatakeyama S, Zhang Q, Chan AC, Loh DY. Essential role for ZAP-70 in both positive and negative selection of thymocytes. Nature. 1995; 376:435-8.

160. Ruutu M, Thomas G, Steck R, Degli-Esposti MA, Zinkernagel MS, Alexander K, Velasco J, Strutton G, Tran A, Benham H *et al*. beta-glucan triggers spondylarthritis and Crohn's disease-like ileitis in SKG mice. Arthritis Rheum. 2012; 64:2211-22.

161. Yoshitomi H, Sakaguchi N, Kobayashi K, Brown GD, Tagami T, Sakihama T, Hirota K, Tanaka S, Nomura T, Miki I *et al*. A role for fungal {beta}-glucans and their receptor Dectin-1 in the induction of autoimmune arthritis in genetically susceptible mice. J Exp Med. 2005; 201:949-60.

162. Hata H, Sakaguchi N, Yoshitomi H, Iwakura Y, Sekikawa K, Azuma Y, Kanai C, Moriizumi E, Nomura T, Nakamura T *et al*. Distinct contribution of IL-6, TNF-alpha, IL-1, and IL-10 to T cell-mediated spontaneous autoimmune arthritis in mice. J Clin Investig. 2004; 114:582-8.

163. Hirota K, Hashimoto M, Yoshitomi H, Tanaka S, Nomura T, Yamaguchi T, Iwakura Y, Sakaguchi N, Sakaguchi S. T cell self-reactivity forms a cytokine milieu for spontaneous development of IL-17+ Th cells that cause autoimmune arthritis. J Exp Med. 2007; 204:41-7.

164. Benham H, Rehaume LM, Hasnain SZ, Velasco J, Baillet AC, Ruutu M, Kikly K, Wang R, Tseng HW, Thomas GP *et al*. Interleukin-23 mediates the intestinal response to microbial beta-1,3-glucan and the development of spondyloarthritis pathology in SKG mice. Arthritis Rheumatol. 2014; 66:1755-67.

165. Kontoyiannis D, Pasparakis M, Pizarro TT, Cominelli F, Kollias G. Impaired on/off regulation of TNF biosynthesis in mice lacking TNF AU-rich elements: implications for joint and gut-associated immunopathologies. Immunity. 1999; 10:387-98.

166. Uderhardt S, Diarra D, Katzenbeisser J, David JP, Zwerina J, Richards W, Kronke G, Schett G. Blockade of Dickkopf (DKK)-1 induces fusion of sacroiliac joints. Ann Rheum Dis. 2009; 69:592-7.

167. Haynes K: **Functional analysis of candidate genes in mouse models of Ankylosing spondylitis (thesis).** The University of Queensland: The University of Queensland; 2011.

168. Armaka M, Apostolaki M, Jacques P, Kontoyiannis DL, Elewaut D, Kollias G. Mesenchymal cell targeting by TNF as a common pathogenic principle in chronic inflammatory joint and intestinal diseases. J Exp Med. 2008; 205:331-7.

169. Jacques P, Lambrecht S, Verheugen E, Pauwels E, Kollias G, Armaka M, Verhoye M, Van der Linden A, Achten R, Lories RJ *et al*. Proof of concept: enthesitis and new bone

formation in spondyloarthritis are driven by mechanical strain and stromal cells. Ann Rheum Dis. 2014; 73:437-45.

170. Adamopoulos IE, Tessmer M, Chao CC, Adda S, Gorman D, Petro M, Chou CC, Pierce RH, Yao W, Lane NE *et al*. IL-23 Is Critical for Induction of Arthritis, Osteoclast Formation, and Maintenance of Bone Mass. The Journal of Immunology. 2011; 187:951-9.

171. Murad YM, Szabo Z, Ludanyi K, Glant TT. Molecular manipulation with the arthritogenic epitopes of the G1 domain of human cartilage proteoglycan aggrecan. Clin Exp Immunol. 2005; 142:303-11.

172. Glant TT, Radacs M, Nagyeri G, Olasz K, Laszlo A, Boldizsar F, Hegyi A, Finnegan A, Mikecz K. Proteoglycan-induced arthritis and recombinant human proteoglycan aggrecan G1 domain-induced arthritis in BALB/c mice resembling two subtypes of rheumatoid arthritis. Arthritis Rheum. 2011; 63:1312-21.

173. Berlo SE, Guichelaar T, Ten Brink CB, van Kooten PJ, Hauet-Broeren F, Ludanyi K, van Eden W, Broeren CP, Glant TT. Increased arthritis susceptibility in cartilage proteoglycan-specific T cell receptor-transgenic mice. Arthritis Rheum. 2006; 54:2423-33.

174. Glant TT, Mikecz K, Arzoumanian A, Poole AR. Proteoglycan-induced arthritis in BALB/c mice. Clinical features and histopathology. Arthritis Rheum. 1987; 30:201-12.

175. Berlo SE, van Kooten PJ, ten Brink CB, Hauet-Broere F, Oosterwegel MA, Glant TT, Van Eden W, Broeren CP. Naive transgenic T cells expressing cartilage proteoglycan-specific TCR induce arthritis upon in vivo activation. J Autoimmun. 2005; 25:172-80.

176. Bárdos T, Szabó Z, Czipri M, Vermes C, Tunyogi-Csapó M, Urban RM, Mikecz K, TT. G. A longitudinal study on an autoimmune murine model of ankylosing spondylitis. Ann Rheum Dis. 2005; 64:981-7.

177. Buzas EI, Brennan FR, Mikecz K, Garzo M, Negroiu G, Hollo K, Cs-Szabo G, Pintye E, Glant TT. A proteoglycan (aggrecan)-specific T cell hybridoma induces arthritis in BALB/c mice. J Immunol. 1995; 155:2679-87.

178. Kezic JM, Glant TT, Rosenbaum JT, Rosenzweig HL. Neutralization of IL-17 ameliorates uveitis but damages photoreceptors in a murine model of spondyloarthritis. Arthritis Res Ther. 2012; 14:R18.

179. Bardos T, Mikecz K, Finnegan A, Zhang J, Glant TT. T and B cell recovery in arthritis adoptively transferred to SCID mice: antigen-specific activation is required for restoration of autopathogenic CD4+ Th1 cells in a syngeneic system. J Immunol. 2002; 168:6013-21.

180. Boldizsar F, Tarjanyi O, Nemeth P, Mikecz K, Glant TT. Th1/Th17 polarization and acquisition of an arthritogenic phenotype in arthritis-susceptible BALB/c, but not in MHC-matched, arthritis-resistant DBA/2 mice. Int Immunol. 2009; 21:511-22.

181. Rodeghero R, Cao Y, Olalekan SA, Iwakua Y, Glant TT, Finnegan A. Location of CD4+ T cell priming regulates the differentiation of Th1 and Th17 cells and their contribution to arthritis. J Immunol. 2013; 190:5423-35.

182. Olalekan SA, Cao Y, Finnegan A. Tissue specific CD4+ T cell priming determines the requirement for interleukin-23 in experimental arthritis. Arthritis Res Ther. 2014; 16:440.

183. Finnegan A, Grusby MJ, Kaplan CD, O'Neill SK, Eibel H, Koreny T, Czipri M, Mikecz K, Zhang J. IL-4 and IL-12 regulate proteoglycan-induced arthritis through Stat-dependent mechanisms. J Immunol. 2002; 169:3345-52.

184. Finnegan A, Mikecz K, Tao P, Glant TT. Proteoglycan (aggrecan)-induced arthritis in BALB/c mice is a Th1-type disease regulated by Th2 cytokines. J Immunol. 1999; 163:5383-90.

185. Hamel KM, Cao Y, Ashaye S, Wang Y, Dunn R, Kehry MR, Glant TT, Finnegan A. B Cell Depletion Enhances T Regulatory Cell Activity Essential in the Suppression of Arthritis. The Journal of Immunology. 2011; 187:4900-6.

186. Szabó Z, Szántó S, Végvári A, Szekanecz Z, Mikecz K, Glant TT. Genetic control of experimental spondylarthropathy. Arthritis Rheum. 2005; 52:2452-60.

187. Vegvari A, Szabo Z, Szanto S, Nesterovitch AB, Mikecz K, Glant TT, Adarichev VA. Two major interacting chromosome loci control disease susceptibility in murine model of spondyloarthropathy. J Immunol. 2005; 175:2475-83.

188. Maksymowych WP, Chiowchanwisawakit P, Clare T, Pedersen SJ, Ostergaard M, Lambert RG. Inflammatory lesions of the spine on magnetic resonance imaging predict the development of new syndesmophytes in ankylosing spondylitis: evidence of a relationship between inflammation and new bone formation. Arthritis Rheum. 2009; 60:93-102.

189. Baraliakos X, Listing J, Rudwaleit M, Sieper J, Braun J. The relationship between inflammation and new bone formation in patients with ankylosing spondylitis. Arthritis Res Ther. 2008; 10:R104.

190. van der Heijde D, Machado P, Braun J, Hermann KG, Baraliakos X, Hsu B, Baker D, Landewe R. MRI inflammation at the vertebral unit only marginally predicts new syndesmophyte formation: a multilevel analysis in patients with ankylosing spondylitis. Ann Rheum Dis. 2012; 71:369-73.

191. Baraliakos X, Heldmann F, Callhoff J, Listing J, Appelboom T, Brandt J, Van den Bosch F, Breban M, Burmester G, Dougados M *et al*. Which spinal lesions are associated with new bone formation in patients with ankylosing spondylitis treated with anti-TNF agents? A long-term observational study using MRI and conventional radiography. Ann Rheum Dis. 2013.

192. Appel H, Loddenkemper C, Grozdanovic Z, Ebhardt H, Dreimann M, Hempfing A, Stein H, Metz-Stavenhagen P, Rudwaleit M, Sieper J. Correlation of histopathological findings and magnetic resonance imaging in the spine of patients with ankylosing spondylitis. Arthritis Res Ther. 2006; 8:R143.

193. Song IH, Hermann KG, Haibel H, Althoff CE, Poddubnyy D, Listing J, Weiss A, Freundlich B, Rudwaleit M, Sieper J. Relationship between active inflammatory lesions in the spine and sacroiliac joints and new development of chronic lesions on whole-body MRI in early axial spondyloarthritis: results of the ESTHER trial at week 48. Ann Rheum Dis. 2011; 70:1257-63.

194. Weber U, Pedersen SJ, Ostergaard M, Rufibach K, Lambert RG, Maksymowych WP. Can erosions on MRI of the sacroiliac joints be reliably detected in patients with ankylosing spondylitis? - A cross-sectional study. Arthritis Res Ther. 2012; 14:R124.

195. Maksymowych WP, Wichuk S, Chiowchanwisawakit P, Lambert RG, Pedersen SJ. Fat metaplasia and backfill are key intermediaries in the development of sacroiliac joint ankylosis in patients with ankylosing spondylitis. Arthritis Rheumatol. 2014.

196. Bennett AN, Rehman A, Hensor EM, Marzo-Ortega H, Emery P, McGonagle D. The fatty Romanus lesion: a non-inflammatory spinal MRI lesion specific for axial spondyloarthropathy. Ann Rheum Dis. 2010; 69:891-4.

197. Chiowchanwisawakit P, Lambert RG, Conner-Spady B, Maksymowych WP. Focal fat lesions at vertebral corners on magnetic resonance imaging predict the development of new syndesmophytes in ankylosing spondylitis. Arthritis Rheum. 2011; 63:2215-25.

198. Heiland GR, Zwerina K, Baum W, Kireva T, Distler JH, Grisanti M, Asuncion F, Li X, Ominsky M, Richards W *et al*. Neutralisation of Dkk-1 protects from systemic bone loss during inflammation and reduces sclerostin expression. Ann Rheum Dis. 2010; 69:2152-9.

199. Vincent C, Findlay DM, Welldon KJ, Wijenayaka AR, Zheng TS, Haynes DR, Fazzalari NL, Evdokiou A, Atkins GJ. Pro-inflammatory cytokines TNF-related weak inducer of apoptosis (TWEAK) and TNFalpha induce the mitogen-activated protein kinase (MAPK)-dependent expression of sclerostin in human osteoblasts. J Bone Miner Res. 2009; 24:1434-49.

200. Hu Z, Xu M, Li Q, Lin Z, Liao Z, Cao S, Wei Q, Zhang YL, Li T, Jin O *et al*. Adalimumab significantly reduces inflammation and serum DKK-1 level but increases fatty deposition in lumbar spine in active ankylosing spondylitis. Int J Rheum Dis. 2012; 15:358-65.

201. Maksymowych WP. Disease modification in ankylosing spondylitis. Nat Rev Rheumatol. 2010; 6:75-81.

202. Baraliakos X, Listing J, Rudwaleit M, Brandt J, Sieper J, Braun J. Radiographic progression in patients with ankylosing spondylitis after 2 years of treatment with the tumour necrosis factor alpha antibody infliximab. Ann Rheum Dis. 2005; 64:1462-6.

203. Braun J, Baraliakos X, Hermann KG, Deodhar A, van der Heijde D, Inman R, Beutler A, Zhou Y, Xu S, Hsu B. The effect of two golimumab doses on radiographic progression in ankylosing spondylitis: results through 4 years of the GO-RAISE trial. Ann Rheum Dis. 2014; 73:1107-13.

204. van der Heijde D, Salonen D, Weissman BN, Landewe R, Maksymowych WP, Kupper H, Ballal S, Gibson E, Wong R. Assessment of radiographic progression in the spines of patients with ankylosing spondylitis treated with adalimumab for up to 2 years. Arthritis Res Ther. 2009; 11:R127.

205. Baraliakos X, Listing J, Brandt J, Haibel H, Rudwaleit M, Sieper J, Braun J. Radiographic progression in patients with ankylosing spondylitis after 4 yrs of treatment with the anti-TNF-alpha antibody infliximab. Rheumatology (Oxf). 2007; 46:1450-3.

206. Haroon N, Inman RD, Learch TJ, Weisman MH, Lee M, Rahbar MH, Ward MM, Reveille

JD, Gensler LS. The impact of tumor necrosis factor alpha inhibitors on radiographic progression in ankylosing spondylitis. Arthritis Rheum. 2013; 65:2645-54.

207. Seo MR, Baek HL, Yoon HH, Ryu HJ, Choi HJ, Baek HJ, Ko KP. Delayed diagnosis is linked to worse outcomes and unfavourable treatment responses in patients with axial spondyloarthritis. Clin Rheumatol. 2014.

208. Braun J, Landewe R, Hermann KG, Han J, Yan S, Williamson P, van der Heijde D. Major reduction in spinal inflammation in patients with ankylosing spondylitis after treatment with infliximab: results of a multicenter, randomized, double-blind, placebo-controlled magnetic resonance imaging study. Arthritis Rheum. 2006; 54:1646-52.

209. Appel H, Kuhne M, Spiekermann S, Ebhardt H, Grozdanovic Z, Kohler D, Dreimann M, Hempfing A, Rudwaleit M, Stein H *et al*. Immunohistologic analysis of zygapophyseal joints in patients with ankylosing spondylitis. Arthritis Rheum. 2006; 54:2845-51.

210. Appel H, Maier R, Wu P, Scheer R, Hempfing A, Kayser R, Thiel A, Radbruch A, Loddenkemper C, Sieper J. Analysis of IL-17+ cells in facet joints of patients with spondyloarthritis suggests that the innate immune pathway might be of greater relevance than the Th17-mediated adaptive immune response. Arthritis Res Ther. 2011; 13:R95.

211. Appel H, Maier R, Bleil J, Hempfing A, Loddenkemper C, Schlichting U, Syrbe U, Sieper J. In situ analysis of interleukin-23- and interleukin-12-positive cells in the spine of patients with ankylosing spondylitis. Arthritis Rheum. 2013; 65:1522-9.

212. Calin A, Elswood J. The relationship between pelvic, spinal and hip involvement in ankylosing spondylitis--one disease process or several? Br J Rheumatol. 1988; 27:393-5.

213. Yang C, Gu J, Rihl M, Baeten D, Huang F, Zhao M, Zhang H, Maksymowych WP, De Keyser F, Veys EM *et al*. Serum levels of matrix metalloproteinase 3 and macrophage colony-stimulating factor 1 correlate with disease activity in ankylosing spondylitis. Arthritis Care & Research. 2004; 51:691-9.

214. Soliman E, Labib W, el-Tantawi G, Hamimy A, Alhadidy A, Aldawoudy A. Role of matrix metalloproteinase-3 (MMP-3) and magnetic resonance imaging of sacroiliitis in assessing disease activity in ankylosing spondylitis. Rheumatol Int. 2012; 32:1711-20.

215. Arends S, van der Veer E, Groen H, Houtman PM, Jansen TL, Leijsma MK, Bijzet J, Limburg PC, Kallenberg CG, Spoorenberg A *et al*. Serum MMP-3 level as a biomarker for monitoring and predicting response to etanercept treatment in ankylosing spondylitis. J Rheumatol. 2011; 38:1644-50.

216. Angyal A, Egelston C, Kobezda T, Olasz K, László A, Glant TT, Mikecz K. Development of proteoglycan-induced arthritis depends on T cell-supported autoantibody production, but does not involve significant influx of T cells into the joints. Arthritis Res Ther. 2010; 12:R44.

217. Uchida K, Yayama T, Sugita D, Nakajima H, Rodriguez Guerrero A, Watanabe S, Roberts S, Johnson WE, Baba H. Initiation and progression of ossification of the posterior longitudinal ligament of the cervical spine in the hereditary spinal hyperostotic mouse (twy/twy). Eur Spine J. 2012; 21:149-55.

218. Loughenbury PR, Wadhwani S, Soames RW. The posterior longitudinal ligament and peridural (epidural) membrane. Clin Anat. 2006; 19:487-92.

219. Tan S, Yao J, Flynn JA, Yao L, Ward MM. Quantitation of Circumferential Syndesmophyte Height along the Vertebral Rim in Ankylosing Spondylitis Using Computed Tomography. J Rheumatol. 2015; 42:472-8.

220. Resorlu M, Gokmen F, Resorlu H, Adam G, Akbal A, Cevizci S, Sariyildirim A, Savas Y, Guven M, Aras AB. Association between apparent diffusion coefficient and intervertebral disc degeneration in patients with ankylosing spondylitis. Int J Clin Exp Med. 2015; 8:1241-6.

221. Joosten LA, Lubberts E, Helsen MM, Saxne T, Coenen-de Roo CJ, Heinegard D, van den Berg WB. Protection against cartilage and bone destruction by systemic interleukin-4 treatment in established murine type II collagen-induced arthritis. Arthritis Res. 1999; 1:81-91.

222. Schurigt U, Stopfel N, Huckel M, Pfirschke C, Wiederanders B, Brauer R. Local expression of matrix metalloproteinases, cathepsins, and their inhibitors during the development of murine antigen-induced arthritis. Arthritis Res Ther. 2005; 7:R174-88.

223. Jacobson PB, Morgan SJ, Wilcox DM, Nguyen P, Ratajczak CA, Carlson RP, Harris RR, Nuss M. A new spin on an old model: in vivo evaluation of disease progression by magnetic resonance imaging with respect to standard inflammatory parameters and histopathology in the adjuvant arthritic rat. Arthritis Rheum. 1999; 42:2060-73.

224. Kong X, Zhang Y, Liu C, Guo W, Li X, Su X, Wan H, Sun Y, Lin N. Anti-angiogenic effect of triptolide in rheumatoid arthritis by targeting angiogenic cascade. PLoS ONE. 2013; 8:e77513.

225. Maksymowych WP, Chiowchanwisawakit P, Clare T, Pedersen SJ, Østergaard M, Lambert RGW. Inflammatory lesions of the spine on magnetic resonance imaging predict the development of new syndesmophytes in ankylosing spondylitis: Evidence of a relationship between inflammation and new bone formation. Arthritis & Rheumatism. 2009; 60:93-102.

226. Walsh NC, Reinwald S, Manning CA, Condon KW, Iwata K, Burr DB, Gravallese EM. Osteoblast function is compromised at sites of focal bone erosion in inflammatory arthritis. J Bone Miner Res. 2009; 24:1572-85.

227. Matzelle MM, Gallant MA, Condon KW, Walsh NC, Manning CA, Stein GS, Lian JB, Burr DB, Gravallese EM. Resolution of inflammation induces osteoblast function and regulates the Wnt signaling pathway. Arthritis & Rheumatism. 2012; 64:1540-50.

228. Nosikova Y, Santerre JP, Grynpas MD, Kandel RA. Annulus fibrosus cells can induce mineralization: an in vitro study. Spine J. 2013; 13:443-53.

229. Ito Y, Fitzsimmons JS, Sanyal A, Mello MA, Mukherjee N, O'Driscoll SW. Localization of chondrocyte precursors in periosteum. Osteoarthritis Cartilage. 2001; 9:215-23.

230. Cai HX, Yayama T, Uchida K, Nakajima H, Sugita D, Guerrero AR, Yoshida A, Baba H. Cyclic tensile strain facilitates the ossification of ligamentum flavum through beta-catenin

signaling pathway: in vitro analysis. Spine (Phila Pa 1976). 2012; 37:E639-46.

231. Bleil J, Maier R, Hempfing A, Schlichting U, Appel H, Sieper J, Syrbe U. Histomorphologic and histomorphometric characteristics of zygapophyseal joint remodeling in ankylosing spondylitis. Arthritis Rheumatol. 2014; 66:1745-54.

232. McQueen F, Lloyd R, Doyle A, Robinson E, Lobo M, Exeter M, Taylor WJ, Jones P, Reid IR, Dalbeth N. Zoledronic acid does not reduce MRI erosive progression in PsA but may suppress bone oedema: the Zoledronic Acid in Psoriatic Arthritis (ZAPA) Study. Ann Rheum Dis. 2011; 70:1091-4.

233. Baraliakos X, Listing J, Buschmann J, von der Recke A, Braun J. A comparison of new bone formation in patients with ankylosing spondylitis and patients with diffuse idiopathic skeletal hyperostosis: a retrospective cohort study over six years. Arthritis Rheum. 2012; 64:1127-33.

234. Matsushima S, Isogai N, Jacquet R, Lowder E, Tokui T, Landis WJ. The nature and role of periosteum in bone and cartilage regeneration. Cells Tissues Organs. 2011; 194:320-5.

235. van Gastel N, Stegen S, Stockmans I, Moermans K, Schrooten J, Graf D, Luyten FP, Carmeliet G. Expansion of murine periosteal progenitor cells with fibroblast growth factor 2 reveals an intrinsic endochondral ossification program mediated by bone morphogenetic protein 2. Stem Cells. 2014; 32:2407-18.

236. Stevens MM, Marini RP, Schaefer D, Aronson J, Langer R, Shastri VP. In vivo engineering of organs: the bone bioreactor. Proc Natl Acad Sci U S A. 2005; 102:11450-5.

237. Schett G, Stolina M, Dwyer D, Zack D, Uderhardt S, Kronke G, Kostenuik P, Feige U. Tumor necrosis factor alpha and RANKL blockade cannot halt bony spur formation in experimental inflammatory arthritis. Arthritis Rheum. 2009; 60:2644-54.

238. Ruiz-Heiland G, Horn A, Zerr P, Hofstetter W, Baum W, Stock M, Distler JH, Nimmerjahn F, Schett G, Zwerina J. Blockade of the hedgehog pathway inhibits osteophyte formation in arthritis. Ann Rheum Dis. 2012; 71:400-7.

239. Pettit AR, Ji H, von Stechow D, Muller R, Goldring SR, Choi Y, Benoist C, Gravallese EM. TRANCE/RANKL knockout mice are protected from bone erosion in a serum transfer model of arthritis. Am J Pathol. 2001; 159:1689-99.

240. Lories RJ, Derese I, Luyten FP. Inhibition of osteoclasts does not prevent joint ankylosis in a mouse model of spondyloarthritis. Rheumatology (Oxf). 2008; 47:605-8.

241. Cesur M, Alici HA, Erdem AF. An unusual cause of difficult intubation in a patient with a large cervical anterior osteophyte: a case report. Acta Anaesthesiol Scand. 2005; 49:264-6.

242. Varsak YK, Eryilmaz MA, Arbag H. Dysphagia and airway obstruction due to large cervical osteophyte in a patient with ankylosing spondylitis. J Craniofac Surg. 2014; 25:1402-3.

243. Shidham V, Chivukula M, Basir Z, Shidham G. Evaluation of crystals in formalin-fixed, paraffin-embedded tissue sections for the differential diagnosis of pseudogout, gout, and tumoral calcinosis. Mod Pathol. 2001; 14:806-10.

244. Yamakawa K, Iwasaki H, Masuda I, Ohjimi Y, Honda I, Saeki K, Zhang J, Shono E, Naito M, Kikuchi M. The utility of alizarin red s staining in calcium pyrophosphate dihydrate crystal deposition disease. J Rheumatol. 2003; 30:1032-5.

245. Dussault RG, Kaye JJ. Intervertebral disk calcification associated with spine fusion. Radiology. 1977; 125:57-61.

246. Chang X, Zheng Y, Yang Q, Wang L, Pan J, Xia Y, Yan X, Han J. Carbonic anhydrase I (CA1) is involved in the process of bone formation and is susceptible to ankylosing spondylitis. Arthritis Res Ther. 2012; 14:R176.

247. Chang X, Han J, Zhao Y, Yan X, Sun S, Cui Y. Increased expression of carbonic anhydrase I in the synovium of patients with ankylosing spondylitis. BMC Musculoskelet Disord. 2010; 11:279.

248. Abhishek A, Doherty M. Pathophysiology of articular chondrocalcinosis--role of ANKH. Nat Rev Rheumatol. 2011; 7:96-104.

249. Sweet HO, Green MC. Progressive ankylosis, a new skeletal mutation in the mouse. J Hered. 1981; 72:87-93.

250. Hristova GI, Jarzem P, Ouellet JA, Roughley PJ, Epure LM, Antoniou J, Mwale F. Calcification in human intervertebral disc degeneration and scoliosis. J Orthop Res. 2011; 29:1888-95.

251. Major NM, Helms CA, Genant HK. Calcification demonstrated as high signal intensity on T1-weighted MR images of the disks of the lumbar spine. Radiology. 1993; 189:494-6.

252. Sakata D, Yao C, Narumiya S. Prostaglandin E2, an Immunoactivator. J Pharmacol Sci. 2010; 112:1-5.

253. Li M, Thompson DD, Paralkar VM. Prostaglandin E2 receptors in bone formation. Int Orthop. 2007; 31:767-72.

254. Kuroda E, Yamashita U. Mechanisms of enhanced macrophage-mediated prostaglandin E2 production and its suppressive role in Th1 activation in Th2-dominant BALB/c mice. J Immunol. 2003; 170:757-64.

255. Mizuno R, Kamioka Y, Kabashima K, Imajo M, Sumiyama K, Nakasho E, Ito T, Hamazaki Y, Okuchi Y, Sakai Y *et al*. In vivo imaging reveals PKA regulation of ERK activity during neutrophil recruitment to inflamed intestines. J Exp Med. 2014; 211:1123-36.

256. Yao C, Sakata D, Esaki Y, Li Y, Matsuoka T, Kuroiwa K, Sugimoto Y, Narumiya S. Prostaglandin E2–EP4 signaling promotes immune inflammation through TH1 cell differentiation and TH17 cell expansion. Nat Med. 2009; 15:633-40.

257. Chen Q, Muramoto K, Masaaki N, Ding Y, Yang H, Mackey M, Li W, Inoue Y, Ackermann K, Shirota H *et al*. A novel antagonist of the prostaglandin E2 EP4 receptor inhibits Th1 differentiation and Th17 expansion and is orally active in arthritis models. Br J Pharmacol. 2010; 160:292-310.

258. Sheibanie AF, Khayrullina T, Safadi FF, Ganea D. Prostaglandin E2 exacerbates collagen-induced arthritis in mice through the inflammatory interleukin-23/interleukin-17 axis. Arthritis Rheum. 2007; 56:2608-19.

259. McCoy JM. The role of prostaglandin E2 receptors in the pathogenesis of rheumatoid arthritis. J Clin Investig. 2002; 110:651-8.

260. Bender AT, Spyvee M, Satoh T, Gershman B, Teceno T, Burgess L, Kumar V, Wu Y, Yang H, Ding Y *et al*. Evaluation of a candidate anti-arthritic drug using the mouse collagen antibody induced arthritis model and clinically relevant biomarkers. Am J Transl Res. 2013; 5:92-102.

261. Okumura T, Murata Y, Taniguchi K, Murase A, Nii A. Effects of the selective EP4 antagonist, CJ-023,423 on chronic inflammation and bone destruction in rat adjuvant-induced arthritis. J Pharm Pharmacol. 2008; 60:723-30.

262. Clark P, Rowland SE, Denis D, Mathieu MC, Stocco R, Poirier H, Burch J, Han Y, Audoly L, Therien AG *et al*. MF498 [N-{[4-(5,9-Diethoxy-6-oxo-6,8-dihydro-7H-pyrrolo[3,4-g]quinolin-7-yl)-3-methylbe nzyl]sulfonyl}-2-(2-methoxyphenyl)acetamide], a selective E prostanoid receptor 4 antagonist, relieves joint inflammation and pain in rodent models of rheumatoid and osteoarthritis. J Pharmacol Exp Ther. 2008; 325:425-34.

263. Kamel MA, Picconi JL, Lara-Castillo N, Johnson ML. Activation of β-catenin signaling in MLO-Y4 osteocytic cells versus 2T3 osteoblastic cells by fluid flow shear stress and PGE2: Implications for the study of mechanosensation in bone. Bone. 2010; 47:872-81.

264. Cheng B, Kato Y, Zhao S, Luo J, Sprague E, Bonewald LF, Jiang JX. PGE(2) is essential for gap junction-mediated intercellular communication between osteocyte-like MLO-Y4 cells in response to mechanical strain. Endocrinology. 2001; 142:3464-73.

265. Li M, Healy DR, Li Y, Simmons HA, Crawford DT, Ke HZ, Pan LC, Brown TA, Thompson DD. Osteopenia and impaired fracture healing in aged EP4 receptor knockout mice. Bone. 2005; 37:46-54.

266. Ninomiya T, Hosoya A, Hiraga T, Koide M, Yamaguchi K, Oida H, Arai Y, Sahara N, Nakamura H, Ozawa H. Prostaglandin E(2) receptor EP(4)-selective agonist (ONO-4819) increases bone formation by modulating mesenchymal cell differentiation. Eur J Pharmacol. 2011; 650:396-402.

267. Miyaura C, Inada M, Suzawa T, Sugimoto Y, Ushikubi F, Ichikawa A, Narumiya S, Suda T. Impaired bone resorption to prostaglandin E2 in prostaglandin E receptor EP4-knockout mice. J Biol Chem. 2000; 275:19819-23.

268. Li X, Okada Y, Pilbeam CC, Lorenzo JA, Kennedy CR, Breyer RM, Raisz LG. Knockout of the murine prostaglandin EP2 receptor impairs osteoclastogenesis in vitro. Endocrinology. 2000; 141:2054-61.

269. Suzawa T, Miyaura C, Inada M, Maruyama T, Sugimoto Y, Ushikubi F, Ichikawa A, Narumiya S, Suda T. The role of prostaglandin E receptor subtypes (EP1, EP2, EP3, and EP4) in bone resorption: an analysis using specific agonists for the respective EPs. Endocrinology. 2000; 141:1554-9.

270. Aguirre JI, Leal ME, Rivera MF, Vanegas SM, Jorgensen M, Wronski TJ. Effects of basic fibroblast growth factor and a prostaglandin E2 receptor subtype 4 agonist on osteoblastogenesis and adipogenesis in aged ovariectomized rats. J Bone Miner Res. 2007; 22:877-88.

271. Kroon F, Landewe R, Dougados M, van der Heijde D. Continuous NSAID use reverts the effects of inflammation on radiographic progression in patients with ankylosing spondylitis. Ann Rheum Dis. 2012; 71:1623-9.

272. Kim SW, Pajevic PD, Selig M, Barry KJ, Yang JY, Shin CS, Baek WY, Kim JE, Kronenberg HM. Intermittent parathyroid hormone administration converts quiescent lining cells to active osteoblasts. J Bone Miner Res. 2012; 27:2075-84.

273. Hodsman AB, Bauer DC, Dempster DW, Dian L, Hanley DA, Harris ST, Kendler DL, McClung MR, Miller PD, Olszynski WP *et al*. Parathyroid hormone and teriparatide for the treatment of osteoporosis: a review of the evidence and suggested guidelines for its use. Endocr Rev. 2005; 26:688-703.

274. Dempster DW, Cosman F, Kurland ES, Zhou H, Nieves J, Woelfert L, Shane E, Plavetic K, Muller R, Bilezikian J *et al*. Effects of daily treatment with parathyroid hormone on bone microarchitecture and turnover in patients with osteoporosis: a paired biopsy study. J Bone Miner Res. 2001; 16:1846-53.

275. Neer RM, Arnaud CD, Zanchetta JR, Prince R, Gaich GA, Reginster JY, Hodsman AB, Eriksen EF, Ish-Shalom S, Genant HK *et al*. Effect of parathyroid hormone (1-34) on fractures and bone mineral density in postmenopausal women with osteoporosis. N Engl J Med. 2001; 344:1434-41.

276. Mutoh M, Watanabe K, Kitamura T, Shoji Y, Takahashi M, Kawamori T, Tani K, Kobayashi M, Maruyama T, Kobayashi K *et al*. Involvement of prostaglandin E receptor subtype EP(4) in colon carcinogenesis. Cancer Res. 2002; 62:28-32.

277. Esaki Y, Li Y, Sakata D, Yao C, Segi-Nishida E, Matsuoka T, Fukuda K, Narumiya S. Dual roles of PGE2-EP4 signaling in mouse experimental autoimmune encephalomyelitis. Proceedings of the National Academy of Sciences. 2010; 107:12233-8.

278. Valdez PA, Vithayathil PJ, Janelsins BM, Shaffer AL, Williamson PR, Datta SK. Prostaglandin E2 suppresses antifungal immunity by inhibiting interferon regulatory factor 4 function and interleukin-17 expression in T cells. Immunity. 2012; 36:668-79.

279. Napolitani G, Acosta-Rodriguez EV, Lanzavecchia A, Sallusto F. Prostaglandin E2 enhances Th17 responses via modulation of IL-17 and IFN-γ production by memory CD4+ T cells. Eur J Immunol. 2009; 39:1301-12.

280. Doodes PD, Cao Y, Hamel KM, Wang Y, Farkas B, Iwakura Y, Finnegan A. Development of proteoglycan-induced arthritis is independent of IL-17. J Immunol. 2008; 181:329-37.

281. Ke HZ, Crawford DT, Qi H, Simmons HA, Owen TA, Paralkar VM, Li M, Lu B, Grasser WA, Cameron KO *et al*. A nonprostanoid EP4 receptor selective prostaglandin E2 agonist restores bone mass and strength in aged, ovariectomized rats. J Bone Miner Res. 2006; 21:565-75.

282. Kato N, Kitahara K, Rittling SR, Nakashima K, Denhardt DT, Kurosawa H, Ezura Y, Noda M. Osteopontin deficiency enhances anabolic action of EP4 agonist at a sub-optimal dose in bone. J Endocrinol. 2007; 193:171-82.

283. Sasaoka R, Terai H, Toyoda H, Imai Y, Sugama R, Takaoka K. A prostanoid receptor EP4 agonist enhances ectopic bone formation induced by recombinant human bone morphogenetic protein-2. Biochem Biophys Res Commun. 2004; 318:704-9.

284. Shamir D, Keila S, Weinreb M. A selective EP4 receptor antagonist abrogates the stimulation of osteoblast recruitment from bone marrow stromal cells by prostaglandin E2 in vivo and in vitro. Bone. 2004; 34:157-62.

285. Clark CA, Schwarz EM, Zhang X, Ziran NM, Drissi H, O'Keefe RJ, Zuscik MJ. Differential regulation of EP receptor isoforms during chondrogenesis and chondrocyte maturation. Biochem Biophys Res Commun. 2005; 328:764-76.

286. Pountos I, Giannoudis PV, Jones E, English A, Churchman S, Field S, Ponchel F, Bird H, Emery P, McGonagle D. NSAIDS inhibit in vitro MSC chondrogenesis but not osteogenesis: implications for mechanism of bone formation inhibition in man. J Cell Mol Med. 2011; 15:525-34.

287. Zhang X, Ziran N, Goater JJ, Schwarz EM, Puzas JE, Rosier RN, Zuscik M, Drissi H, O'Keefe RJ. Primary murine limb bud mesenchymal cells in long-term culture complete chondrocyte differentiation: TGF-beta delays hypertrophy and PGE2 inhibits terminal differentiation. Bone. 2004; 34:809-17.

288. Kitamura T, Itoh M, Noda T, Tani K, Kobayashi M, Maruyama T, Kobayashi K, Ohuchida S, Sugimura T, Wakabayashi K. Combined effects of prostaglandin E receptor subtype EP1 and subtype EP4 antagonists on intestinal tumorigenesis in adenomatous polyposis coli gene knockout mice. Cancer Sci. 2003; 94:618-21.

289. Brown AP, Dinger N, Levine BS. Stress produced by gavage administration in the rat. Contemp Top Lab Anim Sci. 2000; 39:17-21.

290. Li S, Li Y, Ning H, Na L, Niu Y, Wang M, Feng R, Liu L, Guo F, Hou S *et al*. Calcium supplementation increases circulating cholesterol by reducing its catabolism via GPER and TRPC1-dependent pathway in estrogen deficient women. Int J Cardiol. 2013; 168:2548-60.

291. Kuwabara K, Yasui K, Jyoyama H, Maruyama T, Fleisch JH, Hori Y. Effects of the second-generation leukotriene B(4) receptor antagonist, LY293111Na, on leukocyte infiltration and collagen-induced arthritis in mice. Eur J Pharmacol. 2000; 402:275-85.

292. Sakaguchi Y, Shirahase H, Ichikawa A, Kanda M, Nozaki Y, Uehara Y. Effects of selective iNOS inhibition on type II collagen-induced arthritis in mice. Life Sci. 2004; 75:2257-67.

293. Kuroda E, Sugiura T, Zeki K, Yoshida Y, Yamashita U. Sensitivity difference to the suppressive effect of prostaglandin E2 among mouse strains: a possible mechanism to polarize Th2 type response in BALB/c mice. J Immunol. 2000; 164:2386-95.

294. van der Linden S, Valkenburg HA, Cats A. Evaluation of diagnostic criteria for ankylosing spondylitis. A proposal for modification of the New York criteria. Arthritis Rheum. 1984;

27:361-8.

295. Braun J, van der Horst-Bruinsma IE, Huang F, Burgos-Vargas R, Vlahos B, Koenig AS, Freundlich B. Clinical efficacy and safety of etanercept versus sulfasalazine in patients with ankylosing spondylitis: a randomized, double-blind trial. Arthritis Rheum. 2011; 63:1543-51.

296. Karabacakoglu A, Karakose S, Ozerbil OM, Odev K. Fluoroscopy-guided intraarticular corticosteroid injection into the sacroiliac joints in patients with ankylosing spondylitis. Acta Radiol. 2002; 43:425-7.

297. Richter MB, Woo P, Panayi GS, Trull A, Unger A, Shepherd P. The effects of intravenous pulse methylprednisolone on immunological and inflammatory processes in ankylosing spondylitis. Clin Exp Immunol. 1983; 53:51-9.

298. Mintz G, Enriquez RD, Mercado U, Robles EJ, Jimenez FJ, Gutierrez G. Intravenous methylprednisolone pulse therapy in severe ankylosing spondylitis. Arthritis Rheum. 1981; 24:734-6.

299. Haibel H, Fendler C, Listing J, Callhoff J, Braun J, Sieper J. Efficacy of oral prednisolone in active ankylosing spondylitis: results of a double-blind, randomised, placebo-controlled short-term trial. Ann Rheum Dis. 2014; 73:243-6.

300. Klingberg E, Lorentzon M, Gothlin J, Mellstrom D, Geijer M, Ohlsson C, Atkinson EJ, Khosla S, Carlsten H, Forsblad-d'Elia H. Bone microarchitecture in ankylosing spondylitis and the association with bone mineral density, fractures, and syndesmophytes. Arthritis Res Ther. 2013; 15:R179.

301. Donnelly S, Doyle DV, Denton A, Rolfe I, McCloskey EV, Spector TD. Bone mineral density and vertebral compression fracture rates in ankylosing spondylitis. Ann Rheum Dis. 1994; 53:117-21.

302. Viapiana O, Gatti D, Idolazzi L, Fracassi E, Adami S, Troplini S, Povino MR, Rossini M. Bisphosphonates vs infliximab in ankylosing spondylitis treatment. Rheumatology (Oxf). 2014; 53:90-4.

303. Maksymowych WP, Jhangri GS, Fitzgerald AA, LeClercq S, Chiu P, Yan A, Skeith KJ, Aaron SL, Homik J, Davis P *et al*. A six-month randomized, controlled, double-blind, dose-response comparison of intravenous pamidronate (60 mg versus 10 mg) in the treatment of nonsteroidal antiinflammatory drug-refractory ankylosing spondylitis. Arthritis Rheum. 2002; 46:766-73.

304. Santra G, Sarkar RN, Phaujdar S, Banerjee S, Siddhanta S. Assessment of the efficacy of pamidronate in ankylosing spondylitis: an open prospective trial. Singapore Med J. 2010; 51:883-7.

305. Maksymowych WP, Lambert R, Jhangri GS, Leclercq S, Chiu P, Wong B, Aaron S, Russell AS. Clinical and radiological amelioration of refractory peripheral spondyloarthritis by pulse intravenous pamidronate therapy. J Rheumatol. 2001; 28:144-55.

306. Hayami T, Pickarski M, Wesolowski GA, McLane J, Bone A, Destefano J, Rodan GA, Duong le T. The role of subchondral bone remodeling in osteoarthritis: reduction of cartilage

degeneration and prevention of osteophyte formation by alendronate in the rat anterior cruciate ligament transection model. Arthritis Rheum. 2004; 50:1193-206.

307. Neogi T, Nevitt MC, Ensrud KE, Bauer D, Felson DT. The effect of alendronate on progression of spinal osteophytes and disc-space narrowing. Ann Rheum Dis. 2008; 67:1427-30.

308. Heuft-Dorenbosch L, Spoorenberg A, van Tubergen A, Landewe R, van ver Tempel H, Mielants H, Dougados M, van der Heijde D. Assessment of enthesitis in ankylosing spondylitis. Ann Rheum Dis. 2003; 62:127-32.

309. Raj PP. Intervertebral disc: anatomy-physiology-pathophysiology-treatment. Pain Pract. 2008; 8:18-44.

310. Lories RJ, Luyten FP. The bone-cartilage unit in osteoarthritis. Nat Rev Rheumatol. 2011; 7:43-9.

311. Mikecz K, Glant TT, Poole AR. Immunity to cartilage proteoglycans in BALB/c mice with progressive polyarthritis and ankylosing spondylitis induced by injection of human cartilage proteoglycan. Arthritis Rheum. 1987; 30:306-18.

312. Adarichev VA, Nesterovitch AB, Bardos T, Biesczat D, Chandrasekaran R, Vermes C, Mikecz K, Finnegan A, Glant TT. Sex effect on clinical and immunologic quantitative trait loci in a murine model of rheumatoid arthritis. Arthritis Rheum. 2003; 48:1708-20.

313. Melgert BN, Postma DS, Kuipers I, Geerlings M, Luinge MA, van der Strate BW, Kerstjens HA, Timens W, Hylkema MN. Female mice are more susceptible to the development of allergic airway inflammation than male mice. Clin Exp Allergy. 2005; 35:1496-503.

314. Tarjanyi O, Boldizsar F, Nemeth P, Mikecz K, Glant TT. Age-related changes in arthritis susceptibility and severity in a murine model of rheumatoid arthritis. Immun Ageing. 2009; 6:8.

315. Tan S, Yao J, Flynn JA, Yao L, Ward MM. Dynamics of syndesmophyte growth in AS as measured by quantitative CT: heterogeneity within and among vertebral disc spaces. Rheumatology (Oxf). 2014.

8 Appendix

Representative images of each histological score criteria.

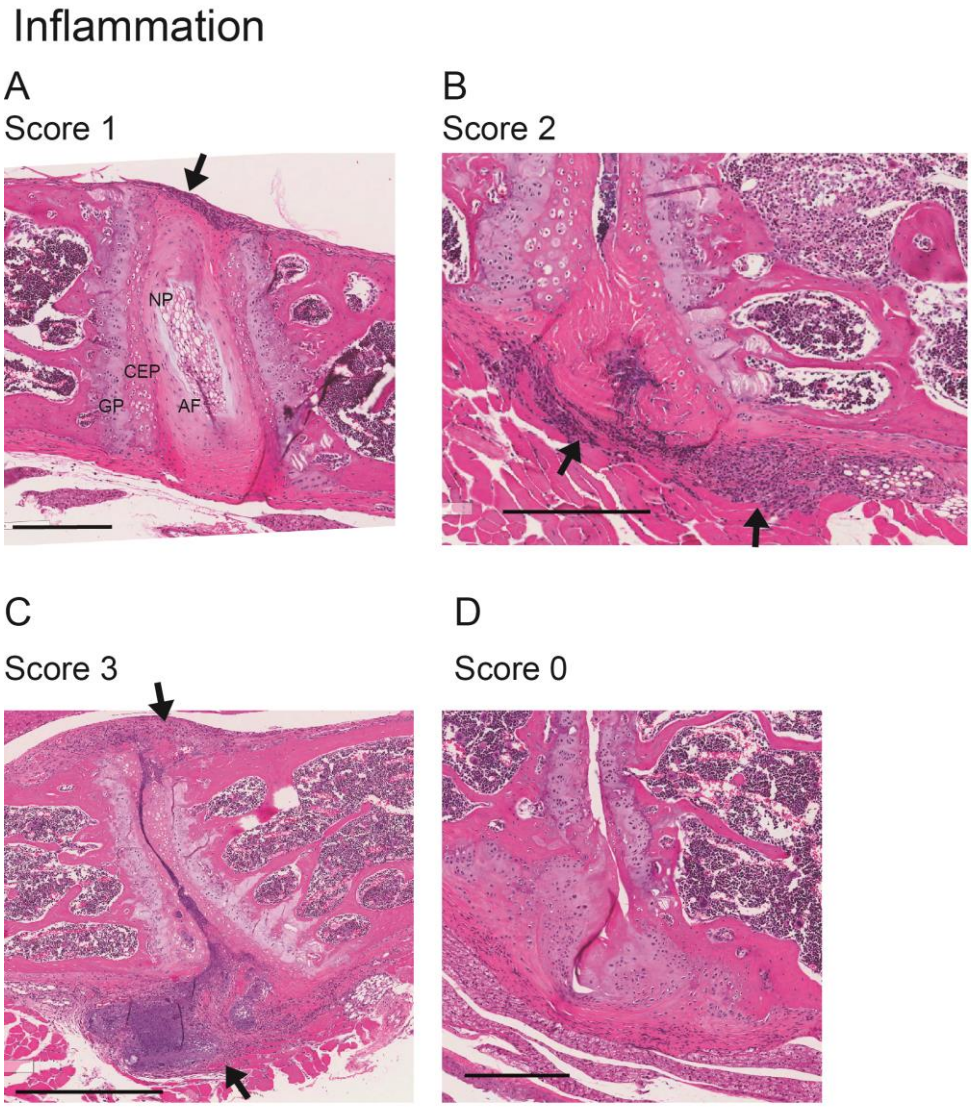

Appendix Figure1: Inflammatory scores.

(A) Score 1: Minor infiltration of inflammatory cells at the periphery of the joint. Black arrows point to inflammatory infiltrates. (B) Score 2: Moderate infiltration – inflammatory pannus < 50% joint area. (C) Score 3: Marked infiltration – inflammatory pannus > 50% joint area. (D) Score 0: inflammatory score 0 can be given to an IVD with normal morphology or advanced disease. The representative image shows an affected IVD without inflammatory cells remain around in IVD space. Scale bar: (A) 400 μm, (B) 300 μm, (C) 600 μm, (D) 300 μm.

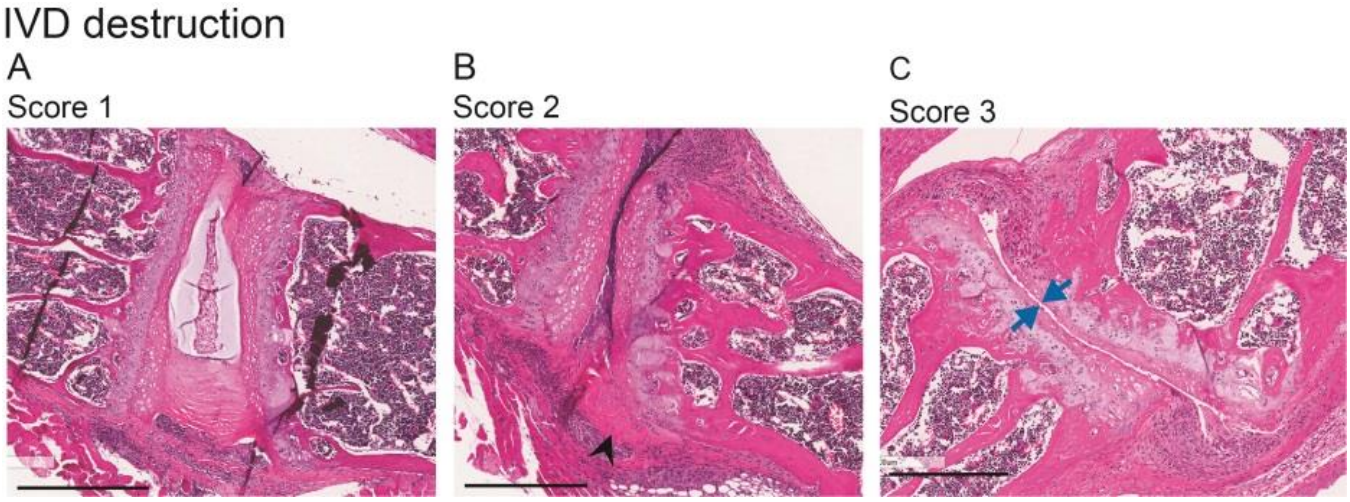

Appendix Figure 2: IVD destruction scores.

(A) Score 1: Less than 50% disc destruction. **(B)** Score 2: more than 50% disc destruction. Black arrowhead indicates remnant IVD tissue. **(C)** Score 3: Total disc destruction/only necrotic disc left. Original IVD space is indicated by blue arrows. Scale bar: (A) 500 μm, (B) 300 μm, (C) 400 μm.

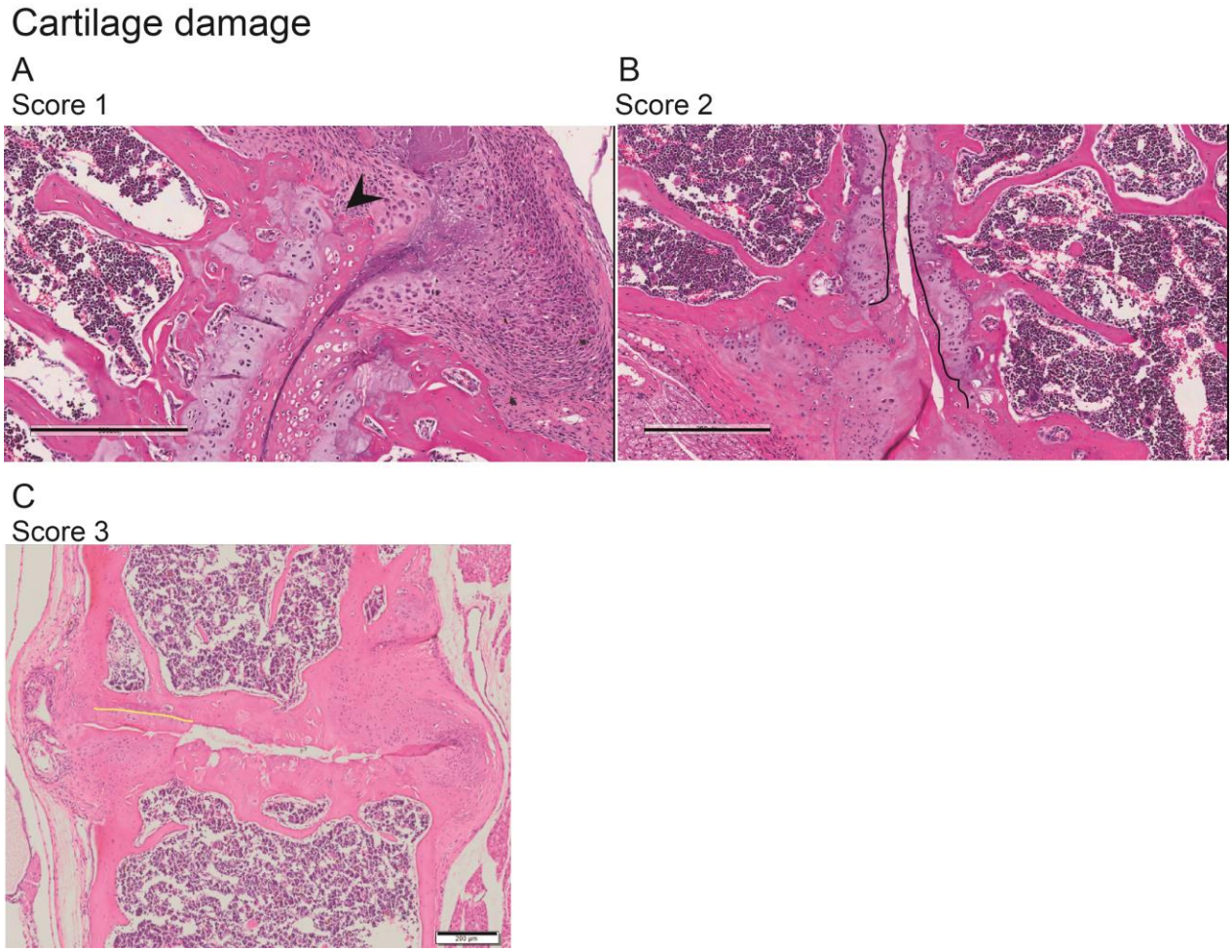

Appendix Figure 3: Cartilage damage.

(A) Score 1: Some erosion of endplate cartilage and/or growth plate cartilage (black arrowhead). **(B)** Score 2: Severe loss of articular cartilage and some growth plate cartilage damage. Black lines outline the interface between endplate and growth plate cartilage. Most endplate cartilage (between IVD space and black line) was severely eroded; whereas the thickness of growth plate cartilage remained. **(C)** Score 3: Severe loss of endplate cartilage and severe growth plate cartilage damage. Yellow line indicates subchondral bone surface that was still covered by growth plate and endplate cartilage. All other endplate and growth plate were damaged. Scale bars: (A-B) 300 μm, (C) 200 μm.

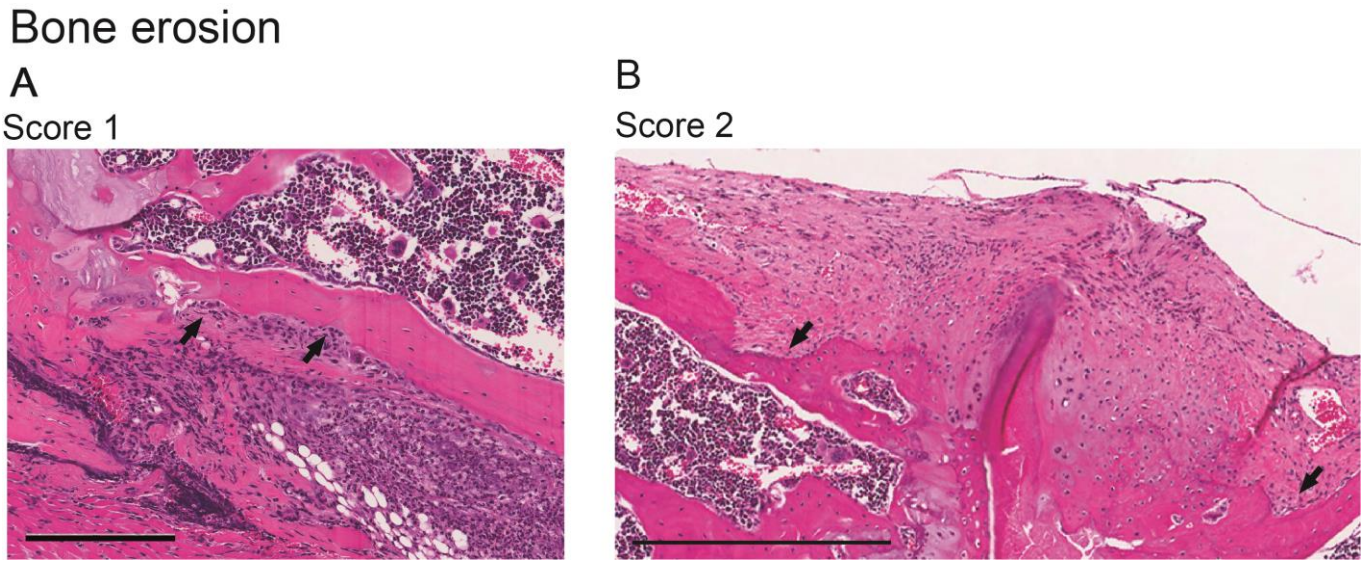

Appendix Figure 4: Bone erosion scores.

(A) Score 1: One or a few small areas of resorption in original vertebral bone. **(B)** Score 2: Numerous areas of obvious focal resorption in original vertebral bone or several areas of severe destruction. Black arrows indicate erosion. (B) Scale bar: (A) 200 μm, (B) 400 μm.

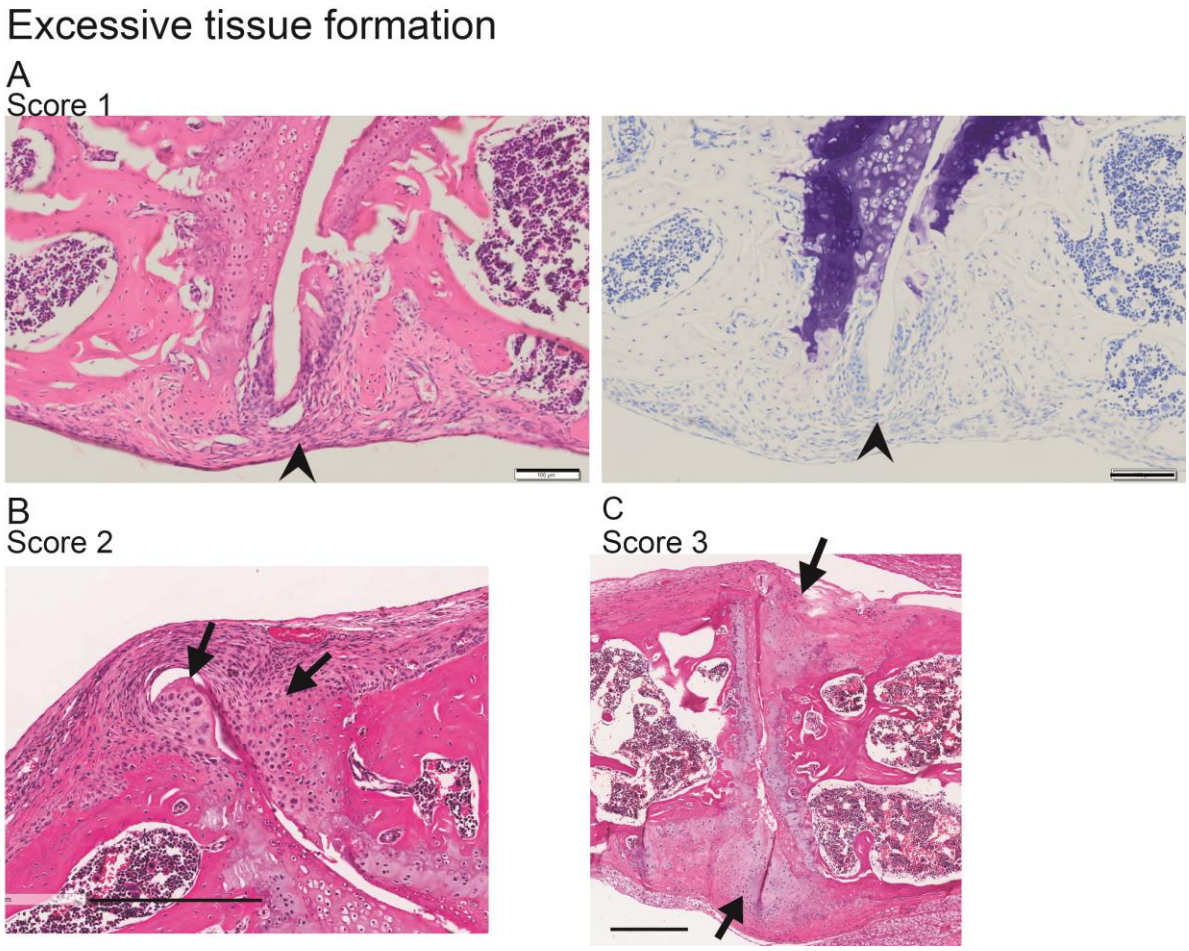

Appendix Figure 5: Excessive tissue formation scores.

(A) Score 1: Mesenchymal cell invasion/ expansion. Black arrowheads indicate mesenchymal cells that present fibroblast morphology and lack of proteoglycan. **(B)** Moderate fibrocartilage formation (<50% of the original disc area) **(C)** Extensive fibrocartilage formation (>50% of the original disc area). Scale bars: 300 μm.

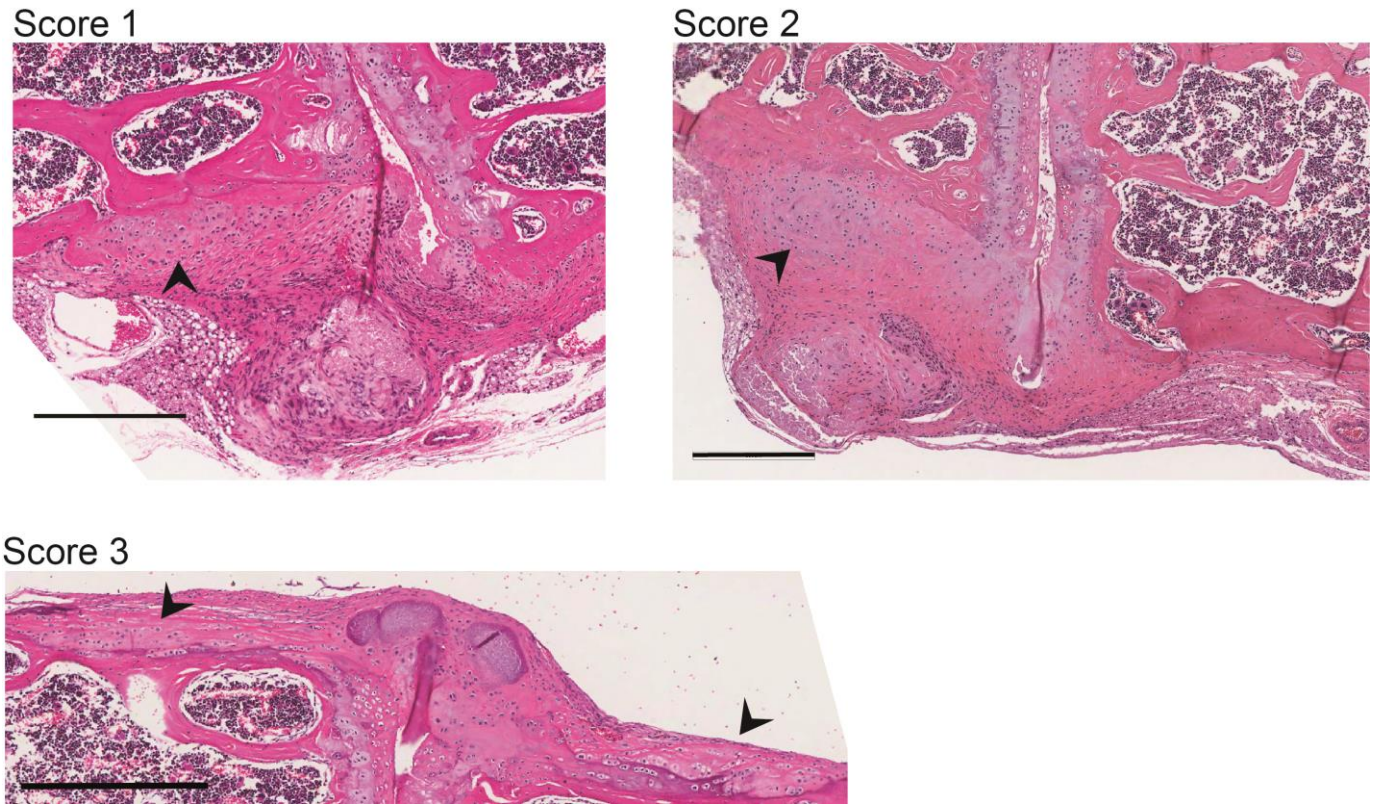

Appendix Figure 6: Ectopic chondrocyte formation scores.

(A) Score 1: single small area. **(B)** Score 2: single large area. **(C)** Score 3: multiple areas. Arrow heads indicate chondrocytes expanding on vertebral bone. Scale bars (A-B) 300 μm, (C) 400 μm**.**